The Study of the Stepwise Hydroxyl Radical-Mediated Oxidation of Alkyl Surfactants at the Air-Water Interface

Thesis by

Kevin M. Barraza

In Partial Fulfillment of the Requirements for

the degree of

Doctor of Philosophy

CALIFORNIA INSTITUTE OF TECHNOLOGY

Pasadena, California

2018

(Defended September 19, 2017)

Kevin M. Barraza
ORCID: 0000-0003-1849-5219

ACKNOWLEDGEMENTS

First, I'd like to thank Jack for being a supportive advisor. Words cannot express how much I appreciate the mentorship Jack has provided me. Thank you so much for the opportunity you've given me at Caltech. I'd like to thank all the past and current members of the Beauchamp group. Kate Upton has always been there to lend an ear about our respective projects, or to talk about non-science things. Daniel Thomas was a great help. When I first joined he was the person who taught me how to use and troubleshoot the FIDI apparatus. I am also appreciative of the postdocs in our lab, Jinshan Gao, Josh Wiley, and Xinxing Zhang, who have each been a source of perspective about science and academia.

There also some important members of the Caltech community who were very important in my development in graduate school. Rick Gerhart is an amazing glassblower. He is responsible for the fabrication of the dielectric barrier discharge source exactly to my specifications. Without his glassblowing expertise, I could never perform hydroxyl radical oxidation, and for that I am very thankful. I'd also like to thank Nathan Dalleska for participating in our group meetings and giving me helpful advice on the data I presented. I can't express how much I appreciate Priscilla Boon for her help on the administrative aspects of the group.

Caltech's CTLO and CPET have been an invaluable resource for my development as an educator. I am thankful for the opportunity to participate in the certificate programs that allowed me to expand my teaching strategies. Mitch Aiken and Kitty Cahalan are incredible at providing the educational resources necessary to go into the community and spread a love of science.

My family has been a source of constant emotional support throughout my life, and that couldn't be truer during my experience in graduate school. I can never thank my mother and father enough for being supportive of me, always being a phone call away whenever I need them. My sister Diana has had a front row seat to my journey as a graduate student, and is always ready to listen to my stories, often over delicious Mexican food. My Aunt Rose and Uncle John are like a second set of parents to me and I can always count on them. Likewise my cousin Tiffany is a second sister, and I always have felt so much support from her. My partner in crime Favian has witnessed my final year of graduate school and has helped me push through the finish line. Finally, I have to voice my appreciation to my cat Marceline, who is ready to jump on my head or meow softly when I need to smile. Thank you to everyone who has helped me reach this point in my life.

ABSTRACT

This thesis presents work on the heterogeneous chemistry of surfactant monolayers adsorbed at the air-water interface with gas phase hydroxyl radicals (OH). A novel hydroxyl radical source utilizing a low-temperature plasma known as the dielectric barrier discharge source (DBDS) is designed, characterized, and implemented as a high concentration OH generator (approximately 1000 fold higher than ambient conditions) in these experiments. Millimeter-sized water droplets containing a monolayer of surface-adsorbed species are exposed to this OH source until a designated level of oxidation. Field-induced droplet ionization mass spectrometry (FIDI-MS), which has been previously proven to be a surface-selective ionization technique, is used as an analytical method to determine the identity and relative quantity of oxidation products at the interface by sampling progeny droplets expelled upon the application of a pulsed electric field. Chapter 2 establishes the utility of the DBDS and FIDI-MS setup by oxidizing the 12-carbon n-alkyl surfactant dodecyltrimethylammonium (DTA^+). Mechanistic details can be determined through the evolution of high mass oxidation products through a nearly complete conversion of the parent monolayer. Carbonyl, hydroxyl, peroxyl, and small amounts of fragmentation products can be discerned from the collision-induced dissociation mass spectra and through hydrogen-deuterium exchange experiments. Psuedo-first order kinetics can also be observed in this system, suggesting a Langmuir-Hinshelwood mechanism of OH-initiated oxidation. Chapter 3 extends the study of oxidation of hydrocarbon surfactants by looking at neighbor chain competition among a bis-quaternary ammonium gemini surfactants, a species that contains two long alkyl chains. Specifically, the experiment assesses the ability of two non-identical

alkyl chains to compete with each other for the impinging gas phase hydroxyl radical. The increased reactivity of singly oxidized chains is evaluated by the oxidation of a gemini surfactant parent with identical alkyl chains. Chapter 4 investigates the oxidation of α,ω-surfactants, those that contain polar functional group separated by methylene spacers, discussing deviations of this class of surfactants with those that contain only one head group (i.e. DTA^+). Chapter 5 demonstrates the DBDS and FIDI-MS system for use as a peptide footprinting technique for the amphiphilic species substance P. Localization of the site of oxidation can be done through FIDI-MS/MS analysis.

PUBLISHED CONTENT AND CONTRIBUTIONS

Chapter 2 is based on the manuscript in preparation:

Barraza, K. M. and Beauchamp, J.L. (2017). "Hydroxyl radical-mediated stepwise Oxidation of the hydrocarbon surfactant dodecyltrimethylammonium ion at the air-water interface." [under preparation]

K. M. B. was the lead researcher and main author of the manuscript.

Chapter 3 is based on:

Barraza, K. M.; Lee, H.; Kim, H.; and Beauchamp, J. L. (2017). "Elucidation of chain competition effects in the hydroxyl radical-mediated oxidation of gemini surfactants at the air-water interface." [under preparation]

K. M. B. was the lead experimental researcher and main author of the manuscript.

Chapter 4 is based on:

Barraza, K. M. and Beauchamp, J. L. (2017). "Heterogeneous OH-mediated oxidation is constrained by restricted motion of looped hydrocarbon chains formed by α, ω-diionic surfactants at the air-water interface." [under preparation]

K. M. B was the lead researcher and main author of the manuscript.

Chapter 5 is based on:

Barraza, K. M. and Beauchamp, J. L. (2017). "Heterogeneous hydroxyl radical-mediated oxidation of the amphiphilic peptide substance P as a footprinting technique." [under preparation]

K. M. B. was the lead researcher and main author of the manuscript.

TABLE OF CONTENTS

LIST OF FIGURES

LIST OF SCHEMES

NOMENCLATURE

OH: Hydroxyl Radical

VOC: Volatile Organic Compound

FIDI-MS: Field-Induced Droplet Ionization Mass Spectrometry

CID: Collision-Induced Dissociation

DBDS: Dielectric Barrier Discharge Source

SOA: Secondary Organic Aerosol

DTA^{+}: Dodecyltrimethylammonium

DM^{2+}: Decamethonium

DAD: 1,12-diaminododecane

H_2TD: Tetradecanedioic Acid

SP: Substance P

Chapter 1

INTRODUCTION

1.1 Background

1.1.1 Air-Water Interfaces – A Frontier in Atmospheric Heterogeneous Chemistry

The atmosphere provides the perfect backdrop for complex chemistry to occur, particularly because volatile organic compounds (VOCs) are continuously emitted from biogenic and anthropogenic sources.[1-12] One of the most important processes that govern the lifetime of VOCs is the oxidative processing of organic species by gas phase oxidants. Reactions between oxidants and VOCs producing highly functionalized and fragmented products of sufficiently low volatility can associate to form nanometer to micrometer-sized solid and semi-liquid particulates known as secondary organic aerosols, which have a large-scale impact on the global climate and human health.[9, 11, 13-16] The hydroxyl radical (OH) represents a dominant oxidant in daytime atmospheric chemistry, and can initiate degradation of a wide variety of compounds to produce the precursors to secondary organic aerosols.[13, 15, 17-30] Present in the troposphere at concentrations of approximately 10^6 molecules/cm^3, [31] OH is produced in two-steps by the photolysis of ozone at wavelengths near 300 nm by solar radiation to produce singlet oxygen $O(^1D)$, followed by a reaction with water ($O(^1D) + H_2O \rightarrow 2OH$).[18, 32] These hydroxyl radicals represent a major gas phase VOC sink. [11, 13-16] In addition, SOAs are a major source of potential reactivity for the hydroxyl radicals, as their surfaces are rich in hydrocarbon groups vulnerable to hydrogen abstraction

by the OH, initiating the process to age them (i.e. functionalize them with oxygen groups).[16, 33-43] In the case of OH-initiated oxidation of aerosols, heterogeneous chemistry, that is, chemistry occurring at the interphase of two distinct phases, has a remarkable impact on observed chemical changes.[44-47] The hydroxyl radical has a high affinity for accommodating on both particulate and aqueous surfaces.[48-51] Heterogeneous OH oxidation experiments have long been found to illuminate the chemical changes of organic particulates and aerosols.[24, 40-41, 50, 52-64] This includes the identification of ketone, alcohol, carboxylic acid, and even transient radical products in numerous low-volatility organic systems.[22, 41, 45, 47, 56-57, 60-61, 65]

This thesis presents work meant to compliment what is already known about the heterogeneous chemistry of OH at the air-water interface with hydrocarbon surfactants by utilizing field-induced droplet ionization mass spectrometry (FIDI-MS) coupled with a novel dielectric barrier discharge source for producing hydroxyl radicals at ambient atmospheric conditions. The system is designed to form millimeter-sized droplets containing a monolayer of surfactant and can be coupled to reactive gas sources for controlled gas-liquid heterogeneous chemistry, elucidating mechanistic, kinetic, and structural details on several systems.[24, 66-70] Here the FIDI-MS/DBDS technique has provided a similar breadth of detail on several pertinent atmospherically-relevant hydrocarbon surfactant system. A potential protein footprinting application of setup is also presented.

1.1.2 Overview of Previous Methods for Generating Gas Phase Hydroxyl Radicals

One of the challenges in studying hydroxyl radical (OH) chemistry under ambient atmospheric conditions is the generation of such a reactive short-lived species. However, reactions of hydroxyl radicals span important topics in biology, industry, and atmospheric

science. Because of these diverse systems in which the hydroxyl radical have played a role, numerous methods to generate hydroxyl radicals have been developed.

The transient nature of the OH radical requires that its production occur *in situ* from a reactive precursor. Ozone is a commonly employed in OH oxidation studies by reacting it with a low molecular weight alkene (e.g. 2,3-dimethylbut-2-ene).[35, 53-54] Such methods have been used to study the degradation of pesticides[54] and the aging of secondary organic aerosols (SOAs)[35, 53] in the absence of UV irradiation, which may convolute the results. Such methods can produce OH at 10^6 molecules/cm^{-3}.[53] Coproducts can also be produced through this method, which can include CO, CO_2, and formaldehyde. The detriment of producing such species in the experimental setup may preclude the use of this generation method.

Photolytic gas phase OH production methods allow precise control of the exposure concentrations. Pulse-photolysis particularly allows for controlled gas phase reaction. Methods can either produce OH directly or indirectly. Direct OH production can be achieved by the photolysis low concentration (5 – 20 ppmv) hydrogen peroxide at 254 nm.[21] Indirect methods involve the photolytic production of a precursor that then reacts to form OH. For example, ozone is photolyzed by 185 nm light to produce singlet oxygen $O(^1D)$, which then reacts with water to form OH.[34, 40, 45] Nitrous oxide (N_2O) has been used as a similar reagent, where photolysis at 193 nm produces $O(^1D)$ and N_2.[25] The organic precursor methyl nitrite (CH_3ONO) has also been used as an OH precursor in atmospheric systems.[26] Irradiation using 360 nm light produces the methoxyl radical (CH_3O) and nitric oxide (NO). The methoxyl radical reacts with oxygen to produce formaldehyde and HO_2, while NO reacts with the HO_2 to produce NO_2 and OH. While these photolytic methods provide an efficient

means to produce gas phase OH, depending on the reactive target of the OH, the UV light may prove to be a competitive source of reactive initiation, or cause uncertainty in the results by the introduction of byproducts and highly reactive intermediates.

Plasma discharges are another method for producing gas phase OH radicals. Similar to photolytic methods, the process requires first energizing a reagent species by exposing it to the plasma, after which it proceeds through one or more subsequent gas phase reactions. For example, passing a flow of H_2/He through a high frequency plasma produces H atoms. The H atoms are carried into a tube filled with O_2 to produce HO_2, which then reacts with another H atom to form two hydroxyl radcials.[50] Radical probe mass spectrometry[71] modifies the electrospray ionization (ESI) technique to produce hydroxyl radicals. A sheath gas of oxygen is used and the voltage bias on the high voltage needle of the ESI source is increased such that a discharge is produced during operation. Within this discharge oxygen is ionized to produce O_2^+ and then reacts with water through a series of reactions to produce OH. In non-ambient studies beams of hydroxyl radicals are produced by passing a mixture of hydrogen peroxide/water through a corona discharge.[64] The resulting beam of OH, unreacted species, and other ions pass through a hexapole filter, which then selects for OH radicals as it passes through the setup. However, hydroxyl radicals produced through discharge methods may produce unwanted excited state species which may be different from the ground state hydroxyl radical chemistry.

We have developed a new electrical discharge methodology that produces hydroxyl radicals under ambient conditions using solely water as the reagent. While aqueous OH radical has been produced by the radiolysis hydrogen peroxide[72-77] and water,[78-81] the content

of this thesis displays the development and utilization of producing OH radicals in the gas phase directly from water vapor. This method not only benefits from simple reagents (a humid helium gas flow), but also limits the amount of byproducts produced or possible contamination of unreacted reagents that may complicate the chemistry of heterogeneous systems.

1.1.3 Dielectric Barrier Discharge as a Useful Means to Generate Hydroxyl Radicals under Ambient Conditions

Electrical discharges have long been used as a means to generate high energy gas phase species such as electrons, metastable excited state species, and radicals.[82-85] Dielectric barrier discharge (DBD) differentiates itself from other discharge methods as it is considered a cold, non-equilibrium plasma. The designation originates from the property of DBD to produce high energy electrons, while keeping the energy of the bulk carrier gas relatively unchanged, evidenced by the low temperature of the plasma. In this regard a DBD is capable of converting more than 99% of the electrical energy into the production of high energy electrons, rather than heating the bulk gas.[86]

While the exact geometry of a setup can vary, the DBD plasma is achieved by placing a dielectric material between two electrodes.[87-88] During operation, one of the electrodes is grounded while a high voltage AC bias is applied to the other. The dielectric material placed between the electrode surface acts as a current limiter, preventing typical equilibrium plasma generation. In order to sustain DBD the applied high voltage to the electrodes must be vary with time so as to prevent charges to accumulate on the dielectric material's surface. For this reason, unlike typical plasma generators, common DBDs require AC power supplies.[86, 89]

The DBD produces as a series of microdischarges typically of 0.1mm in radius in the discharge gap. Electron avalanches produced by the voltage reach a critical point via space charging in the fronts and allow for the microdischarge formation. Only existing for 1 to 10ns, these discharges create a peak current of 100 mA and currents densities of 10^6 to 10^7 A-m^{-2} in a 1mm discharge gap. The total charge ranges between 10^{-10} and 10^{-9} C with electron densities of 10^{20} to 10^{21} m^3. While electrons produced via DBD have energies from 1 – 10 eV the temperature remains unchanged (For comparison, thermal energy at room temperature is roughly 0.03eV).[89]

Mechanistically, the dielectric barrier discharge (DBD) proceeds via four phases. The first is the Townsend phase – a breakdown in the discharge gap occurs when the electric field between electrodes is high enough to sustain an avalanche event. This causes streamers to form conducting channels (i.e. filaments). Charges flow through the channel and deposit on a dielectric surface. Finally, once the voltage across the filament is equalized the discharge dies out. The entire process occurs on the order of nanoseconds. Though the voltage across the gap is close to zero when the discharge extinguishes, the residual conduction channels become sites of preferred initiation of new microdischarges so long as the applied voltage varies with time. Thus with an AC power source, the DBD can be sustained.

The elementary collision processes in plasmas involve the neutral gas molecules in excited and ground states, electrons, positive ions, and negative ions. The electric field directly accelerates electrons rather than atoms, due to their low mass and high mobility. Because of this, it is the electron-impact excitation and ionization processes that are key in understanding the changes in the plasma. Inelastic collisions are the main source of reducing

the mean energy of these electrons. The electron-impact event is crucial because it can produce all excited states of an atom via optically allowed, optically forbidden, and spin-forbidden processes; it can also populate long-lived metastable atomic states, which can further take part in secondary collision processes.[86]

Recently, a relatively new ambient ionization source harnessing dielectric barrier discharge has been studied. Known as Dielectric Barrier Discharge Ionization (DBDI), this processes involves producing low-temperature plasma between two electrodes separated by a dielectric material. When an alternating voltage is applied between the electrodes the electrical discharge is created, capable of ionizing material on the surface of the dielectric material. The product ions can then be directed into a mass spectrometer, suggesting a new class of ambient ionization. This method of ionization was characterized by Na et. al.[90] They conclude that this method of ambient ionization has the advantage of being relatively simplistic in terms of both design and reagents relative to alternative methods such as Direct Analysis in Real Time (DART) and Desorption Electrospray Ionization (DESI). The same group also showed DBDI is capable of detecting explosives at otherwise undetectable levels.[91] The low-temperature plasma ionization techniques have been found to be useful in ionizing analytes of human skin samples *in vivo*,[87] as well as detecting drugs in urine, saliva, and hair,[91] and to image ink pigments from works of art.[92]

The DBD technique has been adapted to produce hydroxyl radicals under ambient conditions for various applications.[93-95] Because the discharge generated produces high-energy electrons at low temperature, the proposed mechanism of producing radicals occurs via electron capture reaction directly ($e^- + H_2O \rightarrow H^- + OH$), or a two-step reaction initiated

by an electron-impact ionization reaction ($e^- + H_2O \rightarrow H_2O^+ + 2e^-$) followed by a reaction of the H_2O^+ cation with water ($H_2O^+ + H_2O \rightarrow H_3O^+ + OH$).

Studies of radical oxidation have used corona discharges in a similar manner to DBD to generate hydroxyl radicals.[64] The method of electrical discharge may create vibrationally excited products, and examination of the LIF spectra of corona discharge-generated OH revealed a high vibrational temperature T_{vib} of 3400 ± 100 K. Other measurements determined the vibrational temperature to be 1700 K.[96] The relative quantities of OH radicals in the $\upsilon = 1$ and $\upsilon = 0$ in the limits of 1700 K $\leq T_{vib} \leq$ 3400 K are calculated using the formula:[64]

$$\frac{n(\upsilon = 1)}{n(\upsilon = 0)} = \exp\left(\frac{-3566 cm^{-1}}{k_B T_{vib}}\right) \tag{1.1}$$

The subsequent amounts are 5 – 22% OH radicals in the $\upsilon = 1$ state, and 95 – 78% in the $\upsilon = 0$ state.

However, the above was calculated assuming there are no collisions among molecules. In the case of the DBD discharge, ambient pressures are used and it can be estimated that the mean-free path under these conditions is approximately 300nm. Probabilistically, a collision with a non-reactive buffer gas (e.g. helium) will stabilize the hydroxyl radical before it reaches the outlet of the glass DBD chamber.

1.2 Content of Thesis

1.2.1 Stepwise Oxidation of a Linear Alkyl Surfactant at the Air-Water Interface

A surge of interest in hydroxyl radical (OH) chemistry has arisen in the field of atmospheric science over the decades as OH-mediated oxidation has been identified as the primary sink of hydrocarbons in the atmosphere. Gas phase studies have shed light on the details of the oxidation process for various organic compounds. However, organics and the hydroxyl radical have a significant affinity to accommodate to air-water interfaces. While such interfaces are prevalent in the atmosphere in the form of cloud droplets, fog, mist, and aerosols, the challenge of creating OH at ambient conditions and sampling the air-water interface effectively while excluding components of the bulk aqueous phase has precluded the same level of analysis that has been seen for gas phase systems. In Chapter 2 we implement field-induced droplet ionization mass spectrometry (FIDI-MS) to sample from millimeter-sized water droplets with adsorbed dodecyltrimethylammonium (DTA^+) as a charged, surface-active species with a long hydrocarbon chain. Gas phase hydroxyl radicals are generated within a dielectric barrier discharge source (DBDS) and are flowed over the droplet, allowing for controlled oxidation of the DTA^+ present on the droplet's surface. Sampling the water droplet after OH exposure via FIDI-MS provides a means to characterize the initial products of the heterogeneous oxidation of DTA^+. Varying exposure lengths elucidates the product evolution over the course of oxidation, and can be traced to known mechanisms of OH chemistry. The time-resolved data is used to deduce the kinetics of the system.

1.2.2 Comparative Hydroxyl Radical-Mediated Oxidation of Fraternal and Identical Hydrocarbon Groups in Gemini Surfactants

Hydrocarbon surfactant monolayers formed at air-water interfaces are ubiquitous in aerosols and lipid membrane systems. The hydrocarbon moieties present themselves into the gas phase and are therefore the first targets for oxidants such as OH. The heterogeneous chemistry of monolayers of hydrocarbon surfactants has subsequently been the focus of much study. However, questions still remain on how relatively closely spaced neighbor alkyl chains (as are found in lipid systems where they are tethered together by the head group) impact each other's relative reactivity with the hydroxyl radical. Chapter 3 investigates neighbor chain competition in the heterogeneous oxidation of bis-quaternary ammonium gemini surfactants (general formula: $(C_nH_{[2n-1]})N^+(CH_3)_2(C_sH_{2s})N^+(CH_3)_2(C_mH_{[2m-1]})$, abbreviated n-s-m), at the air-water interface using the DBDS for OH generation and FIDI-MS for interface sampling. Two gemini surfactants were designed and synthesized to address two important questions concerning inter-chain competition. First, a monolayer of dissymmetric gemini (DG) with chain lengths 16-4-12 is oxidized by gas phase OH to determine to what extent a longer alkyl group at the air-water interface outcompete its shorter chain neighbor. Second, a symmetric gemini (SG) system of chain lengths 16-4-16 is heterogeneously oxidized until a considerable amount of oxidation product containing two oxygen atoms is present. FIDI-MS/MS analysis is used to determine to what extent the first functionalization on one of the chains of the SG changes the susceptibility of this chain to oxidation relative to its neighbor. The results are then compared to molecular simulations describing each surfactant system.

1.2.3 The Heterogeneous Oxidation of α,ω-Surfactants: The Influence of Hydrocarbon Conformation at the Air-Water Interface on Oxidation Pathways

Secondary organic aerosols (SOAs) are often composed of α,ω-surfactants, those that carry polar head groups separated by a hydrophobic interior of methylene units. For example, unsaturated fatty acids are an important precursor to dicarboxylic acids found in SOAs. Similarly, amines are commonly found in boreal forest and marine environments, with diamine species being suggested as an important part of particulate formation in those climates. Chapter 4 discusses the oxidative fate of a model α,ω-surfactant, the decamethonium ion at the air-water interface via hydroxyl radical-mediated oxidation. Field induced-droplet ionization mass spectrometry (FIDI-MS) coupled with the dielectric barrier discharge source (DBDS) is utilized to analyze the oxidative pathways of the decamethonium system, based on known OH chemistry. The observed chemistry of decamethonium is directly compared to the DTA^+ system studied in Chapter 2 by exposing a droplet containing an equimolar mixture of the two species to OH. To assess the possibility that head group interactions are responsible for the observed chemistry, α,ω-surfactants containing carboxylic acid head groups and amine head groups are also oxidized.

1.2.4 Heterogeneous Hydroxyl Radical-Mediated Oxidation of the Amphiphilic Peptide Substance P as a Footprinting Technique

The need to characterize the properties of both natural and synthetic proteins and peptides has become crucial as this class of biomolecules is seriously considered for novel materials or biomedical applications. Oxidative footprinting represents one technique used to determine structural information of a protein by chemically modifying the protein's residues

and determining the locations of the chemical changes by mass spectrometry. Several radiolysis or catalytic methodologies have been developed to generate a controlled amount of oxidant in solution, and residues in contact with the aqueous phase are modified. Conventional oxidative footprinting elucidates the sites of the most solvent-accessible residues. Chapter 5 presents the application of the coupled DBDS and FIDI-MS setup as a novel peptide footprinting technique to determine the gas phase-accessible residues of a surface active peptide substance P. Heterogeneous reaction of OH with a monolayer of substance P determines gas-accessible residues of peptides and acts as a complimentary footprinting technique for systems in which a surface active peptide adopts a unique conformation at the air-water interface.

Chapter 2

Hydroxyl Radical-Mediated Stepwise Oxidation of the Hydrocarbon Surfactant Dodecyltrimethylammonium Ion at the Air-Water Interface

2.1 Abstract

A dielectric barrier discharge source (DBDS) producing a concentration of hydroxyl radicals of 2 x 10^9 molecules/cm^3 coupled with Field-Induced Droplet Ionization Mass Spectrometry (FIDI-MS) has been developed to monitor the stepwise hydroxyl radical-mediated oxidation of a hydrocarbon surfactant dodecyltrimethylammonium (DTA^+) ion at the air-water interface of a 1.6 mm diameter droplet under ambient atmospheric temperature and pressure. The step-wise conversion of 92% of the nascent DTA^+ to oxidation products occurs in 60 sec, resulting in the formation of carbonyl, hydroxyl, and peroxyl-containing species. Structural assignments are supported by collision-induced dissociation (CID) and H/D exchange experiments, the latter conducted with D_2O droplets. The low ratio of hydroxyl to carbonyl functionalization in the alkyl chain suggests the Russell mechanism commonly described in the hydroxyl radical-mediated oxidation of other systems is not operative. Rather, the carbonyl and peroxyl-forming pathways, as well as radical site migration pathways, play an important role in the evolution of products. Low mass products were identified as a series of aldehydes produced from beta cleavage of a C–C bond, and their relative intensities suggest that the hydroxyl radicals react preferentially with the methylene groups near the methyl terminus of the alkyl chain. Detailed analysis of the kinetics of oxidation suggests the hydroxyl radical is accommodated on and has a significant

diffusion period in the interfacial layer, rather than reacting with the most accessible and previously oxidized species first, implicating Langmuir-Hinshelwood reaction kinetics. Exchange of unreacted subsurface excess surfactant products occurs on a 1 minute timescale.

2.2 Introduction

Volatile organic compounds (VOCs) are released into the atmosphere from both biogenic sources[10, 12] as well as anthropogenic sources such as the burning of fossil fuels.[1-2] The organic aerosols formed from VOCs in the atmosphere have far-reaching effects on visibility, health, cloud formation, and reactive pathways of atmospheric species.[11, 13-14] Of all the degradation processes for saturated VOCs (e.g. alkanes) in the atmosphere, hydroxyl radical (OH)-mediated oxidation reactions account for greater than 90% of their loss in the troposphere, and constitute their major loss pathway in the stratosphere, forming secondary organic aerosols (SOAs).[11, 13-16] The reactivity of OH toward VOCs is dominant over other gas phase radical species such as ozone (O_3) and nitrate radical (NO_3), even in the presence of NO_x.[9] In both rural and urban locations oxidized organic aerosols are found to constitute the majority oxidized aerosol composition, comprising 64% to 95% of total organic aerosols.[38] Furthermore, the properties of oxidized organic aerosols (such as volatility, oxidation state, density, and cloud droplet nucleation activity) can vary widely based on oxygen-carbon ratios over the course of oxidative aging.[37-38, 40, 53]

The majority of VOCs are hydrophobic or slightly amphiphilic, either as nascent VOCs (e.g. oleic acid) or as partially oxidized species containing heteroatoms (O, N, S functionalities),[4, 47] and show a thermodynamic drive to adsorb and remain on air-water interfaces (e.g. fog, rain, and cloud droplets) rather than diffuse into to a bulk aqueous

environment.[97] In addition, the OH radical has been shown to have an affinity for adsorbing to air-water interfaces where it can react with other adsorbed organic species.[48-49] In collected droplets in polluted urban environments, oxidized hydrocarbons and OH are found in substantially higher concentrations in atmospheric water droplets,[98] indicating that OH-mediated oxidation of VOCs is facilitated in aqueous droplet systems. Thus, a major question in atmospheric chemistry is understanding the initial heterogeneous OH-mediated oxidation pathways occurring for surface active hydrocarbon species, particularly at air-water interfaces.

Several reactor flow tube studies have investigated the heterogeneous reactions of OH and organic solid particulates under conditions mimicking atmospheric conditions.[20, 22, 41, 50-52, 54, 56-58, 65] From these studies it was found that the heterogeneous reaction of OH radicals with particulates occurs efficiently, quantified with uptake coefficients ranging from 0.51± 0.10 to values as high as 1.3 ± 0.4.[51, 65] However, the uptake coefficient is dependent on the surface, with organic coatings of varying thickness increasing the uptake coefficient.[56] The subsequent heterogeneous chemistry between the adsorbed VOCs and gas phase OH radical can be slowed drastically relative to the homogeneous gas phase chemistry,[52] implicating the air-water interface as a chemically unique system.

Mass spectrometry analysis of OH-oxidized VOC solid particulates show that higher mass species comprise multi-functionalized oxygenated species, which include ketones, aldehydes, alcohols, and carboxylic acids for the gas-particulate interface.[22, 41, 45, 47, 56-57, 65] Under highly oxidizing conditions evidence of fragmentation of VOCs is seen via the detection of lower molecular weight species including carboxylic acids of varying chain

length, methanol, acetaldehyde, formic acid, and acetic acid.[22, 36, 47, 50, 62, 65] Furthermore, structural features of the surface species impact the exact nature of the observed products, with fragmentation and alcohol products favored for particles coated with branched alkanes and carbonyl products in higher abundance for linear alkane precursor species.[22] Physical properties of the solid particulates and liquid microdroplets, such as hygroscopicity, surface tension, cloud condensation nucleation activity, and particle size have been found to be impacted by OH exposure.[40, 58, 65]

For heterogeneous chemistry occurring at air-liquid interfaces, theoretical studies have found that the local solvent environment has a tremendous impact on the hydrogen abstraction event with an organic species, with aprotic environments inhibiting hydrogen abstraction from the hydrocarbon by OH due to their inability to stabilize the transition state via hydrogen bonding.[99] Studies at the air-water interfaces with OH radicals have shown that short exposures produce an array of oxygenated products and fragmentation products including carbonyls, alcohols, peroxides, and carboxylic acids.[60-61] These studies used aqueous microjets containing an organic species and exposure to OH produced via laser flash photolysis of $O_3/O_2/H_2O$ mixtures over an exposure time of nanoseconds, monitoring the composition changes using electrospray ionization mass spectrometry (ESI-MS). By limiting the OH exposure period of these microdroplets to that of the electrospray ionization event, transient peroxyl radical species were detected.[61] While the initial products of heterogeneous OH chemistry were detected with this method, the sequential reactions of a monolayer of a hydrocarbon surfactant have not been monitored over the course of nearly complete oxidative processing. While the controlled exposure of surfactant monolayers to gas phase

OH at ambient conditions in combination with temporally well-defined product sampling and analysis has been viewed as a challenge to atmospheric chemists, it remains an important goal in the understanding of reactions of OH with amphiphilic species at the air-water interface.

The general mechanism of the hydroxyl radical-mediated oxidation of alkyl-containing organic compounds in ambient air is shown in **Scheme 2.1** and is based on known gas phase and known heterogeneous OH oxidation pathways.[13, 17, 25, 39, 60-61, 100-104] The process is initiated via abstraction of a hydrogen atom from the hydrocarbon by OH (reaction [1]), followed by the addition of oxygen to form the peroxyl radical (reaction [2]). This peroxyl radical can convert to the subsequent peroxide according to reaction [3] by ambient HO_2, which is 100 times more abundant than ambient OH.[31] However, the formation of the tetroxide intermediate by the reaction of two alkyl peroxyl radicasl via reaction [4] presents an alternative pathway, and is found to be nearly diffusion-limited in solution.[100] This intermediate can decompose in a number of ways. According to the Russell mechanism, decomposition of the intermediate to an alcohol, carbonyl, and oxygen occurs via a six-membered intermediate (reaction [5]).[102] The Bennett-Summers mechanism (reaction [6]) converts the tetroxide intermediate to two carbonyls and hydrogen peroxide via a bicyclic intermediate, and is often invoked in low-temperature systems.[100-101] Finally, the loss of oxygen from the tetroxide intermediate produces two alkoxyl radicals (reaction [7]). However, in the presence of NO, which is present at concentrations around 10 ppbv in ambient city air,[105] the alkoxyl radical can be formed from the addition of NO to the peroxyl radical, followed by the loss of NO_2 (reaction [8]). In aqueous environments, water catalyzed

a 1,2-hydrogen shift produces the more stable α-hydroxyalkyl radical on the microsecond timescale, which then reacts with oxygen to form the carbonyl (reaction [9a]).[60, 106-107] In the gas phase, unimolecular rearrangement to form the α -hydroxylalkyl radical is considered less favorable under atmospheric conditions,[108] and formation of the carbonyl likely occurs by direct reaction of O_2 to form a trioxy intermediate, followed by the release of HO_2 to form the carbonyl (reaction [9b]).[27] For primary and secondary alkoxyl radicals, this process occurs quickly relative to the scission of the β C–C bond[13] (reaction [10]) to generate an aldehyde and a new alkyl radical. Reaction [11] generates an alcohol via a hydrogen abstraction event. Radical termination may occur via the dimerization of two alkoxyl radicals to form an organic peroxide (reaction [12]). Finally, alkoxyl radicals formed from long chain alkyl species undergo not only the intramolecular 1,2-hydrogen shift, but also the 1,5-hydrogen shift via a six-membered transition state (reaction [13]), forming an alcohol and a new radical site capable of further reaction.[103] This radical site migration gains importance as the number of carbon atoms in the alkyl chain increases.[19] In the present study the reaction pathways illustrated in Scheme 1 form the basis for interpreting the OH-mediated oxidation of the dodecyltrimethylammonium ion at the air-water interface.

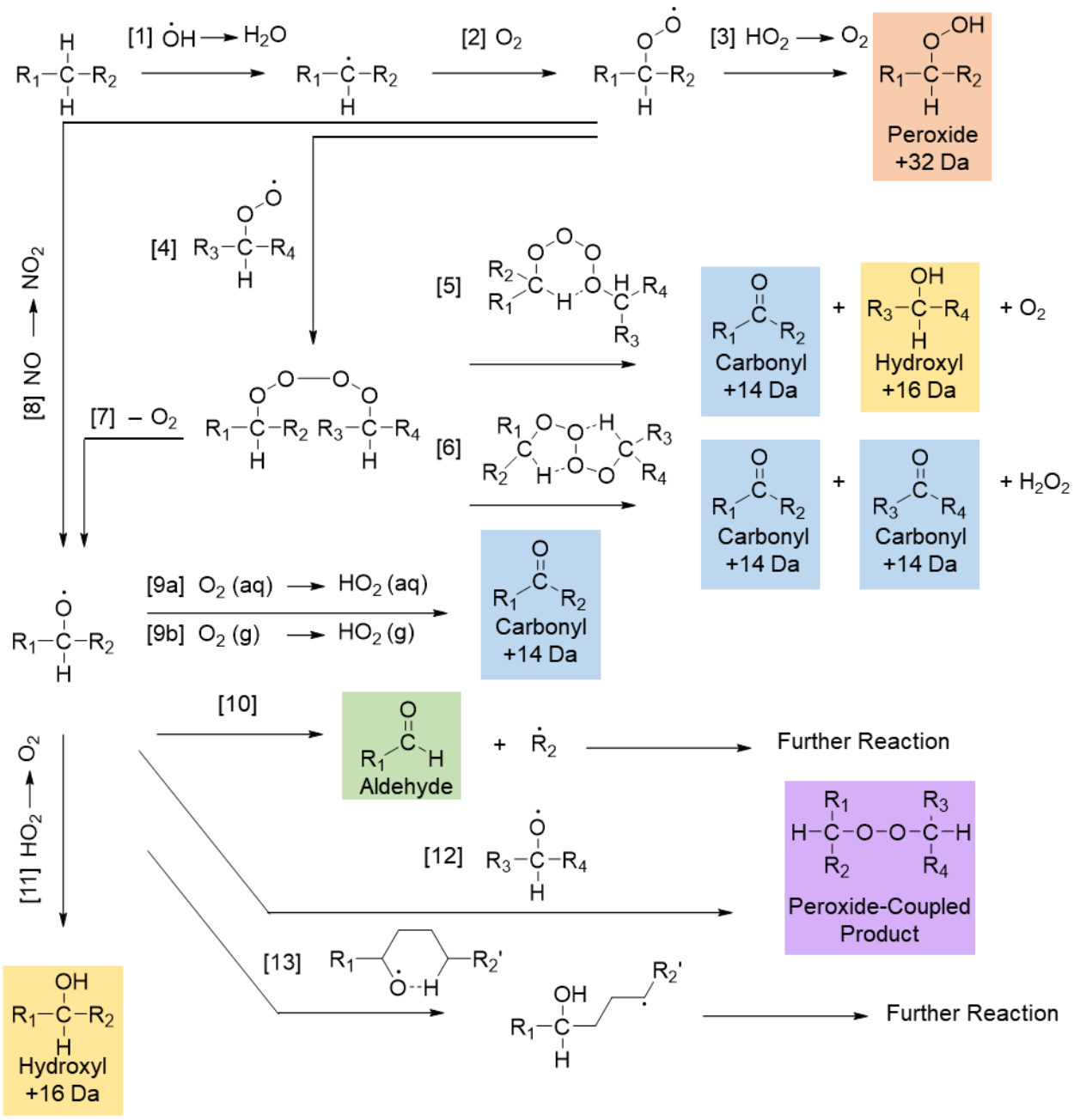

Scheme 2.1. Known mechanisms of hydroxyl radical-mediated oxidation of a hydrocarbon.

The air-water interface presents a unique and relatively unexplored environment of heterogeneous OH chemistry. In the gas phase all interactions are sequential, binary encounters. Activated intermediates retain excitation, leading to further unimolecular

rearrangement and dissociation. In aqueous environments, intermediates are thermalized by collisions with the solvent, removing internal energy that would favor unimolecular rearrangement and dissociation. Because reactants are solvated, the aqueous phase reactions are diffusion-controlled. The air-water interface exemplifies a hybrid of the two regimes. The surfactant's hydrophobic domain protrudes into the gas phase, where it interacts with incident OH. However, the hydrophilic head group extends into the aqueous phase, providing a means to thermalize species during the oxidative processing.

In the present study we use the technique of Field-Induced Droplet Ionization-Mass Spectrometry (FIDI-MS) coupled with a dielectric barrier discharge hydroxyl radical generator that operates at ambient atmospheric conditions. FIDI-MS is a surface selective technique to sample from aqueous droplets,[24, 66-70] while the ambient OH generator passes water-saturated helium through a dielectric barrier plasma discharge to produce OH. In the present study these combined experimental methodologies are employed to examine the stepwise heterogeneous reactions of OH with the hydrocarbon surfactant dodecyltrimethylammonium ion (DTA^+) at an aqueous surface. The temporal evolution of the various oxidation products are monitored over time until depletion of the parent species at the surface is nearly complete. Despite the simplicity of a single unbranched saturated alkyl chain, over 100 oxidation products are observed in less than one minute of OH exposure.

2.3 Materials and Methods

2.3.1 Materials

Dodecyltrimethylammonium bromide (DTA^+ bromide) was purchased from Aldrich Chemical Company, Inc. and used as is. Solutions were made using HPLC grade water (OmniSolv). Deuterium oxide (D_2O) was purchased from Cambridge Isotope Laboratories (99.9% purity) and used as is. Stock solutions were prepared at 1 mM concentrations and stored at 25 °C and diluted to a final concentration of 150 μM for experiments.

2.3.2 Field-Induced Droplet Ionization Mass Spectrometry (FIDI-MS)

FIDI-MS has been developed as an effective means to probe the air-water interface of hanging millimeter-sized droplets,[66-68] and has been applied to the real-time monitoring of heterogeneous chemistry of air-water interfaces.[24, 68-70] **Figure 2.1a-b** depict the important components of the FIDI apparatus in a side and top view, respectively, and all FIDI experiments are conducted with ambient conditions in laboratory air. The FIDI apparatus is mounted to an LTQ-XL mass spectrometer (Thermo-Fischer, Waltham, MA). The mass spectrometer syringe pump delivers 150 μM solution of DTA^+ bromide to a stainless steel capillary in the FIDI apparatus, forming approximately 1.6 mm diameter droplets (2.5 μL volume) exactly between two plate electrodes spaced 6.3 mm apart. This concentration ensures an excess of one monolayer for a droplet of this size, while being well below its critical micelle concentration.[109] Upon formation of the droplet, a 1 min equilibration period allows the surface active species to diffuse to the surface (See **Appendix A** for relevant calculations for a monolayer concentration and the diffusion timescale.). After this period the droplet is exposed to a flow of hydroxyl radicals in a helium carrier gas for up to 60 s. When sampling, the front plate electrode is kept at ground and a high voltage (3-5 kV) pulse

is sent to the back plate electrode. A voltage divider applies half the back plate voltage to the capillary, establishing a homogeneous electric field. This electric field induces a dipole in the droplet aligned with the electric field that culminates in the formation of two Taylor cones from opposite ends of the stretched droplet, ejecting charged progeny microdroplets of opposite polarity. One stream of the progeny droplets passes through an aperture in the grounded plate electrode where it enters the atmospheric pressure inlet of the mass spectrometer (**Figure 2.1c**). Mass spectra are collected with the settings tuned to the DTA^+ peak at m/z 228, and only one FIDI-MS spectrum is taken for the droplet at each exposure time. Since FIDI sampling causes significant fluid flow within the distorted droplet, each measurement proceeds with a fresh droplet. A total of 8 repetitions per DBDS exposure condition are performed by removing the previous droplet and forming a fresh droplet. Collision-induced dissociation (CID) spectra are obtained for the products containing 1 to 2 oxygen functional groups by adjusting the mass spectrometer settings prior to the FIDI sampling. The parameters for spectrum collection are adjusted from their default settings to an isolation width of 0.8 m/z and a collision excitation parameter of 25%. Product CID spectrum collection is repeated 5 times per isolated product.

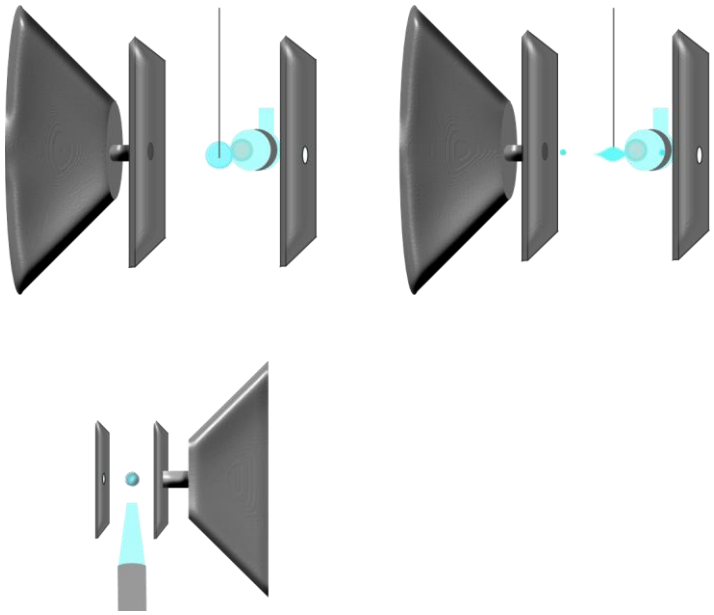

Figure 2.1. The FIDI-MS setup for surfactant oxidation experiments. a) Depiction of setup during droplet equilibration phase. 1) Stainless steel capillary; 2) Aqueous 1.6 mm diameter droplet containing surfactant; 3) Grounded plate electrode; 4) High voltage plate electrode; 5) Mass spectrometer; 6) hydroxyl radical source. b) Top view of experimental setup. c) Depiction of setup during FIDI-MS sampling. Progeny droplets containing analytes are ejected from Taylor cones and sent through the atmospheric pressure inlet of the mass spectrometer.

2.3.3 Production of Hydroxyl Radicals through the Dielectric Barrier Discharge Source (DBDS)

The dielectric barrier discharge source (DBDS) comprises a 38 mm borosilicate tube (6.45 mm O.D., 3.91 mm I.D.) with a tungsten rod (1.02 mm diameter) inner electrode, and a conductive silver epoxy outer electrode. A bubbler provides water-saturated helium through the DBDS with flow monitored by a Type πMFC Digital Mass Flow Controller (model PFC-50, MKS Instruments). A high voltage AC power supply (Trek PM04015; Trek, Inc, NY) biases the inner electrode during experiments, while the outer electrode remains grounded. A low temperature plasma is generated inside the tube, producing hydroxyl

radicals in the gas stream. Confirmation of hydroxyl radical production was evidenced two ways: 1) identification of excited state OH fluorescence ($A^2\Sigma \rightarrow X^2\Pi$ transition) in the plasma emission spectrum and 2) observing the oxidation product of a solid caffeine sample, a known hydroxyl radical scavenger,[110-112] upon desorption by the DBDS gas flow into the inlet of the mass spectrometer. From these diagnostic procedures the DBDS was optimized and installed in the FIDI apparatus with its OH outlet 5 mm from the droplet and operated at 12 kV_{pp}, 1 kHz sine waveform, 1.414 mA current, and 1000 cm^3/min He/H_2O flow. For details on the construction, characterization, and optimization of the DBDS see **Appendix B**.

2.4 Results and Discussion

2.4.1 Kinetics of Heterogeneous Oxidation of DTA^+ at the Air-Water Interface at Ambient Conditions

The FIDI mass spectra for the hydroxyl radical-mediated oxidation of DTA^+ at the air-water interface for DBDS exposures of 10 – 60 s is shown in **Figure 2.2**. Over the course of the 60 s exposure to OH, oxidized products accumulate combinations of carbonyl, hydroxyl, and peroxyl functionalizations evidenced by m/z shifts of +14, +16, and +32, respectively. Assignment of oxidation generations is based on the number of oxygen atoms incorporated into the alkyl chain, where the n^{th} generation contains n oxygen atoms. At least seven generations of DTA^+ oxidation products are observed over the course of approximately 90% conversion of the monolayer. The first generation is dominated by the m/z 242 carbonyl product, with only minor contributions from the hydroxyl product at m/z 244. This bias in

the first generation distribution toward the carbonyl functionalization remains throughout the course of the 60 s oxidation.

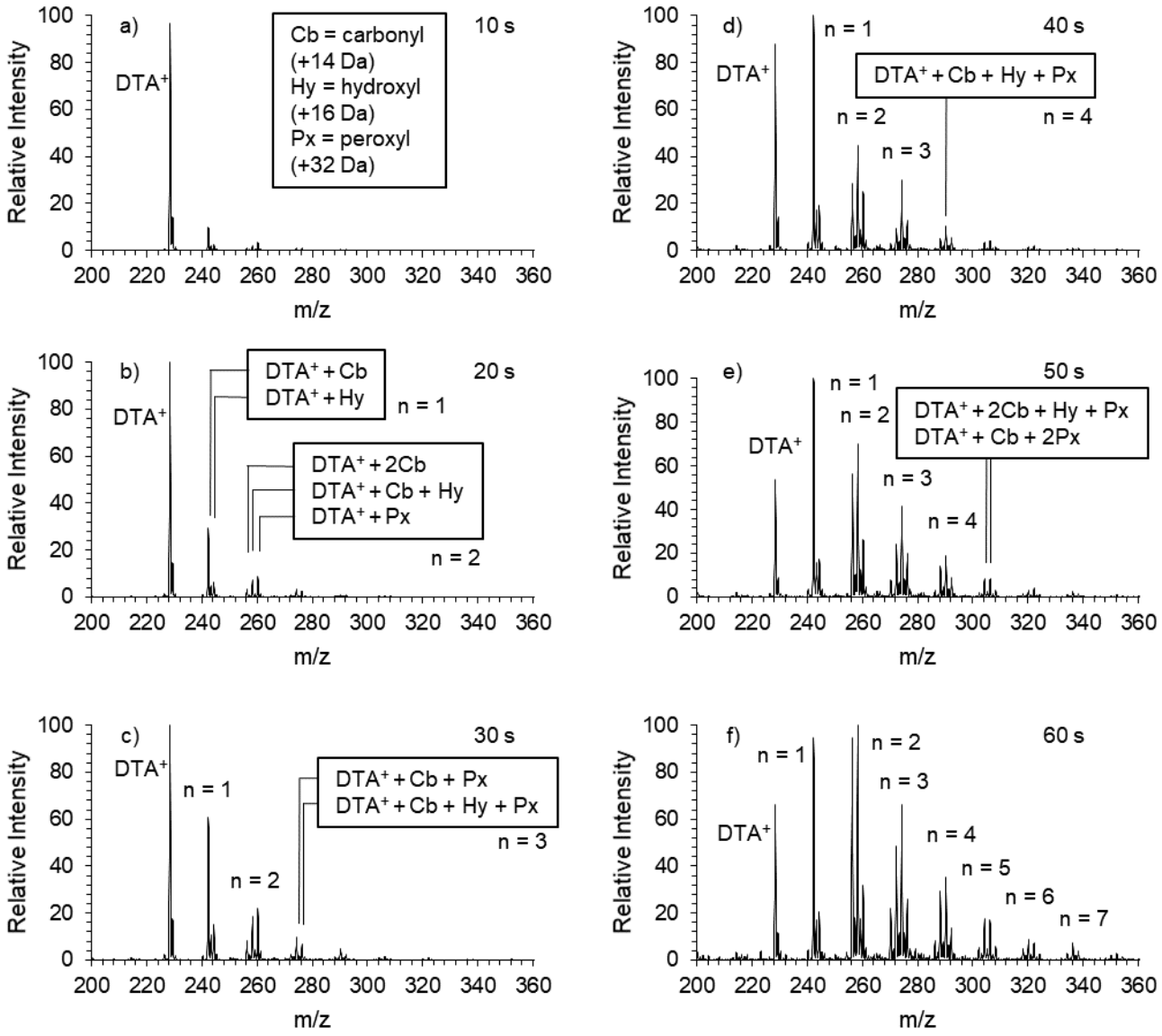

Figure 2.2. The hydroxyl radical-mediated oxidation of DTA^+ at the air-water interface monitored over 60 s. The 1st generation oxidation products are represented by the label n = 1, the 2nd by n = 2, and so forth. N = 8. a) 10 s DBDS exposure. b) 20 s DBDS exposure. c) 30 s DBDS exposure. d) 40 s DBDS exposure. e) 50 s DBDS exposure. f) 60 s DBDS exposure.

The second generation consists of m/z 256, 258, and 260, the dicarbonyl, hydroxycarbonyl, and the peroxy product, respectively. The identity of these species' functional groups is confirmed by collision-induced dissociation (CID) analysis shown in **Figure 2.3**. The CID of the first generation products (**Figure 2.3a-b)** undergo cyclization and head group loss by nucleophilic attack of the oxygen atom, resulting in the $[M - 59]^+$ species (**Scheme 2.2a**). However, the numerous distinct products in the CID spectrum of m/z 244 are attributed to the hydroxyl chemistry, including the product formed from the loss of methanol (For mechanistic details see **Scheme 2.2b**).

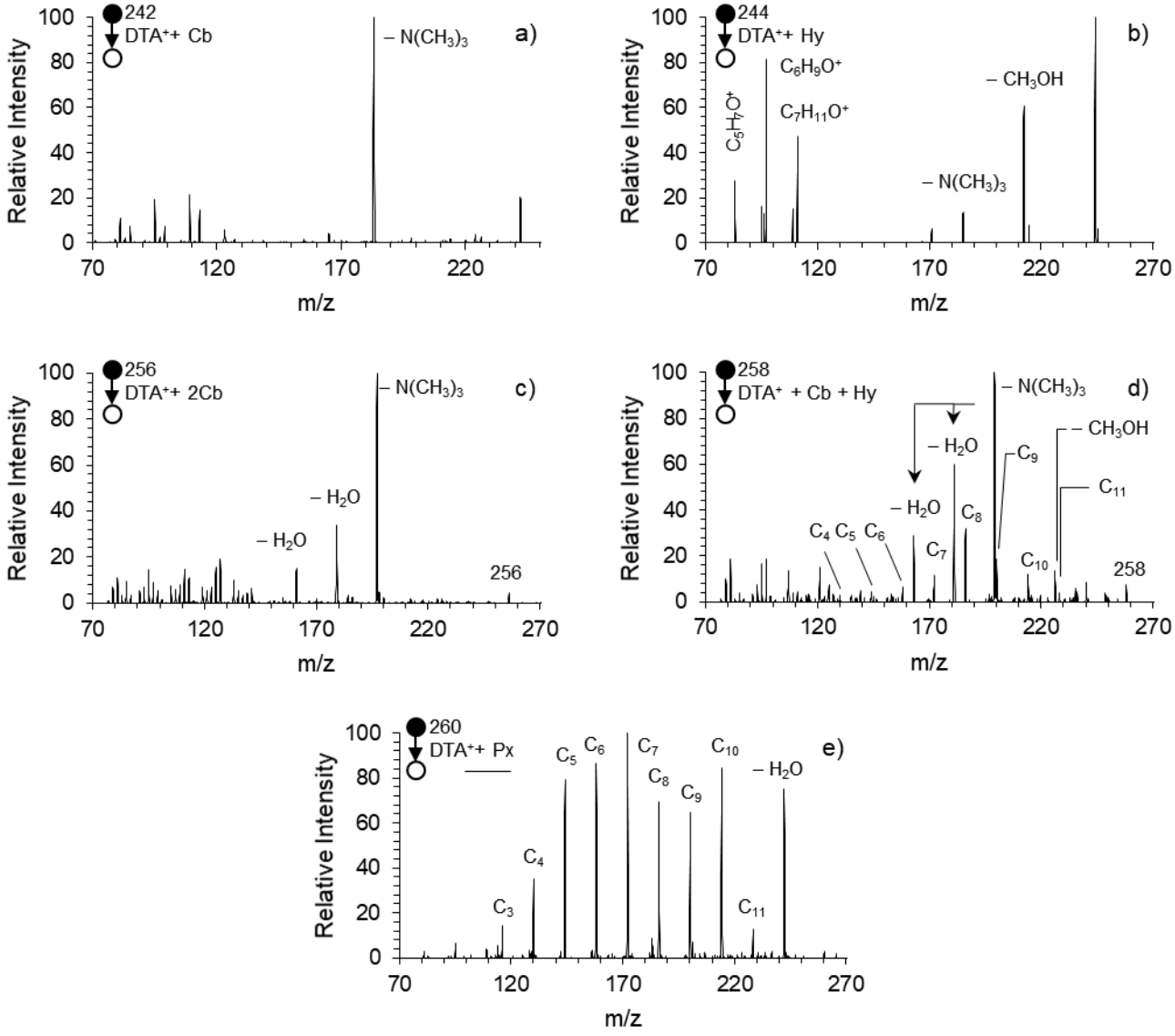

Figure 2.3. FIDI-MS collision-induced dissociation (CID) spectra of the first and second generation DTA^+ oxidation products after a 20 s DBDS exposure. N = 5. a) CID spectrum of m/z 242, the DTA^+ + Cb species. b) CID spectrum of m/z 244, the DTA^+ + Hy species. c) CID spectrum of m/z 256, the DTA^+ + 2Cb species. d) CID spectrum of m/z 258, the DTA^+ + Cb + Hy species. e) CID spectrum of m/z 260, the DTA^+ + Px species.

These spectra provided the basis for identifying the bifunctionalized second generation products. The CID spectrum of m/z 256 (**Figure 2.3c**) shows head group-loss indicative of the nucleophilic displacement caused by carbonyl groups. The CID spectrum of m/z 258 (**Figure 2.3d**) shows a combination of products found in the CID spectra of m/z 242 and 244, signifying the presence of both the carbonyl and hydroxyl functional groups, namely the cyclization process and methanol loss pathway. However, the series of products spaced by 14 mass units – m/z 228, 214, 200, 186, 172, 158, 144, and 130 – indicate a C–C bond breakage pathway not observed in the CID spectra of the singly functionalized species. The series conforms to aldehydes with chain lengths of 11 to 4 carbon atoms. While aldehyde formation is possible for the first generation products, no such series of products is observed in **Figure 2.3a** or **Figure 2.3b**, indicating that the interaction of neighboring hydroxyl and carbonyl groups is important in the generation of this aldehyde series. A proposed mechanism is shown in **Scheme 2.2c**, in which aldehyde formation occurs for the α-hydroxyketone species. Assuming this mechanism, the aldehyde product occurs at a carbon that has previously been functionalized. Therefore, for a given C_n aldehyde species it can be deduced that carbon n is the site of the carbonyl. Because the other functionalized site is lost after fragmentation, the hydroxyl group resides at the n + 1 carbon.

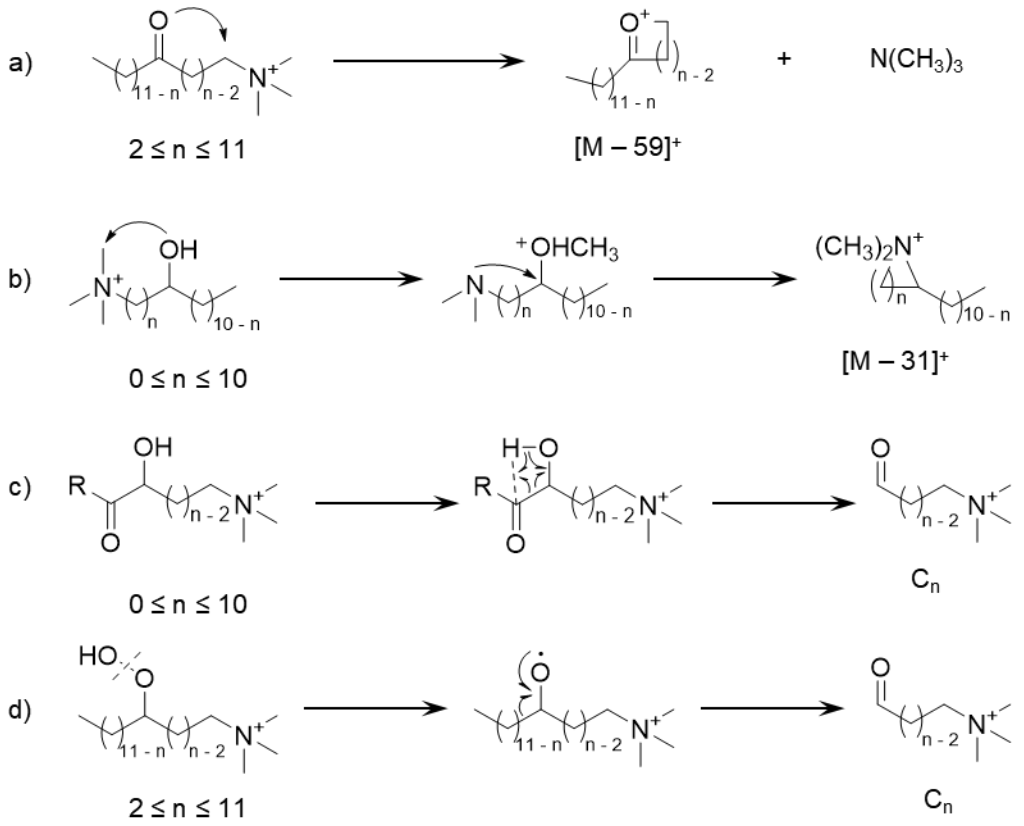

Scheme 2.2. Possible mechanisms for observed fragmentation products in CID analysis of DTA^+ oxidation products. a) Mechanism of head group loss to produce the $[M - N(CH_3)_3]^+$ product. b) Mechanism of methanol loss to produce the $[M - CH_3OH]^+$. c) Mechanism for aldehyde series formation from an α-hydroxyketone product m/z 258. d) Mechanism for aldehyde series formation from peroxide m/z 260.

It should be noted that m/z 258 also conforms to a carboxylic acid. However, the absence of characteristic water and/or decarboxylation losses suggests these species are not carboxylic acids.[113] Furthermore, gas phase rate constants suggest the terminal methyl group of DTA^+ is not likely to be the site of oxidation (the only site on the chain that can produce a carboxylic acid) in the presence of numerous more reactive methylene groups.[28, 30]

Figure 2.3e shows the CID spectrum of m/z 260, and elucidates the structural information of the species. This species, representing a mass increase of 32 Da, suggests either the incorporation of two hydroxyl groups or one peroxyl group, both of which can be formed via pathways in **Scheme 2.1**. The spectrum is dominated by the series of previously mentioned aldehyde C_n peaks, indicating that bond scission is not only favorable, but outcompetes head group loss as a fragmentation pathway in the spectrum. This type of fragmentation is commonly seen in organic peroxides,[114-115] and so suggests that the intensity of m/z 260 is dominated by the peroxide species. The weak O–O bond fragments via the mechanism in **Scheme 2.2d**. The cleavage of the peroxide O–O bond generates an alkoxyl radical. In the absence of ambient oxygen, the radical undergoes β cleavage, forming an aldehyde species. Like the CID spectrum of m/z 258 (**Figure 2.3d**), there is a significant decrease in relative intensity for C_n aldehydes with fewer than five carbon atoms.

The kinetics for the average incorporation of oxygen into the DTA^+ monolayer is shown in **Figure 2.4a**, showing significant linearity ($R^2 = 0.987$). Furthermore, the timescale for an average of one oxygen incorporated into the DTA^+ alkyl chain can be used to estimate an effective OH concentration of 2×10^9 molecules/cm^3 (See **Appendix A**). Extraction of a pseudo first-order rate constant from a fit to the decay of parent DTA^+ relative intensity ($R^2 = 0.954$), as shown in **Figure 2.4b** gives a value of $k = 0.0169\ s^{-1}$. The observed kinetic behavior implicates the oxidation of the DTA^+ monolayer occurs in a stepwise fashion:

$$DTA^+ \xrightarrow{[O]} [DTA^+ + O] \xrightarrow{[O]} [DTA^+ + 2O] \xrightarrow{[O]} \text{etc.}$$

Figure 2.4c shows the relative fractions of each generation of products over the 60 s oxidation. The population of each generation on the interface experiences a period at which

they constitute a majority on the droplet surface. Fitting the data for generation 1 to a polynomial function (R^2 = 0.9991), these species experience maximum rate of formation at 9.25 s. This population experiences a shift from net production to net degradation at 36.1 s. The data for the second generation also fits to a polynomial regression (R^2 = 0.998174), with a maximum production rate of [DTA^+ +2O] species at 31.6, and a turning point to net degradation occurring at 55.3 s.

The relative abundances of the second generation products are shown in **Figure 2.4d**, and shows unique behavior. While the relative abundance of m/z 258 remains constant, the amount of m/z 256 and 260 significantly changes. The fraction of m/z 260, shows a decrease as the other two products comprise a larger share of the second generation intensity in the mass spectra. The constant fraction of m/z 258 suggests that the reactivity of this species is elevated relative to the dicarbonyl species, resulting in the rate of its production and destruction to be comparable, preventing it from accumulating to levels beyond its initial value.

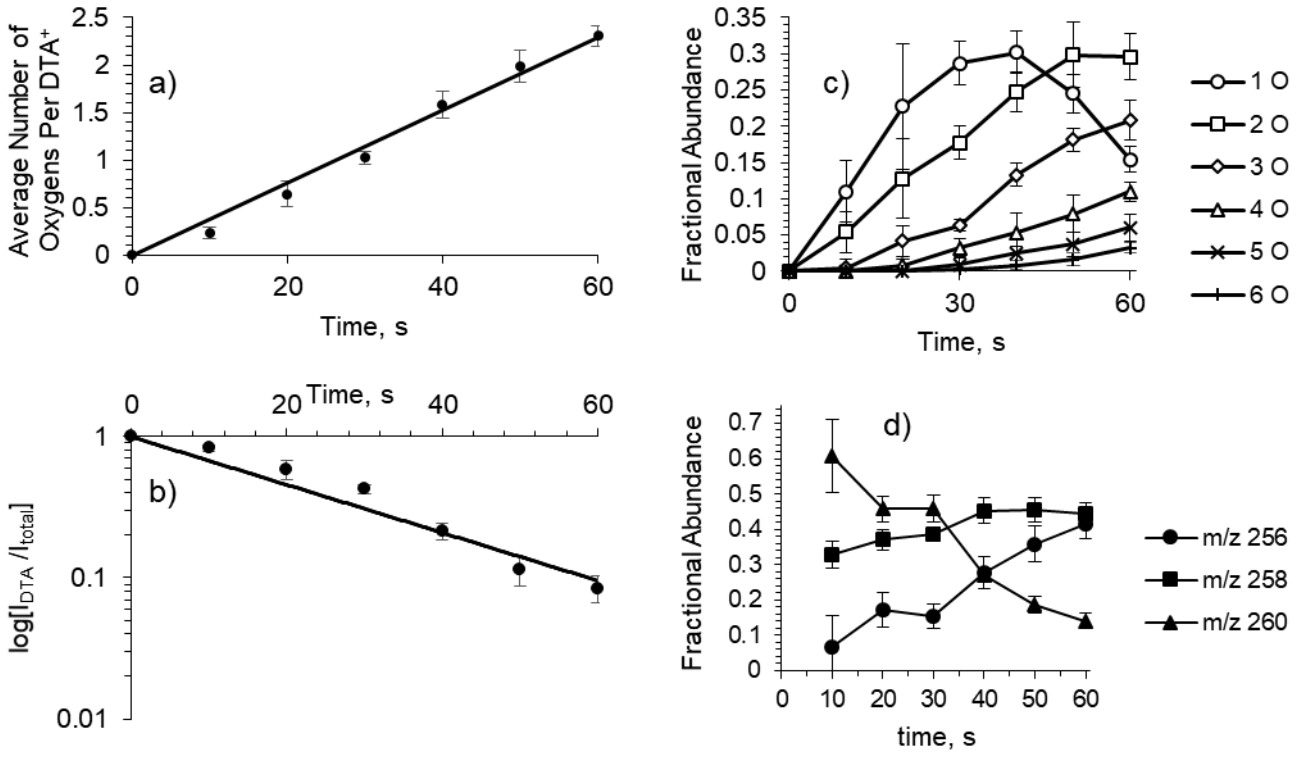

Figure 2.4. Kinetics data for the oxidation of DTA^+ by the hydroxyl radical at the air-water interface. N = 8. All error bars are standard deviations. a) The average number of oxygen atoms incorporated into the DTA^+ alkyl chain over the 60 s exposure to the DBDS, with linear regression (R^2 = 0.987). b) The logarithmic plot of the disappearance of DTA^+ fraction intensity (I_{DTA}/I_{total}) over the course of the 60 s exposure with linear regression shown (R^2 = 0.954). c) The fractional abundance of each generation of DTA^+ oxidation products versus time. d) The fractional abundance of individual products within the second generation of products over the course of DTA^+ monolayer oxidation, with m/z 256, 258, and 260 representing the dicarbonyl, hydroxycarbonyl, and peroxyl product, respectively.

2.4.2 Mechanistic Details of the Oxidation

The kinetics data and identification of oxidation products suggest the mechanism by which the hydroxyl radical interacts with a hydrocarbon surfactant at the air-water interface

under ambient conditions. The excellent agreement of the kinetics data with a first order process suggests the termination of the OH-initiated oxidation event results in the formation of products with functional groups with single oxygen atoms in **Scheme 2.1**, namely the carbonyl and hydroxyl products. As these first generation products are formed they accumulate at the surface until they become the probabilistic targets of impinging hydroxyl radicals. The major abundance of solely singly-oxygenated products at short times dismisses pathways that result in alternative products on these timescales (e.g. fragmentation products and peroxide coupled dimers). This sequential addition of oxygen into the hydrocarbon chain predicts the rising and falling behavior of each generation seen in **Figure 2.4c**.

The linear trend in total amount of oxygen incorporation seen in **Figure 2.4a**, coupled with the steady accumulation and reduction of each generation found in **Figure 2.4c** suggest that prior oxidation of a chain does not impact reaction rate. Given that oxygen-incorporation of hydrocarbons is known to weaken adjacent C–H bonds,[116] it would be expected to see the relative amount of later generations increase at a faster rate than earlier ones. It can be argued that this lack of acceleration is due to the hydroxyl radical having significant diffusion time on the droplet's surface. It is therefore likely that the observed kinetics in **Figure 2.4a** is resulting from the accommodation and diffusion of the hydroxyl radical prior to reaction, the characteristic behavior of Langmuir-Hinshelwood kinetics, making its reactive partner more random than the thermodynamics would suggest.

The second generation products provide a second source of evidence for the mechanism. One of the most important features of the evolution of second generation products is the large fraction of mixed functional group products [DTA^+ + Cb + Hy], despite the evidence that

hydroxyl functionalization is not a major pathway for oxidation. While reaction [13] in **Scheme 2.1** can account for a pathway resulting in a mixed functional product, the possibility of the α-hydroxyketone products suggested by CID analysis (**Figure 2.3d**) does not support this mechanism as it does not fit with a six-membered transition state required for this pathway. Rather, two distinct radical abstraction events are more plausible, and fit well with the kinetics of the system. The proposed formation of the α-hydroxyketone m/z 258 product from secondary oxidation of m/z 242 at the weakened alpha C–H location[116] is shown in **Scheme 2.3**.

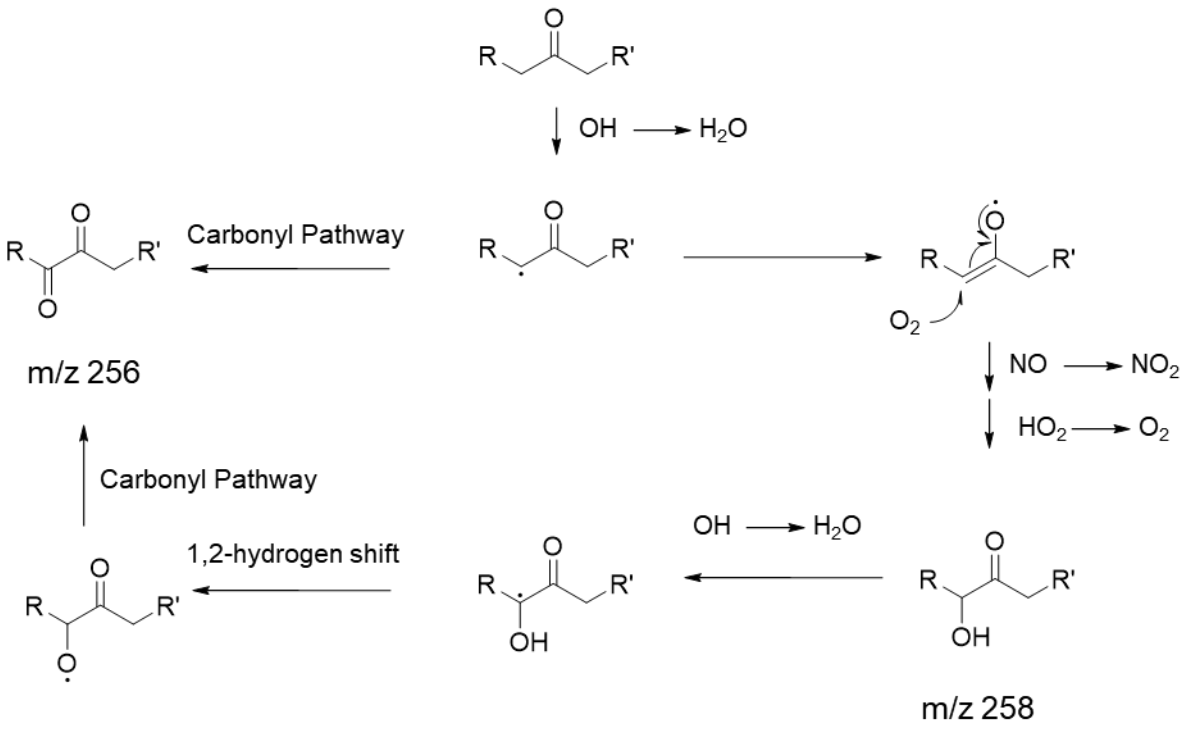

Scheme 2.3. Possible branching mechanism for the formation of m/z 256, the dicarbonyl product, and m/z 258, the α-hydroxyketone product from the precursor carbonyl m/z 242.

The second unique feature of the evolving distribution of second generation oxidation products is the linear increase in the ratio of m/z 256/258 implied by **Figure 2.4d**. Again assuming a sequential means of producing the second generation products, the oxidation of m/z 242 can immediately form m/z 256. However, the significant increase relative to m/z 258 suggests a new pathway for producing the dicarbonyl product emerges as the DTA^+ monolayer oxidizes. A possible mechanism for this phenomenon, in which the hydroxyl of m/z 258 is converted to a carbonyl thereby effectively increasing the relative ratio of m/z 256/258, is shown in **Scheme 2.3**. The progressive shift in relative quantities of the second generation species over time provides evidence that the second sequential oxidation occurs as the amount of m/z 258 on the surface increases. The hydroxyl radical only begins initiating the conversion of these species as their meeting over the course of its diffusion through the surfactant monolayer becomes more likely.

The remaining generation products (generation n > 2) show similar distributions, with mixed functional species constituting the majority species for a given generation. The process involves sequential reactions in which an initial precursor $DTA^+ + nO$ is converted to the next generation product $DTA^+ + (n+1)O$ from a single hydroxyl radical event. Multiple carbonyl-containing products tend to favor forming hydroxyl groups, resulting in mixed functional products, and some of those hydroxyl groups are converted back to carbonyl groups. The CID of m/z 260 suggests that initial products containing even numbers of oxygen atoms (multiples of +32 mass shifts) have a significant contribution from the peroxide species.

2.4.3 Observed Replenishment of DTA^+ in an Oxidized Monolayer via Exchange Processes with the Subphase

Heterogeneous processing of aerosols shows that surface properties related to the increased hydrophilicity shift substantially under prolonged exposure to OH.[40, 58, 65] Furthermore, the exchange of oxidized products with unreacted organics in the subphase has been invoked in the mechanism of heterogeneous OH oxidation of an organic-coated solid particulate system.[63] **Figure 2.5** reveals that such exchange is observable in the FIDI mass spectra of surface species post-oxidation at the air-water interface after a 60 s delay prior to FIDI sampling. The percentage changes illustrated in **Figure 2.5** show that the oxidized monolayer, formerly dominated by a mixture of high mass products of generations 1, 2, and 3, undergoes a shift in species relative amounts. Particularly striking is the significant increase (31.0%) in DTA^+, while nearly every oxidized product peak shows a decrease. The likely mechanism for this phenomenon is the exchange occurring between the interfacial population of surfactants and the bulk DTA^+ within the droplet. As oxidation imparts oxygen functional groups that increase hydrophilicity of the surfactant alkyl chain, the product species diffuse to the bulk aqueous phase, leaving a site on the droplet surface available for the hydrophobic chain of an unoxidized DTA^+ species to replace it.

The reduction in intensity is most pronounced in the series of products with sequentially more carbonyl groups – m/z 242 (DTA^+ + Cb), 256 (DTA^+ + 2Cb), and 270 (DTA^+ + 3Cb) – indicating the carbonyl functional group has a more pronounced and consistent effect on diffusive behavior at the interface than the hydroxyl group. The mixed functional group products also see decreases. However, the hydroxyl series m/z 244, 260, 276 shows a deviation. While the fraction of m/z 244 and 276 decreases as a result of the delay period,

the increase in relative abundance of m/z 260 indicates that this species resists exchange with solubilized DTA^+ in solution. The distinct behavior suggests there may be a structural difference in this species. Hydrogen-deuterium exchange experiments and collision-induced dissociation experiments are implemented to identify the possible structural differences among the product species.

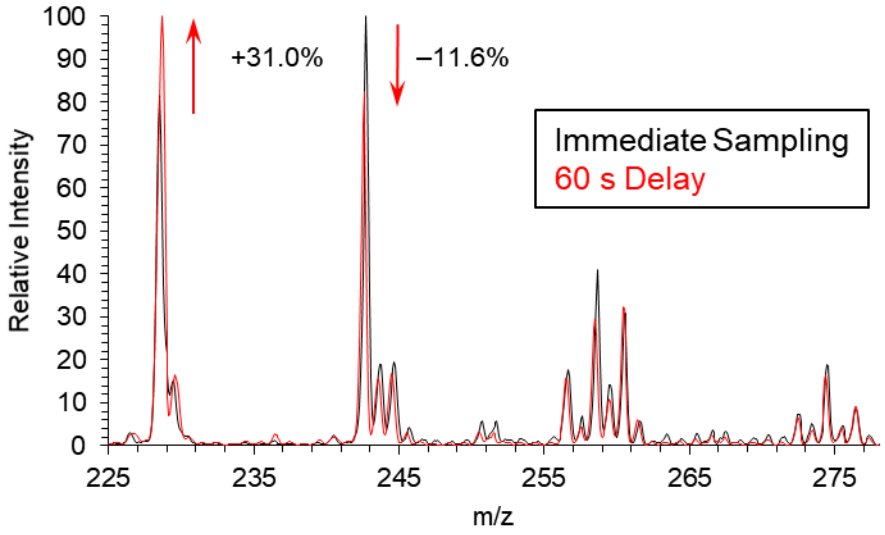

Figure 2.5. Comparison of FIDI mass spectra of the DTA^+ monolayer immediately after a 60 s OH exposure and after a 60 s delay prior to sampling. Arrows emphasize major changes in intensity.

2.4.4 Confirmation of Product Identities through Hydrogen-Deuterium (H/D) Exchange Experiments

As a means to confirm the identity of product functional groups of the initial oxidation products, particularly the m/z 260 product that could represent a dihydroxy or a peroxide product, the heterogeneous DTA^+ oxidation was carried out as mentioned previously in 90/10 D_2O/H_2O solvent. The resultant increase in mass for each H/D exchange event that a species undergoes correspondingly increases the observed m/z by 1 unit. While it is not assumed that

H/D exchange will be fast or complete during the timescale of the reaction, the change in intensity among the m/z 242 (DTA^+ + Cb) and m/z 244 (DTA^+ + Hy) and their respective neighbor peaks give a baseline for the extent of H/D exchange caused by the carbonyl and hydroxyl functional groups at the air-water interface under the experimental conditions. This change in intensity is expressed as a percent deviation from the relative intensity in the H_2O condition (See Appendix A for calculations). **Figure 2.6** shows the comparison of the FIDI spectrum of the first and second generation products in the presence and absence of D_2O for a 60 s DBDS exposure. During the analysis of the percent intensity change ($\Delta_{m/z}$ in Figure 2.6), the data were corrected for ^{13}C signal. While the percent intensity changes agree for purely carbonyl products m/z 242 and 256 and for products with unequivocally one hydroxyl group (m/z 244 and m/z 258), the m/z 260 exhibits relatively low H/D exchange under the assumption that it is a dihydroxy product. The result indicates that the m/z 260 contains a single exchangeable proton, providing evidence for the assignment of m/z 260 as a peroxide product.

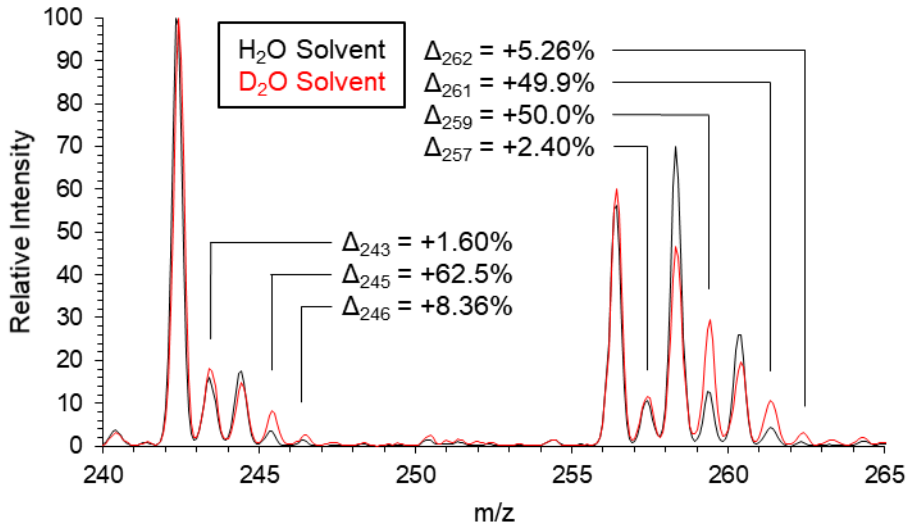

Figure 2.6. Comparison of relative intensities of the first two generations of oxidation products for DTA^+ at the air-water interface in H_2O solvent (black) and 90% D_2O solvent (red). The differences in relative intensities for each m/z ($\Delta_{m/z}$) are written as a percent deviation from the expected isotopic proportion.

2.4.5 Identification of Low Mass DTA^+ Oxidation Products

Figure 2.7 depicts the low mass products generated in the 50 s DBDS exposure condition. The series of peaks separated by 14 m/z reflect scission of the alkyl chain at different C–C bond locations, resulting in the loss of consecutively more methylene units. The longest discernable fragmentation product is the 10 carbon aldehyde (labeled C_{10} in **Figure 2.7**), which resulted from the loss of an ethyl group at the end of the chain. The C_4 fragment species is found at lowest intensities in the series. The C_{11} fragmentation was found to be present via CID of m/z 228 for a 90% oxidation condition (See **Appendix A**). Compared to a DTA^+ standard, isolated m/z 228 post-oxidation contains a fragment generated from the loss of trimethylamine, a product common to nucleophilic displacement of a carbonyl. The low abundance of the fragmentation series suggests that initial oxidation promotes functionalization rather than fragmentation, as is seen in the heterogeneous OH oxidation of squalene particles[117] and secondary organic aerosols.[34]

The relative intensities of these low mass products suggest the location of the initial hydrogen abstraction event. As **Scheme 2.1** reaction [10] indicates, C–C bond cleavage occurs adjacent to the alkoxyl radical site. For example, the C_{10} low mass product is formed by one of two scenarios. In the first case C_{10} was the site of hydrogen abstraction. Fragmentation of the C_{10}–C_{11} formed the C_{10} aldehyde low mass product and an ethyl radical.

In the second case C_{11} was the site of hydrogen abstraction. Scission of the C_{10}–C_{11} bond resulted in the formation of acetaldehyde and a radical site now on the terminal C_{10} methylene unit. This radical reacts to produce the final C_{10} product. While both are plausible mechanisms, gas phase data, at least for small hydrocarbons, suggests that upon bond breakage the formation of the larger alkyl radical (i.e. the radical with higher molecular weight) is more stable.[118] Using this as the model, a C_n product is indicative of the oxidation of the C_{n+1} site for $n > 6$. Low mass products C_8 through C_{10} account for approximately 50% of the total low mass product intensity, indicating that the site of abstraction is biased toward the last third of the alkyl chain.

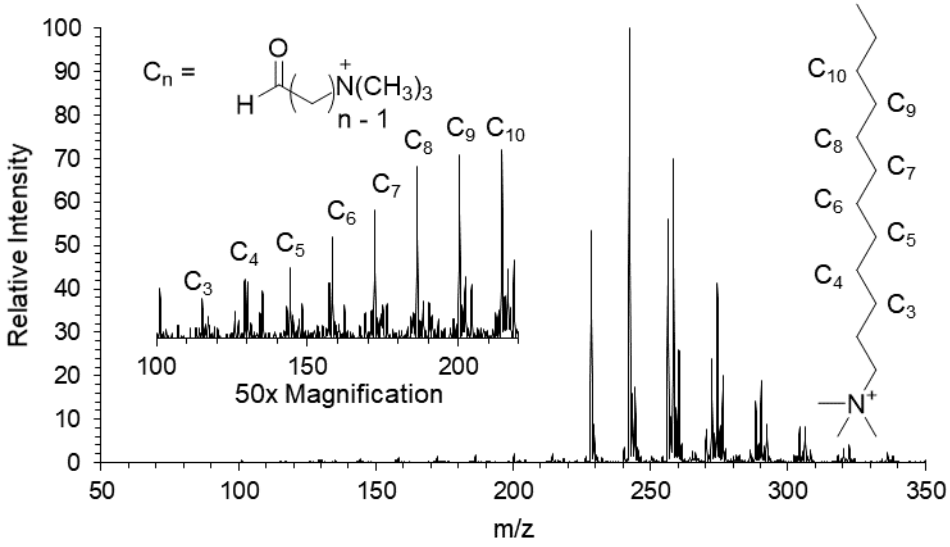

Figure 2.7. FIDI spectrum of DTA^+ at a 50 s DBDS exposure. Inset: 50x magnification of the low mass products.

2.5 Conclusions

A monolayer of hydrocarbon surfactant at the air-water interface is historically a challenging system to study with the hydroxyl radical due to the challenge surrounding

generating the highly reactive OH radical at ambient conditions, and the difficulty in sampling the chemical changes of the monolayer over a controlled exposure. The development of the DBDS has proven to be a simple and reliable instrument for the generation of OH at ambient conditions, and coupled with FIDI-MS has shown to be an effective experimental design for the study of hydroxyl radical chemistry at the air-water interface. For the first time, time-resolved oxidation studies of hydrocarbon surfactants have been performed, capable of discriminating the initial oxidation products and their stepwise conversion to the highly complex and multiply oxygenated product mixtures.

The results of the DTA^+ + OH interfacial reaction agree with previous studies that indicate that hydrocarbons under oxidative processing form various carbonyl, hydroxylated, and peroxyl species in addition to fragmentation products. Furthermore, the kinetic data of the air-water system in this work provides further support that the heterogeneous chemistry of the hydroxyl radical obeys Langmuir-Hinshelwood kinetics.

The utility of the quaternary ammonium ion DTA^+ is demonstrated through these studies because of its efficiency in forming monolayers, the ease of its detection, and the unique fragmentation this ion undergoes in the presence of carbonyl, hydroxyl, and peroxyl groups, allowing for the effective identification of the initial oxidation products as well as localizing the oxidation site for the peroxyl product. As another novelty of this work, hydrogen-deuterium exchange has successfully aided in the identification of oxidation products containing labile protons. The successful characterization of the evolution of products in the stepwise OH-mediated oxidation of a linear alkyl surfactant using the DBDS-FIDI-MS systems suggests that this system can be used to discern mechanistic details of the

heterogeneous oxidation of other atmospherically and biologically relevant species at the air-water interface.

Chapter 3

Comparative Hydroxyl Radical-Mediated Oxidation of Fraternal and Identical Hydrocarbon Groups in Gemini Surfactants

3.1 Abstract

Lipids consisting of two alkyl chains joined by a polar head group are prevalent throughout nature, notably in biological membranes that act as a buffer to ambient gases such as in the lining of the lungs. The ability of a lipid or surfactant system to retain its properties depends on their susceptibility to oxidation to gas phase oxidants. One such important question about the oxidation of saturated lipid monolayers is the effect of the proximity of neighboring chains on the reactivity of the lipid, specifically on the possible effect on oxidation site. We present a study designed to answer two questions: 1) In the case when two unequal linear alkyl chains are present at the air-water interface, to what extent will the longer chain's increased projection into the gas phase outcompete its shorter neighbor for reaction gas phase oxidant; and 2) For initially identical hydrocarbon neighbor chains present at the air-water interface, to what extent does an oxidative functionalization affect the subsequent relative reactivity of one neighbor over the other? The method of field-induced droplet ionization mass spectrometry (FIDI-MS) coupled with the dielectric barrier discharge source (DBDS) as a hydroxyl radical generator is implemented to initiate heterogeneous oxidation followed by direct sampling of oxidize a monolayer of bis-quaternary ammonium gemini surfactants of the form $R(CH_3)_2N^+(CH_2)_4N^+(CH_3)_2R'$ to study chain oxidation competition among neighboring alkyl groups. Oxidation of a dissymmetric gemini surfactant

(R = $C_{16}H_{33}$ group, R' = $C_{12}H_{25}$) by the DBDS followed by immediate FIDI-MS analysis shows that no such preference is observed toward the longer chain. Oxidation and analysis of a symmetric gemini surfactant (R = R' = $C_{16}H_{33}$) indicate that a second oxidation event is biased to occur on the same chain as the first oxidation event. These results are in agreement with molecular dynamic simulations which suggest the alkyl groups are significantly tangled rather than extended to the gas phase.

3.2 Introduction

Lipids represent an important class of molecules as they are extensively utilized in biological systems as both an energy source and as a major structural component of cells. Biological lipids are amphiphilic molecules containing a hydrophobic domain (usually a long chain hydrocarbon) and a hydrophilic domain. The utility of lipids lies in their thermodynamic drive to form various macromolecular structures in aqueous systems including monolayer or bilayer membranes, vesicles, and micelles, which are capable of internalizing small molecules and maintaining conditions that differ from the external medium.[119-124] Lipid chemical compositions can vary widely, and the chemical nature of the lipid components has far-reaching effects on its vesicle properties, such as the mechanism of small molecule internalizaton.[125-126]

Because biological function of the cell rests on its cellular membrane integrity, the degradation of lipid membranes in the presence of oxidants has been studied extensively and has been linked to human disease.[127-133] Furthermore, lipid oxidation is intensely studied in the context of monitoring and understanding the aging and rancidity processes of high fat content food products, in the effort to improve their shelf life and storage.[44, 134-136] In both

cases, unintended oxidation occurs when oxidants such as metal cations or reactive oxygen species first encounter lipids at their hydrophobic-hydrophilic interface.[137-138] A large number of studies on lipid oxidation focus on lipids containing one or more double bond, due to that functionality's propensity to undergo radical-induced oxidation from molecular oxygen, singlet oxygen ($^1O_2$), peroxides, superoxide, and the hydroxyl radical.[139-145] Variations in lipid membrane composition, particularly the addition of hydrophobic antioxidants such as vitamin E, are found to inhibit oxidation as they incorporate into the lipid and quench free radicals.[127, 146]

While unsaturated lipids are well-studied due to their prevalence in foods and membranes, pulmonary tissues represent a key system in which saturated lipids are major membrane constituents. Assays of lipid compositions conclude that dipalmitoyl phosphatidylcholine (DPPC), a lipid whose hydrophobic domain consists of two saturated hydrocarbon chains, is present in the range of 41 – 70%.[147-149] Relatively few studies focus on saturated lipids, partly due to the fact that saturated lipids are inherently more stable than unsaturated lipids.[44] Interfacial ozone oxidation studies of DPPC with unsaturated lipid palmitoyl-oleoyl-phosphatidylcholine (POPC) show that the unsaturated species is the only species susceptible to ozone on the experimental timescale.[69, 150-152] While ozone is a major atmospheric pollutant and health hazard, one of the most potent oxidants of saturated hydrocarbons, the hydroxyl radical (OH), has an ambient daytime of 10^6 molecules/cm^3,[31] and gas phase hydrocarbon reactive rate constants on the order of 10^{12} cm^3/molecule–s,[17, 29] making it a key species in saturated lipid degradation. Hydrocarbon lipids are under constant oxidative pressure from this species under ambient conditions. Studies of hydroxyl radical

processing of saturated lipids and lipid analogues at air-water interfaces under ambient atmospheric conditions has been sparse, but DPPC coated NaCl particles show that the heterogeneous OH oxidation of the lipid produces oxygenated, fragmented, and nitrate compounds.[63]

However, it is still not well understood how lipids undergo hydroxyl radical-mediated oxidation in a heterogeneous system in light of having two competing hydrocarbon chains. Heterogeneous oxidation of large hydrocarbons indicate that the methylene hydrogens extending the furthest from the aqueous phase are preferentially the site of oxidation for OH generated in the gas phase,[22] suggesting that larger hydrocarbon chains that extend further into the gas phase should show increased reactivity at the air-water interface. Additionally, for initially identical hydrocarbon chains the oxidation of one chain to form an oxygen functional group may make that chain's oxygen adjacent C – H bonds susceptible enough to oxidation to bias the product distribution toward functionalizing a single chain. The following study investigates how influential the proximity of neighbor alkyl groups is in the heterogeneous OH reaction.

The choice of an appropriate lipid for the study of inter-chain competition during oxidation is crucial. For mass spectrometry analysis, the species requires high detection (preferably one or more permanently charged sites) and well-understood fragmentation behavior. The class of molecules known as gemini surfactants holds an interesting prospect. These surfactants are composed of two long hydrophobic hydrocarbon groups, each terminated with a polar head group linked to the other by either a rigid or flexible hydrocarbon spacer.[153-155] They show enhanced surface activity at the air-water interface,

including high surface adsorption and large decreases in surface tension,[155] while solution phase properties include relatively sensitive temperature-dependent micelle formation.[156-157] The influence of spacer chain length on critical micelle concentration has also been investigated, suggesting gemini surfactants can be engineered to have comparable surface properties to biological lipids.[158-160] In fact, the similar structural and amphiphilic properties allow gemini surfactants to easily incorporate into phospholipid membranes,[161-163] and this ability of gemini surfactants to incorporate into macromolecular structures such as vesicles, micelles, and membranes has resulted in their observed antifungal and antibacterial properties.[164-166] For their apparent analogous structural and interfacial behavioral similarities to biological phospholipids, gemini surfactants make a suitable system to study the stepwise oxidation of lipid-like hydrocarbon chains at the air-water interface. Specifically, bis-quaternary ammonium gemini surfactants are dicationic species of the form $(C_nH_{[2n-1]})N^+(CH_3)_2(C_sH_{2s})N^+(CH_3)_2(C_mH_{[2m-1]})$, abbreviated using the chain lengths as n-s-m. They provide hydrophilic ammonium head groups with long chain alkyl groups that, when adsorbed to the air-water interface, present themselves to the gas phase. Thus these surfactants undergo OH-mediated oxidation pathways similar to saturated biological lipids. Two distinct gemini surfactants are studied. The dissymmetric gemini (DG) 16-4-12 contains unequal linear alkyl chains for the study of competition among unequal hydrocarbon chain length with the OH reaction, and the symmetric gemini (SG) 16-4-16 oxidation is investigated to determine how multiple oxygenation sites are distributed among two initially identical neighbor hydrocarbon chains.

The generalized pathways for hydroxyl radical-mediated oxidation of a gemini surfactant pertinent to this study are shown in **Scheme 3.1**, [13, 17, 25, 39, 60-61, 100-104] and highlights the interplay two alkyl chains exhibit in a dialkyl lipid. The reactivity of hydrocarbon groups with hydroxyl radicals stems from the susceptibility of the C – H bond to hydrogen abstraction (reaction [1]), producing a carbon-centered radical. For long chain linear hydrocarbons, the more numerous and reactive methylene hydrogens are probabilistically the most likely sites of oxidation. Under atmospheric conditions, molecular oxygen adds to the carbon-centered radical (reaction [2]). While this peroxyl radical is known to undergo a wide variety of pathways, in the presence of nitric oxide the peroxyl radical forms the transient ROONO before rearranging to produce nitrogen dioxide and an alkoxyl radical (reaction [3]). By means of oxygen or the hydroperoxyl radical, the alkoxyl species forms a carbonyl or hydroxyl product (reactions [4] and [5]). Alternatively, for particularly long-chained hydrocarbons the radical can abstract a hydrogen from a C–H bond in a 1,5-radical shift, producing a hydroxyl group and a new radical site on the hydrocarbon (reaction [6]). In the presence of another chain, the radical can abstract from its neighbor hydrocarbon tail (reaction [7]). In this way a new radical site can be generated from the original radical from a single oxidation event, rather than requiring a second hydroxyl radical initiating oxidation. Whether the radical site is generated through this route, or via a second hydroxyl radical hydrogen abstraction event, the cascade of reactive events results in a doubly functionalized surfactant. However, in the case of a gemini surfactant (or phospholipid) the position of the two functional groups on one or both hydrocarbon chains is the result of several factors. If the series of pathways results in the termination of the radical site on the

surfactant, specifically by reactions [4] and [5], then the second functional group must come about by a second hydroxyl radical abstraction event. The degree to which the functionalization of one of the chains makes it more vulnerable to the second oxidation initiation is unknown. If a hydrogen shift generates the second radical site, then the proximity and interaction of the two hydrocarbon tails will influence whether reaction [6] or reaction [7] dominates. Ultimately, the interplay of all pathways leads to a potential bias for surfactants with either a difunctionalized chain, or two monofunctionalized chains.

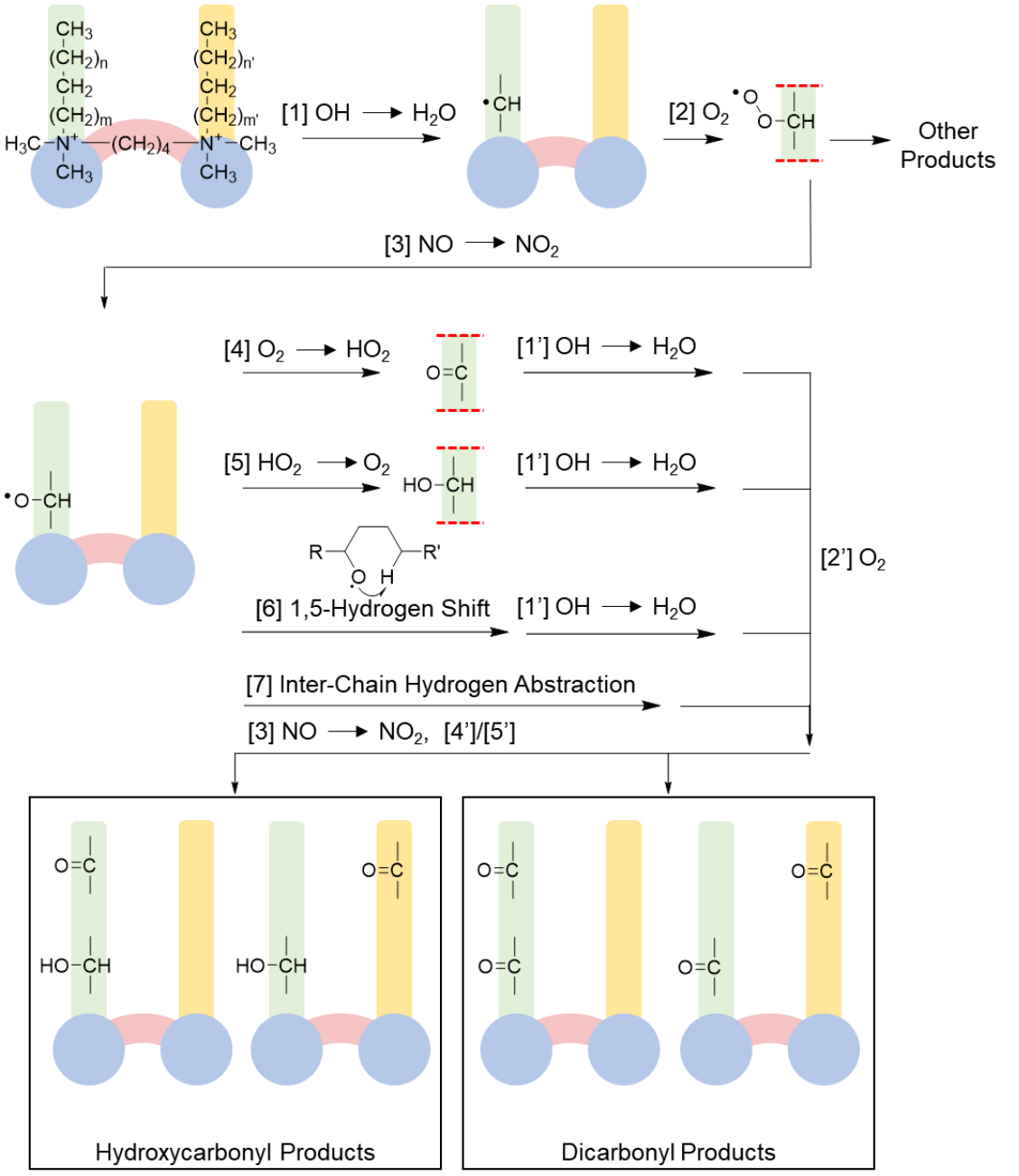

Scheme 3.1. The reaction mechanism of hydroxyl radical-mediated oxidation of a generic gemini surfactant leading to the formation of dicarbonyl and hydroxycarbonyl products.

Quaternary ammonium dicationic gemini surfactants provide a uniquely informative system for determining the relative hydroxyl radical reactivity of competing neighbor

hydrocarbon chains at the air-water interface through the unambiguous fragmentation patterns of oxidized alkylammonium to produce oxonium ions during collision-induced dissociation (CID), a common fragment seen in CID mass spectra.[167] **Scheme 3.2** shows the mechanism of fragmentation for DG and SG. In the case of DG, an oxidation product containing a carbonyl produces characteristic CID ions dependent on whether the carbonyl is located on the longer hexadecyl or the shorter dodecyl chain. Given that the carbonyl is on the hexadecyl chain (**Scheme 3.2a.i**), the oxygen atom attacks the carbon adjacent to the nitrogen, freeing the newly formed cyclic oxonium (m/z 239) from the rest of the gemini surfactant. The dimethylamino group can cyclize the remaining spacer to form the five-membered cyclic quaternary ammonium ion (m/z 100). An identical reaction can occur for the case in which the carbonyl is on the dodecyl chain (**Scheme 3.2a.ii**), with the cyclic oxonium appearing at m/z 183. Therefore, the CID data illuminates the location of the carbonyl functionalization by the relative abundances of the m/z 183 and m/z 239 products.

For SG, the location of two functionalization groups is determined by similar ion formation. The dicarbonyl product ($[SG + 2Cb]^{2+}$) forms a oxo-oxonium ion (m/z 253) if the carbonyls are on the same hexadecyl chain (**Scheme 3.2b.i**), or two oxonium ions at m/z 239 (**Scheme 3.2b.ii**) if the carbonyls are on different hexadecyl chains; the two oxonium products are due to the fact that each oxo-hexadecyl chain can cyclize independently. Identical logic rationalizes the fragmentation products in the case of the hydroxycarbonyl product ($[SG + Cb + Hy]^{2+}$). Cyclized oxonium ions bearing the hydroxyl group are indicative of oxidation occurring sequentially on the same chain (**Scheme 3.2c.i**). Otherwise, the two chains of SG form their respective cyclized species based on the functionalization of

each chain – an oxonium for the carbonyl product and a protonated ether for the hydroxyl product (**Scheme 3.2c.ii**).

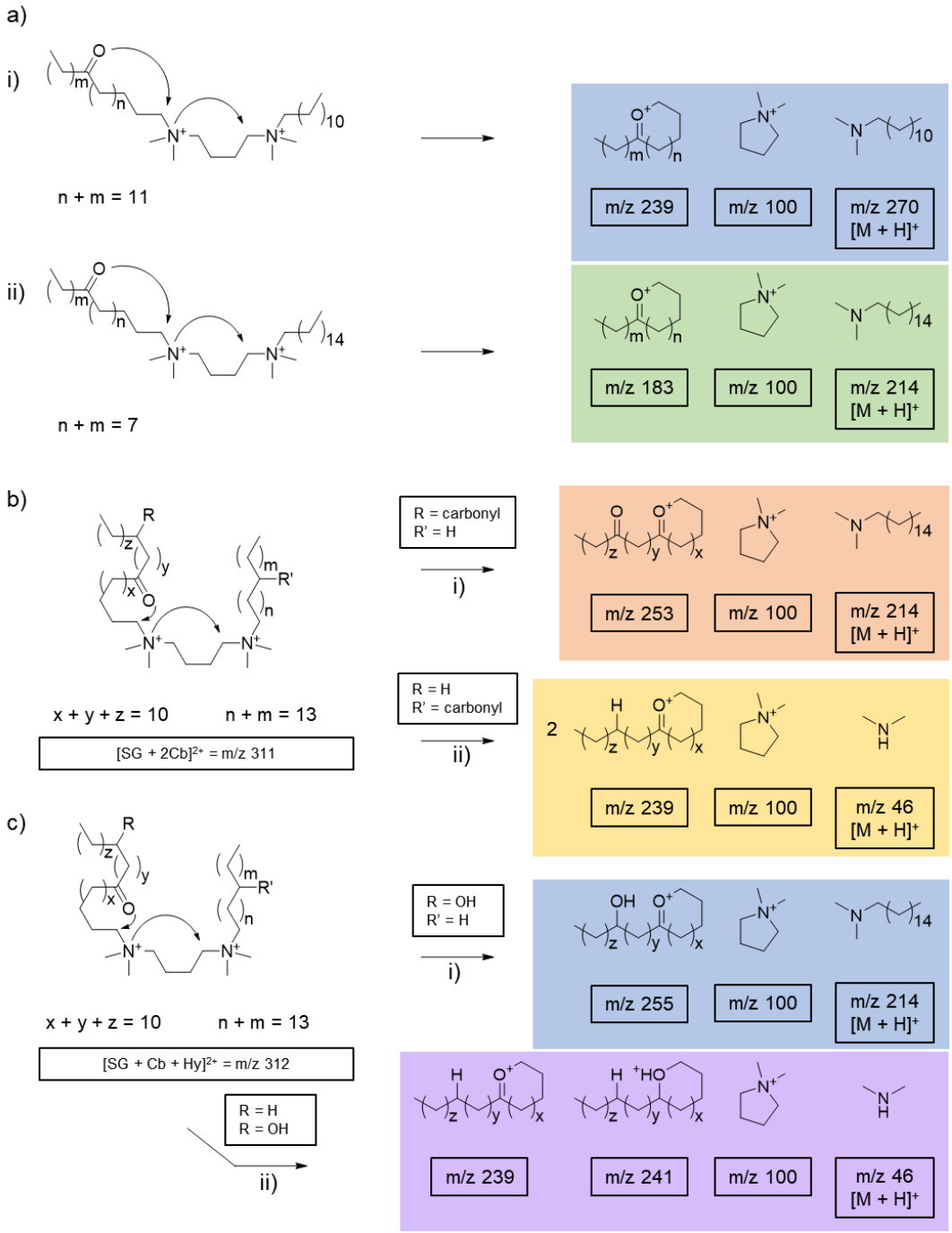

Scheme 3.2. Possible mechanisms of fragmentation for oxidized gemini surfactants during collision-induced dissociation. a) Fragmentation mechanism of $[DG + Cb]^{2+}$, where the carbonyl

functionalization resides on i) the hexadecyl chain; ii) the dodecyl chain. b) Fragmentation mechanism of $[SG + 2Cb]^{2+}$, where each carbonyl group: i) resides on the same hexadecyl chain; ii) resides on different hexadecyl chains. c) Fragmentation of $[SG + Cb + Hy]^{2+}$, where each functional group: i) resides on the same hexadecyl chain; ii) resides on different hexadecyl chains.

The heterogeneous oxidation of the two surfactants DG and SG are monitored in real-time using field-induced droplet ionization mass spectrometry (FIDI-MS). Monolayers of DG provide insight on the effect of chain length on the relative reactivity of two unique neighbor chains. Findings on oxidized hydrocarbons suggest the more gas phase-accessible longer tail will show enhanced reactivity relative to the shorter tail. In the second experiment, the effect of prior oxidation is investigated as a factor enhancing the propensity of an alkyl chains

3.3Materials and Methods

3.3.1 Materials

All reagents used in synthesis were purchased from Sigma-Aldrich (St. Louis, MO) at the highest available purity and used as is. Isopropyl alcohol (ACS grade, Millipore Sigma), water (HPLC grade, OmniSolv), and acetonitrile (HPLC grade, OmniSolv) were used as solvents as is. Glassware used for synthesis was baked for 16 hours at 130 °C prior to use. Stock solutions were made at 1 mM concentrations and stored at – 20 °C.

3.3.2 Synthesis of Gemini Surfactants

Syntheses of gemini surfactants 16-4-12 and 16-4-16 proceeded via modified protocols of gemini surfactant syntheses in the literature[157, 168] and are outlined in **Scheme 3.3**. Synthesis of 16-4-12 required a two-step process involving an intermediate compound. To synthesize intermediate 1, A 100 mL 2-necked round bottom flask was fitted with a

condenser and dropping funnel, and a solution of 40 mmol 1,4-dibromobutane in 30 mL isopropyl alcohol was added, followed by the dropwise addition of 20 mmol N, N-dimethylhexadecylamine over 30 minutes. The mixture was refluxed for 24 hours at 50 °C. Excess solvent was evaporated in air until a white powder was obtained. The identity of intermediate 1 was verified by electrospray ionization mass spectrometry (ESI-MS) of a small crystal of the product dissolved in acetonitrile using an LTQ-XL mass spectrometer (Thermo-Fischer, Waltham, MA). The mass spectrum can be found in **Appendix C**. The crude yield of 1 was 52%.

The surfactant DG (16-4-12) was obtained by combining 3 mmol intermediate 1 and 3 mmol N, N-dimethyldodecylamine in 20 mL isopropyl alcohol. The mixture was refluxed for 24 hours at 50 °C. The solvent was evaporated in air until a white product was crystallized. The crude yield of DG was 73%. Product identity was verified by mass spectrometry (See **Appendix C** for details.). The product was recrystallized in dichloromethane.

Synthesis of SG (16-4-16) proceeded as follows. To a 100 mL 2-necked round bottom flask containing 10 mmol 1,4-dibromobutane was added 20 mmol N,N-dimethylhexadecylamine in 30 mL isopropyl alcohol, and refluxed at 50 °C for 24 hours. The solvent was evaporated in air and the solid product was collected. The product was recrystallized in dichloromethane. The identity of the product was verified by ESI-MS (See **Appendix C** for details.).

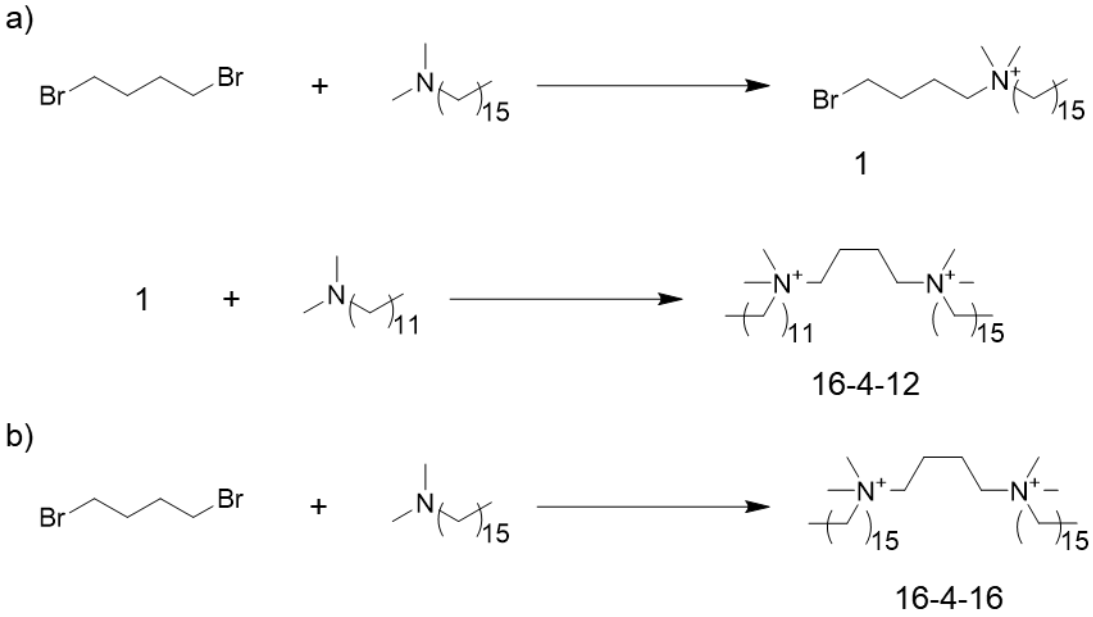

Scheme 3.3. Synthesis of gemini surfactants. a) Synthetic route for the gemini surfactant 16-4-12. b) Synthetic route for the gemini surfactant 16-4-16.

3.3.3 Field-Induced Droplet Ionization Mass Spectrometry (FIDI-MS)

The FIDI source has been described extensively elsewhere and has been used to investigate changes in chemical composition on the surface of millimeter-sized droplets.[24, 66-70] Briefly, the FIDI apparatus is mounted to an LTQ-XL mass spectrometer (Thermo-Fischer, Waltham, MA). Aqueous droplets of 2.5 μL volume (1.6 mm diameter) containing 60 μM gemini surfactant are formed on a 28 gauge stainless steel capillary resting exactly between two plate electrodes (spaced 6.3 mm apart) via syringe pump. A 1 minute equilibration time allows the surfactant to partition to the interface from the bulk aqueous phase, forming a monolayer. After this period a flow of gas phase hydroxyl radicals, generated via passing a flow of water-saturated through plasma discharge, is delivered to the droplet. During sampling, a high voltage (3-5 kV) pulse is sent to the back plate electrode

while keeping the front plate at ground, and a half voltage pulse is simultaneously sent to the capillary, ensuring the establishment of a homogeneous electric field. A critical field strength perturbs the droplet and causes it to elongate along the field, forming Taylor cones on each end, ultimately ejecting microdroplets from the interfacial layer of the droplet. The atmospheric pressure inlet is aligned with an aperture designed in the grounded plate electrode, allowing a microdroplet to be aspirated into the mass spectrometer. Prior to FIDI-MS experiments the settings of the mass spectrometer are optimized for the surfactant of interest. With these settings the droplet is sampled post-oxidation. The procedure is repeated five times, each time with a new droplet. For FIDI-MS/MS analysis, collision-induced dissociation (CID) spectra are collected for oxidation products containing two oxygen atoms with the following settings: isolation width of 0.8 m/z and a collision excitation parameter of 25%. Product CID spectrum collection is repeated 5 times per isolated product.

3.3.4 Production of Hydroxyl Radicals

Hydroxyl radicals are produced using the dielectric barrier discharge source (DBDS) described previously in **Chapter 2**. Discussion of its optimization is found in **Appendix B**. Briefly, a specially designed borosilicate tube is fitted with a tungsten rod along its length and a conductive coating on its outer surface These conductive materials are used as electrodes to form a low temperature plasma when the inner rod electrode is biased. A flow of He/H_2O (approximately 1% H_2O) sent through the plasma discharge by means of a gas inlet near the back end of the tube promotes dissociation of water molecules to hydroxyl radicals and exits through a 2 mm ID outlet. The flow rate is monitored by a Type πMFC Digital Mass Flow Controller (model PFC-50, MKS Instruments). A power supply (Trek PM04015; Trek, Inc, NY) provides the AC voltage necessary to generate the plasma. During

operation in conjunction with FIDI-MS sampling, the DBDS is placed with its OH outlet 5 mm from the droplet and operated at 12 kV_{pp}, 1 kHz sine waveform, 1.414 mA current, and 1000 cm^3/min He/H_2O flow.

3.3.5 Molecular Dynamic Simulations of the Gemini Surfactant at the Air-Water Interface

Molecular simulations are performed using Large-scale Atomic/Molecular Massively Parallel Simulator (Sandia National Laboratories) by our collaborators (H. Lee and H. Kim, Korea Advanced Institute of Science and Technology). The system utilizes a Nosé-Hoover thermostat, Verlet integration method with a 1 fs integration time (20 ns total simulation), OPLS-AA force field parameters,[169] and SHAKE algorithm for TIP3P-Ewald for solvent water molecules. The system consisted of 32 surfactant ions (either 16-4-12 or 16-4-16) with bromide counterions and 3,312 water molecules in a 41.5 x 47.9x 150 simulation box $Å^2$. Initially, water molecules were arranged in a column with a depth of 54 Å, having a monolayer of surfactant on each interfacial boundary in the z-direction. The surface area of the surfactant was taken to be 124 $Å^2$. Simulations proceeded in three phases. In the first phase, the system was heated from 10 K to 300 K in the first 0.5 ns using NVT dynamics. Following this initial phase, the system is allowed to equilibrate at 300 K over the remaining 20 ns period. The final 15 – 20 ns period undergoes trajectory analysis.

3.4 Results and Discussion

3.4.1 Oxidation of 16-4-12: Effect of Neighbor Alkyl Chain Length on Relative Reactivity of Alkyl Chains

The result of a 30 s exposure of a monolayer of dissymmetric gemini (DG) 16-4-12 to the DBDS is shown in **Figure 3.1**. Hydroxyl-radical mediated oxidation results in a variety of oxygen-containing functional groups commonly seen in gas phase OH-mediated oxidation, namely carbonyl, hydroxyl, and peroxyl groups. The high mass oxidation products are found in groups of generations, each representing sequentially more incorporated oxygen functional groups. The first generation, representing DG + O, is observed with the most abundant product being the carbonyl $[DG + Cb]^{2+}$ product. At roughly 50% the carbonyl product intensity is the hydroxyl product, $[DG + Hy]^{2+}$. This contrasts the similar study of dodecyltrimethylammonium ion, which exhibited much lower production of the single hydroxylated product. Generation 2 consists of dicarbonyl, hydroxycarbonyl, and peroxyl product formation. Beyond this, a rich diversity of product distributions is seen for the higher n = 3 to 6 generations.

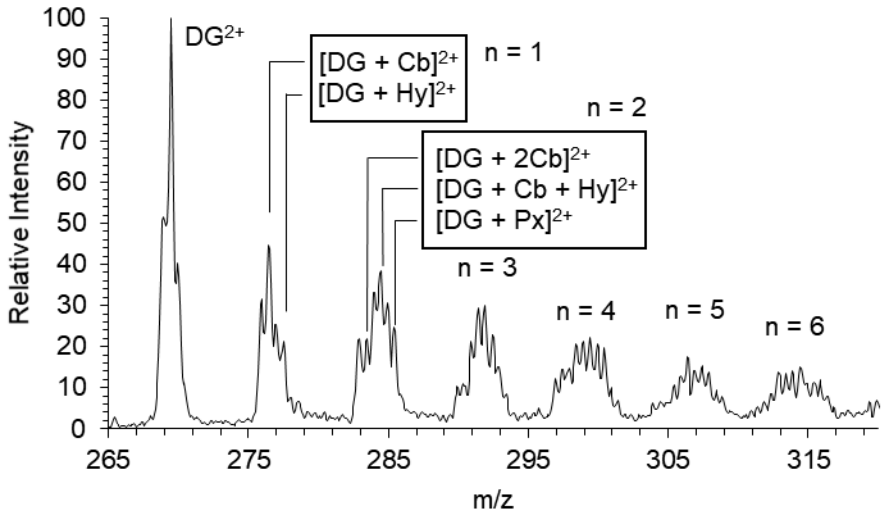

Figure 3.1. FIDI mass spectrum of dissymmetric gemini (DG) 16-4-12 after a 30 s OH exposure. Generations of products $[DG + nO]^{2+}$ are shown for n = 1 through n = 6.

The CID spectra of the carbonyl product $[DG + Cb]^{2+}$ is shown in **Figure 3.2**. The carbonyl product represents a single oxidation event initiated by a gas phase hydroxyl radical. It is therefore interesting to understand how the two chains of unequal length compete with each other to produce the first generation product. Based on the fragmentation pathways in **Scheme 3.2**, the presence of m/z 183 and m/z 239 represent cyclized oxonium ions from the dodecyl (Ox_{12}^{+}) and hexadecyl (Ox_{16}^{+}) chains, respectively. In addition, a pair of ions found at m/z 228 and 284 reflect the adduction of these oxonium ions with dimethylamine, a species originating from the alkylammonium head group of the original gemini species. The ratio of $[Ox_{12}^{+}]$:$[Ox_{16}^{+}]$ is 0.75. Under the assumption that all methylene groups exhibit identical C–H bond reactivity, the reactivity of each chain in the DG species is related to the number of methylene C–H bonds in the chain (The terminal methyl group hydrogens are omitted as gas phase data indicates that their C–H reactivity is nearly 100 times slower than methylene C–H bonds.[29]). Within this scenario the ratio of oxidized dodecyl and hexadecyl chains among a population of DG is 0.73. The agreement between the empirical and theoretical ratios indicate that the hydroxyl radical abstraction event (**Scheme 3.1** reaction 1) is a statistical event, reflecting the number of available methylene units at the air-water interface. This kind of randomized behavior can only be seen if the hydroxyl radical is long-lived enough on the monolayer to interact with many methylene units. Mechanistically, the observed DG oxidation results reflect Langmuir-Hinshelwood kinetics: the hydroxyl radical accommodates to the monolayer surface, diffusing long enough to react with methylene units

on a statistical basis. The CID spectrum of the other first generation product $[DG + Hy]^{2+}$ can be found in the **Appendix C**. Poor fragmentation yields prevented effective characterization of the CID products.

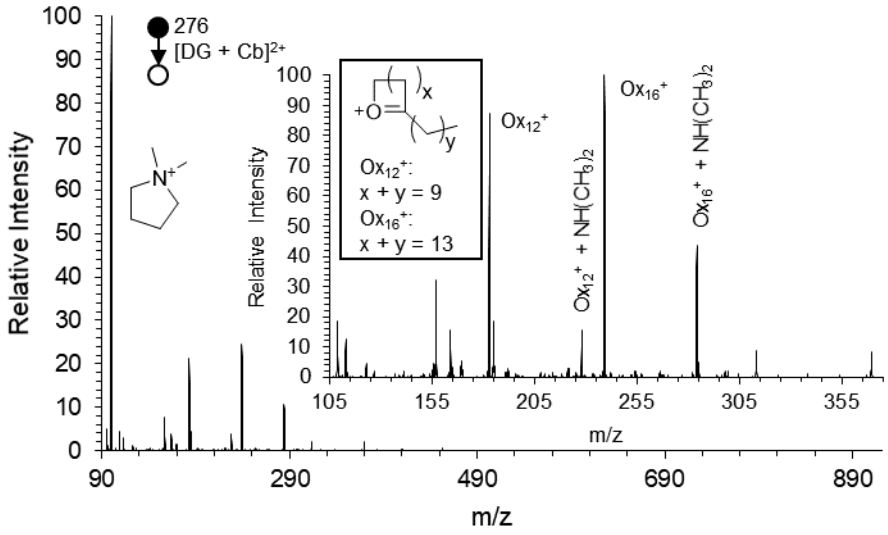

Figure 3.2. FIDI collision-induced dissociation spectrum of m/z 276, the $[DG + Cb]^{2+}$ product of DG after a 30 s OH exposure.

3.4.2 Oxidation of 16-4-16: Effect of Prior Oxidation on the Relative Reactivity of Alkyl Chains

The FIDI-MS spectrum of the symmetric gemini (SG) 16-4-16 after a 30 s exposure to the DBDS is shown in **Figure 3.3**. Over the exposure to OH, the monolayer is functionalized to carbonyl, hydroxyl, and peroxyl groups. The first generation of oxidation products is dominated by the carbonyl species at m/z 304; however, the intensity of the SG + Hy species is significantly large relative to the amount seen in DTA^+ (**See Chapter 2**). This observed deviation in oxidation is likely due to the fact that inter-chain abstraction pathways to quench the alkoxyl radical and form a hydroxyl group are enhanced in systems where hydrocarbon chains are in close proximity. The second generation products include the dicarbonyl species

(m/z 311), hydroxycarbonyl species (m/z 312), and peroxyl species (m/z 313). Based on the known reaction pathways of hydrocarbons, formation of the dicarbonyl and hydroxycarbonyl functionalities on a hydrocarbon surfactant must proceed through the interaction of two radical species. Specifically, a cascade of reactions initiated by two separate hydroxyl radical abstractions can ultimately lead to the difunctionalized species. Alternatively, carbon-centered radical generation can occur via the 1,5-hydrogen shift seen in **Scheme 3.1**. With two hexadecyl chains presented to the gas phase on the droplet surface, it becomes important to understand the interaction of the two neighboring hydrocarbon groups on the distribution of products. In one instance, functionalization of one hydrocarbon chain makes it thermodynamically more susceptible to a second functionalization. However, the known propensity of the hydroxyl radical to undergo accommodation and diffusion on the surface prior to reaction may make this inherent susceptibility less relevant to its abstraction from its final reactive partner. Similarly, intra-chain and inter-chain abstraction may show prominent deviations from known reactivity based on the proximity of the neighboring hydrocarbon chain.

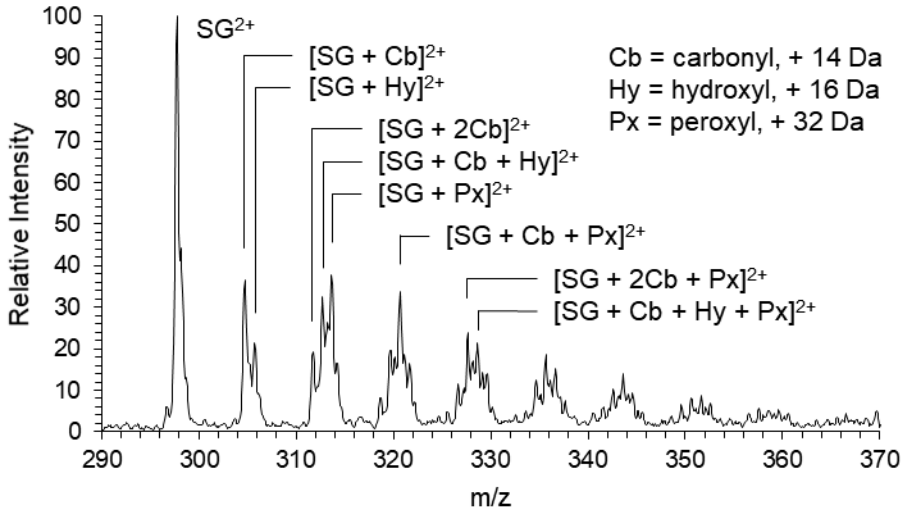

Figure 3.3 FIDI spectrum of symmetric gemini 16-4-16 (SG) after a 30 s OH exposure.

The CID of the second generation product $[SG + 2Cb]^{2+}$ is shown in **Figure 3.4a**. The dominant species in the spectrum is the cyclized fragment from the former head group and methylene linker of the parent SG species (m/z 100). While this species provides no information about the sites of functionalization, it does indicate that the fragmentation pathways provided in **Scheme 3.2** are occurring. It should also be noted that there is no evidence that this methylene linker-derived species carries functionalization, suggesting that gas phase accessible C–H bonds in the longer hydrocarbon chains are the favored reaction site.

The dicarbonyl species cyclizes via the mechanism in **Scheme 3.2b** to produce the oxonium ion at m/z 239 (Ox_{16}^{+}). This species carries no additional carbonyl group and so its presence implies that the second functionalization of SG occurs on the neighbor chain. Additionally, Ox_{16}^{+} forms an adduct with free dimethylamine ($NH(CH_3)_2$) at m/z 284 during CID fragmentation. The free dimethyl amine is released as a second Ox_{16}^{+} forms from the neighbor chain (See **Scheme 3.4a** for detailed mechanism). A peak at m/z 253 indicates the existence of the $[Ox_{16}^{+} + Cb]$ product, evidence of both carbonyl groups residing on the same hexadecyl chain. The adduct $[Ox_{16}^{+} + Cb + N(CH_3)_2]$ can be found at m/z 298.

Assuming that the extent of cyclization of the parent $[SG + 2Cb]^{2+}$ is 100%, two Ox_{16}^{+} are produced per parent $[SG + 2Cb]^{2+}$ species, due to the fact that each chain can cyclize independently. This means that the true relative intensity of m/z 311 that contains carbonyl groups on each hexadecyl chain is represented by half the intensities of the m/z 239 and m/z

284 peaks. Correcting for this, the ratio of relative amounts of difunctionalized hexadecyl products to monofunctionalized hexadecyl products is 1.33. In a case in which the likelihood of hydrogen abstraction from any methylene carbon is truly equal, the probability of reaction on a given hexadecyl chain is proportional to the number of methylene C – H bonds in the chain. Not surprisingly, this means the first oxidation event is equally likely to occur at any of the 30 methylene C–H bonds on each chain. The second oxidation event can occur on either the previously oxidized chain, which now has 2 fewer hydrogen atoms, or the unreacted chain. The probabilities are therefore 0.483 for the oxidized chain and 0.517 for the unreacted chain. The theoretical ratio of difunctionalized chains to monofunctionalized chains should therefore be 0.934. The deviation from this ratio suggests a preference for the second oxidation site to occur on the previously oxidized chain.

The CID spectrum of m/z 312 is shown in **Figure 3.4b**. The spectrum contains the oxonium ion Ox_{16}^+ at m/z 239 and a hydroxylated oxonium ion at m/z 255. There is also another pair of ions at m/z 268 and 282 that correspond to a 16-carbon cyclized ammonium ion (Amm_{16}^+). A possible mechanism for the formation of Amm_{16}^+ is shown in **Scheme 3.4b**. A freed hexadecyldiamine chain containing a hydroxyl group undergoes a proton-catalyzed nucleophilic displacement of water by the nitrogen atom, forming the Amm_{16}^+ species. The m/z 282 represents the complimentary [Amm_{16}^+ + Cb]. The presence of this pair suggests the plausibility of the mechanism, as the loss of the hydroxyl functionality upon cyclization of $[SG + Hy + Cb]^{2+}$ should produce the cyclized alkylammonium species for a monofunctionalized chain, or a oxo-containing ammonium in the difunctionalized chain. It is therefore suggested that Ox_{16}^+ and Amm_{16}^+ represent evidence that the original second

generation product $[SG + Hy + Cb]^{2+}$ is oxidized on two-separate chains, while the Ox_{16}^{+} + Hy and Amm_{16}^{+} + Cb reflect difunctionalization of a single chain.

Using the same assumption as in the case of $[SG + 2Cb]^{2+}$, the cyclized fragmentation products that do not carry an oxygen atom will produce two cyclic species per original $[SG + 2Cb]^{2+}$. Correcting for this, the ratio of difunctionalized to monofunctionalzied species is 1.79. This is dramatically higher than the ratio for which the oxidation site is randomly determined. One explanation for this observation is the importance of abstraction of the alkoxyl radical (reaction [6] in **Scheme 3.1**) for the formation of the hydroxyl functional group. Unlike the carbonyl pathways, the formation of the hydroxyl group requires the propagation of the radical reaction by a hydrogen abstraction event. Because surfactant species are not as mobile as gas phase molecules, they are limited in finding a reactive partner to their local environment, which may mean favoring abstraction from along their own chain. If this is the case, difunctionalization of single chains dominates monofunctionalization. A second explanation lies in the enhanced reactivity of the first generation $[SG + Cb]^{2+}$ species. The methylene hydrogens alpha to the carbonyl group are weakened, causing them to be the preferred site of a second OH abstraction event (Refer to **Scheme 2.3**). In either scenario the hydroxyl radical is influenced by the composition of the surfactant monolayer.

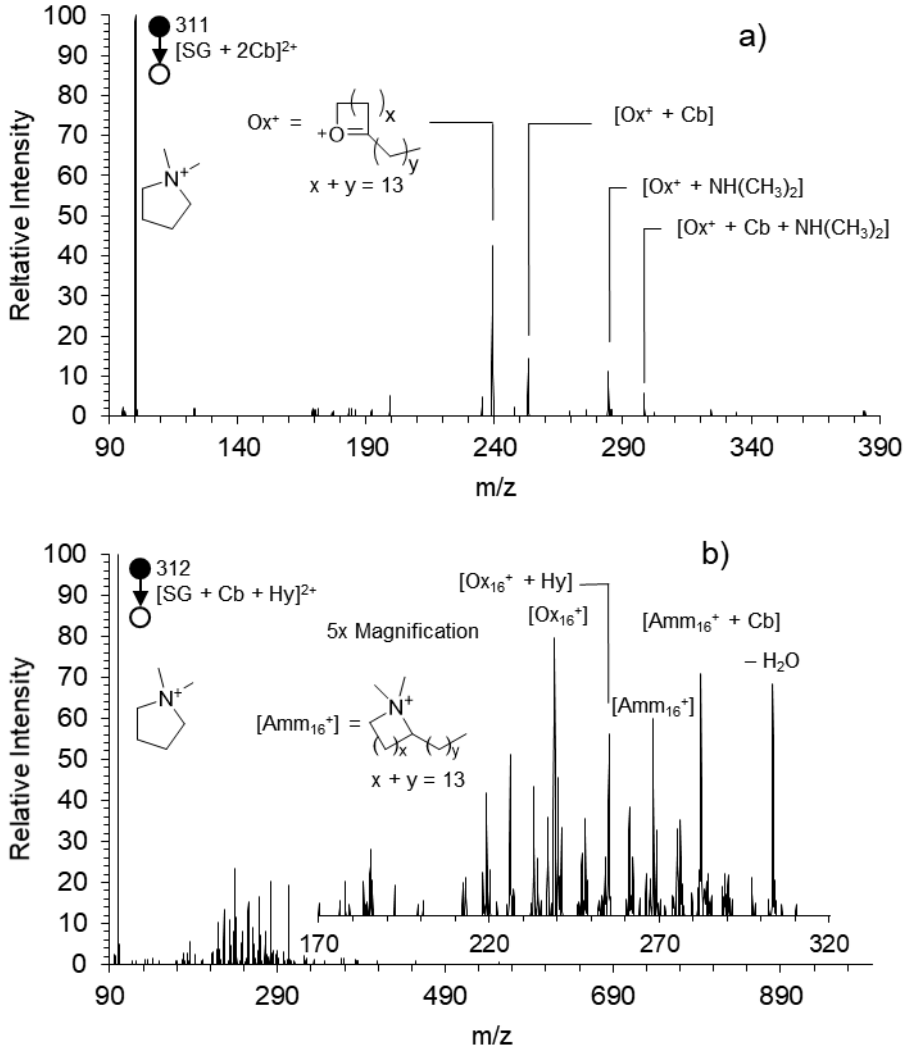

Figure 3.4. FIDI collision-induced dissociation (CID) spectra of second generation oxidation products of symmetric gemini (SG) 16-4-16 after a 30 s OH exposure. a) CID spectrum of m/z 311 $[SG + 2Cb]^{2+}$. b) CID spectrum of m/z 312 $[SG + Cb + Hy]^{2+}$.

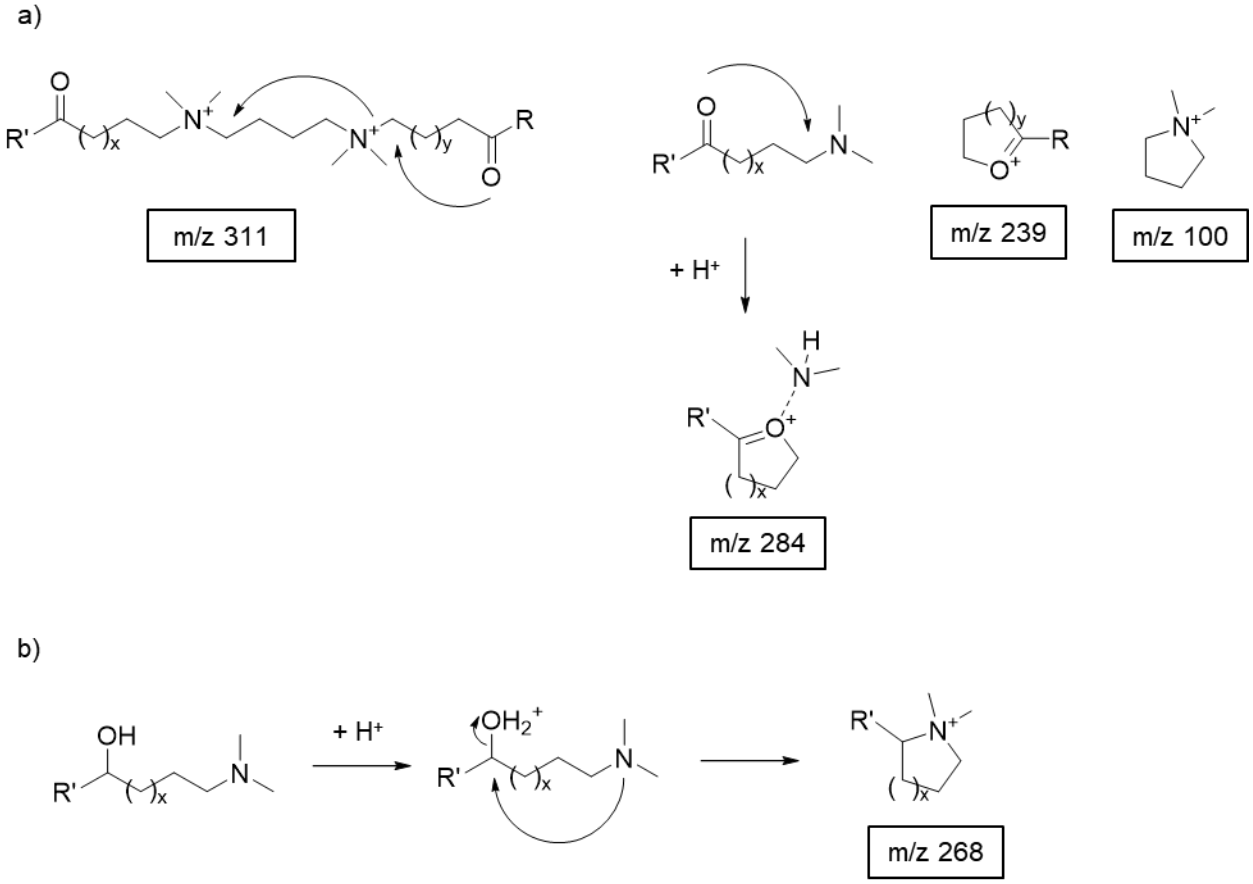

Scheme 3.4. Possible mechanisms for the formation of fragmentation products found in the CID spectra of the second generation oxidation products of SG. a) Mechanism of the formation of m/z 284 from a previously freed gemini chain.

Figure 3.5 shows the CID spectrum of m/z 313 the $[SG + Px]^{2+}$ species. Much like the analogous product for $DTA^+ + Px$ species discussed in **Chapter 2**, this species has a unique fragmentation pattern not observed in the spectra in **Figure 3.4**. The series conforms to doubly charged aldehydes formed through the fragmentation of the peroxyl group similar to that species (See **Scheme 2.2d** for mechanistic details.). Sizable amounts of chain fragments ranging in length from 3 to 14 carbon atoms are present, indicating that OH oxidation can be initiated on nearly the complete length of the original hexadecyl chain. The prevalence of product at nearly every methylene site suggests that all methylene groups appear to be

accessible to the hydroxyl radical, possibly indicating that the individual surfactant species at the air-water interface are not tightly packed, but rather have gaps and openings for the hydroxyl radical to reach the methylene units close to the head group. The ability of the hydroxyl radical to diffuse through the surface to reach these chains also suggests the lifetime of the OH radical is significant after it adsorbs, again suggesting a Langmuir-Hinshelwood mechanism at work.

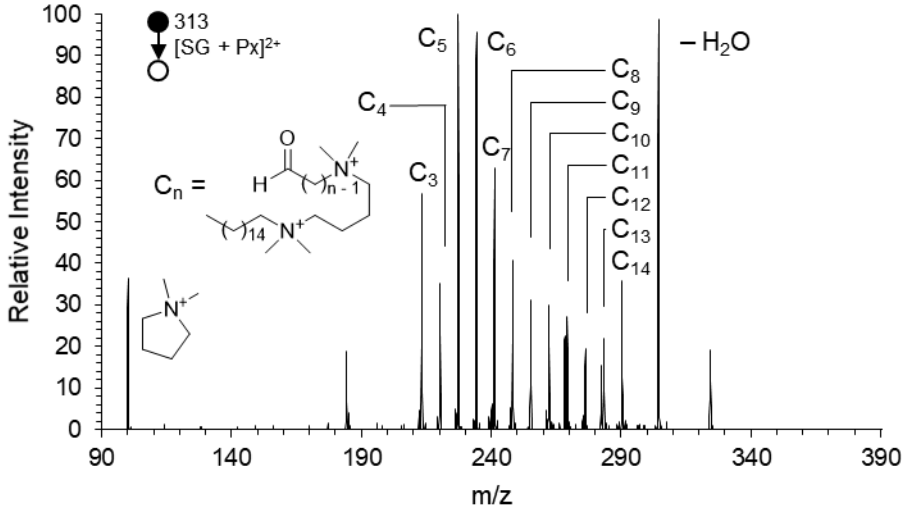

Figure 3.5. The collision-induced dissociation spectrum of m/z 313, the $[SG + Px]^{2+}$ product. Peaks labeled C_n are those in which the SG fragmented at the oxidation site, forming a truncated n-carbon chain terminating in an aldehyde group.

3.4.3 Molecular Dynamic Simulations

The results of the molecular simulations of the DG and SG monolayers are shown in **Figure 3.6**. In the context of the snapshot shown in **Figure 3.6a**, the observed relative reactivity of the hexadecyl and dodecyl chains in DG becomes apparent. At 300 K the individual chains do not form an ordered monolayer but rather form an interlaced tangle of chains at the air-water interface. The number density profile of the hexadecyl and dodecyl

chain shown in **Figure 3.6b** indicates that both chains present themselves to the gas phase to the same degree, and so the longer chain does not have a significant conformational advantage at the air-water interface. It is therefore apparent that the impinging hydroxyl radical has an equal likelihood of interacting all methylene hydrogen atoms. The ratio of singly oxidized dodecyl to hexadecyl groups similarly suggests the random nature of the heterogeneous chemistry of DG.

Figure 3.6c shows the distribution of surfactant SG over a 20 ns equilibration period along with the number density profile of atoms during the simulation (**Figure 3.6d**). The similarly disordered layer of hexadecyl chains indicates that the hydroxyl radical is capable of interacting with all chains similarly. The evidence of more than statistical amounts of doubly functionalized hexadecyl chains therefore indicates that the hydroxyl radical's selection of a chain must come from something other than an accessibility factor, implicating a thermodynamic drive to react with the previously oxidized alkyl groups.

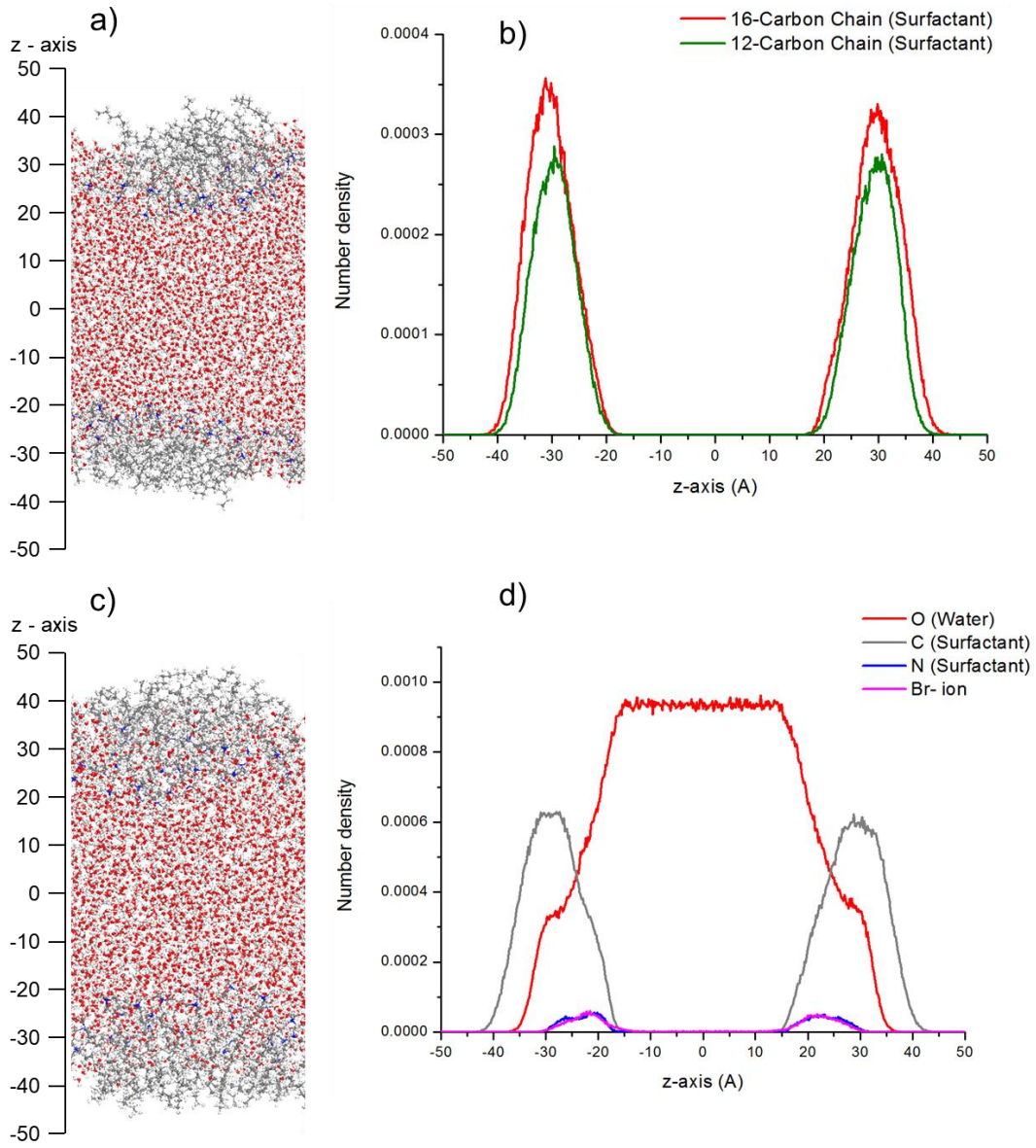

Figure 3.6. Molecular simulations for the dissymmetric gemini (DG) and symmetric gemini (SG). a) Representative snapshot of a monolayer of DG (t = 20 s). b) Average number density profile (n = 500) for the DG system. c) Representative snapshot of a monolayer of SG (t = 20 s). d) Average number density profile (n = 500) for the SG system.

3.5 Conclusions

The doubly charged gemini surfactants DG and SG served as excellent system to determine the mechanistic behavior of neighboring alkyl chain lengths in their competitive reactivity towards the hydroxyl radical at the air-water interface, specifically due to their ability to discern chain oxidation sites under CID analysis. The reactivity exhibited by both DG and SG suggests that the hydroxyl exhibits both random and particular partner-selecting behavior. For an initial oxidation, the nearly statistical ratio of oxidized C_{12} and C_{16} chains suggests no preference in reactive partner by the OH radical. This is in direct violation of the assumption that the OH radical is so reactive that it will initiate oxidation with the most prominent methylene group, i.e. those of the longer C_{16} chain. The FIDI-MS/MS data upholds this conclusion, as the CID spectrum of $[SG + Px]^{2+}$ show that the oxidation sites are distributed significantly from the third to the fourteenth carbon.

However, the FIDI-MS/MS data for $[SG + 2Cb]^{2+}$ and $[SG + Cb + Hy]^{2+}$ suggests the OH radical is more likely to oxidize a previously oxidized chain. We conclude that this is direct evidence of the diffusive behavior of the hydroxyl radical with an alkyl surfactant at the air-water interface. The OH radical is long-lived enough to sample multiple C – H bonds, making it more likely to initiate abstraction on the oxidized chain's weakened C – H bonds.

Molecular dynamic simulations by our collaborators complement our results, as the droplet surface is not an ordered array of surfactants, but rather a mass of interwoven alkyl groups from neighboring chains. Because of the disordered nature of the alkyl chains, longer chains do not project into the gas phase to an appreciable extent beyond the shorter chains. This also aligns with the observed increased reactivity of oxidized chains, as the OH radical

diffuses through the surfactant layer it is more likely to react with the weakened C – H bonds of the oxidized chain. In addition, the winding nature of the chains increases the likelihood of intramolecular isomerization. The results of this study suggest how alkyl groups in membrane lipid molecules interfere with their neighbor chains at the air-water interface.

Chapter 4

The Heterogeneous Oxidation of α,ω-Surfactants: The Influence of Hydrocarbon Conformation at the Air-Water Interface on Oxidation Pathways

4.1 Abstract

Oxidized hydrocarbons are an important component of secondary organic aerosols (SOAs). One class of oxidized organics, α,ω-surfactants, are composed of hydrophilic functional groups separated by multiple methylene spacers, and are thought to constitute up to half the composition of SOAs in the form of dicarboxylic acids. However, it is not well understood how adsorbed α,ω-surfactants on water droplet surfaces are processed by oxidants in the atmosphere. Like other hydrocarbon-derived species, α,ω-surfactants are particularly susceptible to atmospheric hydroxyl radicals (OH) at the air-water interface. The decamethonium ion ($(CH_3)_3N^+(CH_2)_{10}N^+(CH_3)_3$) is used as a model system to study the chemistry of these surfactant species. Heterogeneous OH-initiated oxidation is carried out under ambient atmospheric conditions by exposing 1.6 mm droplets to OH using the dielectric barrier discharge source (DBDS) and sampling and analyzing the oxidation products at the air-water interface via field-induced droplet ionization mass spectrum (FIDI-MS). The major initial product of the oxidation is the peroxyl product with the carbonyl functionalized species as a minor product, with extensive oxidation producing carboxylic acids. Product identities were confirmed by FIDI-MS/MS analysis. Comparative experiments of an equimolar mixture of DM^{2+} with a linear alkyl surfactant dodecyltrimethylammonium (DTA^+) shows they undergo different reactive pathways, likely

due to conformational organization at the air-water interface. A C_{14} dicarboxylic acid and C_{12} diamine α,ω-surfactant are also oxidized to determine if the oxidation pathway is influenced by head group-head group interactions. Results indicate that the reaction pathway is independent of head group interactions and surface charge of the droplet, but rather stem from conformational availability of methylene sites at the air-water interface.

4.2 Introduction

Aerosols have a dramatic impact on the climate and ecosystems of the earth, and so much interest has been invested in understanding the composition and chemical processes influencing their behavior and properties. The composition of aerosols can vary based on the local environment, but for aerosols in both urban and rural climates hydrocarbons and their oxidized products are the most widespread contributors to the mass of aerosols. While saturated and unsaturated hydrocarbons from anthropogenic[3] and biogenic sources constitute an important source of volatile species in the atmosphere, functionalized species are a major component of secondary organic aerosols (SOA) as hydrocarbons are processed by gas phase processes. The chemistry of such processes is known to be promoted at the air-water interface. It is therefore of interest to understand the stepwise chemistry of surfactants adsorbed to air-water interfaces of droplet systems with heterogeneous oxidants such as the hydroxyl radical and ozone in order to understand the progressively changing composition of aqueous aerosols.

One such class of semi-processed hydrocarbons are α,ω-surfactants, or those with hydrophobic linear chain of methylene subunits terminating on each end with polar head groups. For example, due to the prevalence of these precursor species and ambient levels of

gas phase oxidants such as ozone and the hydroxyl radical (OH), α,ω-dicarboxylic acids ($HOOC\text{-}[CH_2]_n\text{-}COOH$) are consistently found to be components of secondary organic aerosols (SOA).[5-8, 170-171] The source of such α,ω-dicarboxylic acids can be traced to pathways such as the ozonolysis of oleic acid to form azelaic acid[46, 68, 172-176] Adsorbed oleic acid on aqueous droplets and aerosols and the low volatility of the dicarboxylic acid product suggest that these species remain adsorbed after reaction, and the continual processing of these species is governed by their heterogeneous chemistry with ambient gas phase oxidants in the atmosphere.[46, 68, 172] Initial experiments involving the heterogeneous oxidation of carboxylic acids and dicarboxylic acids at the air-water interface by OH in the presence of molecular oxygen have detected that these species undergo functionalization on short (microsecond) timescales, producing carbonyl, hydroxylated, peroxyl, and under the experimental conditions transient peroxyl radical products.[60-61]

However, α,ω-dicarboxylic acids are not the only relevant α,ω-surfactant species that undergo heterogeneous chemistry in atmospheric aerosol systems. Amines and α,ω-diamines are an important class of compounds that have been given far less attention than oxygenated organic species, yet volatile amines are suggested to be major initiators of cloud condensation nuclei and atmospheric particulates,[177-178] with over 150 different amines identified in atmospheric systems.[179] Atmospheric amines are detectable in boreal forests[180-182] as well as marine environments, and are crucial to the initial formation of aerosols in systems with high amine concentration.[43, 183] The high levels of amines in forests relative to urban environments and high levels in soil and fungal samples suggest biogenic sources, and reservoirs of amines dominate their emission to the atmosphere.[181] Furthermore, volatile organic amines are found

to be highly reactive toward hydroxyl radicals,[182] and have been suggested to be important in the discussion of OH chemistry in boreal forest settings where reactivity with volatile hydrocarbons and oxygenated species cannot account for its total reactivity.[23, 184]

Because of their importance to the composition of aerosols, a study which follows the oxidative processing of a surrogate for an atmospheric α,ω-surfactant, the decamethonium ion $(CH_3)_3N^+–(CH_2)_{10}–N^+(CH_3)_3$ on the surface of microliter volume aqueous droplets is presented by gas phase hydroxyl radical. Time-resolved oxidation and sampling of a monolayer of decamethonium under ambient atmospheric conditions is achieved via field-induced droplet ionization mass spectrometry (FIDI-MS)[24, 66-70] coupled with the dielectric barrier discharge source (DBDS) discussed previously. The decamethonium ion has the advantage of the presence of two permanent charges on each head group, allowing for easier detection of fragment products that are known to be produced from oxidation. Fragmentation products of a mono-head group surfactants like fatty acid caused by the scission of C–C bonds ultimately can produce ionizable carboxylic acids, or non-ionizable aldehydes, alcohols, or peroxides.[60-61] Because only one of the two fragmentation products carries the charged head group, the other product containing a non-ionizable functionality cannot be detected using ambient mass spectrometry as the FIDI-MS method, like other ambient mass spectrometry techniques, requires samples to carry a charge, either as an adduct (e.g. protonated, sodiated, or deprotonated) or as a permanent ion.[185-188] The issue is irrelevant for decamethonium, which will carry a permanent charge on each fragment. Furthermore, the presence of a permanent charge avoids the issue of ionization suppression seen in samples that are only weakly acidic or basic.[189-191] Finally, the alkylammonium head groups in

decamethonium eliminate the volatility of fragmentation products with non-charged functionalities, meaning these species will not escape to the gas phase and be lost.

The surrogate DM^{2+} by the gas phase hydroxyl radical is followed from the incorporation of oxygen atoms to the formation of fragmentation products over a complete oxidation. Product identities are confirmed by MS/MS analysis and oxidation pathways based on known hydroxyl radical chemistry are proposed. The results are compared to a similar surfactant system with a linear alkyl chain, dodecyltrimethylammonium ion, and two other types of α,ω-surfactants, tetradecanedioic acid and 1,12-diaminododecane.

4.3 Materials and Methods

4.3.1 Materials

Decamethonium bromide (DM^{2+} bromide), dodecyltrimethylammonium (DTA^+ bromide), 1,12-diaminododecane (DAD), and tetradecanedioic acid (H_2TD) were purchased from Sigma Aldrich at the highest available purity and were used without further purification. Solutions of 150 μM concentrations were prepared and used on the same day using HPLC grade water (Omni-Solv). For experiments involving a 1:1 mixture of DM^{2+}:DTA^+, the stock 150 μM solutions of each surfactant were mixed in equal amounts to form a solution with a final concentration of 75 μM of each species.

4.3.2 Field-Induced Droplet Ionization Mass Spectrometry (FIDI-MS)

Field-induced droplet ionization mass spectrometry (FIDI-MS) was performed as described previously.[24, 66-70] Experiments involved forming a droplet (1.6 mm diameter) of the 150 μM solution of a given surfactant at the end of a 28 gauge capillary suspended between two plate electrodes spaced 0.63 cm apart. These electrodes contain apertures that

align with the atmospheric pressure inlet of an LTQ-XL mass spectrometer (Thermo-Fischer, Waltham, MA) controlled by the XCalibur software. An equilibration time of 1 minute was allowed for the surfactant to diffuse to the air-water interface, forming a monolayer of the species. The monolayer is then exposed to the dielectric barrier discharge source (DBDS), capable of generating hydroxyl radicals at ambient conditions at concentrations of approximately 10^9 cm^{-3}, positioned 0.5 cm from the surface of the droplet. After exposure, a 3 – 5 kV pulsed potential is applied between the electrodes using a LabView program, creating an electric field that induces a dipole that elongates the droplet in opposite directions. The field directs the elongating droplet toward the mass spectrometer inlet. The polarity of the pulse is chosen such that surfactant ions move with the elongating droplet in the direction of the inlet of the mass spectrometer through the plate electrode apertures. At a critical voltage, Taylor cones on each end eject microdroplets; the one containing surfactant ions is sent into the mass spectrometer where it is analyzed. The settings of the mass spectrometer are optimized for the surfactant species prior to the FIDI-MS oxidation experiment via electrospray ionization mass spectrometry (ESI-MS) and using the Xcalibur program's tune function. Repetitions of the experiment are performed by flushing the droplet from the capillary and repeating the experiment with a fresh droplet. Collision-induced dissociation (CID) experiments are performed with an isolation width of 0.8 m/z and a collisional excitation parameter of 25%.

4.3.3 Production of Hydroxyl Radicals

Hydroxyl radicals are produced using the dielectric barrier discharge source (DBDS) as described in detail previously (see **Appendix B** for construction details and characterization). The DBDS is operated at 12 kV_{pp} voltage, 1 kHz frequency, and 1.42 mA current.

4.4 Results and Discussion

4.4.1 Oxidation of Decamethonium Ion (DM^{2+})

Figure 4.1 shows the progression of the OH-initiated oxidation of a monolayer of DM^{2+} at the air-water interface under ambient conditions. Non-fragmented products are assigned to a generation based on the number of oxygen atoms added to the parent molecule, with the n^{th} generation containing n oxygen atoms. An initial 10 s oxidation produces a product at m/z 145 (**Figure 4.1a**), corresponding to two possible second generation products, the dihydroxy or peroxy isomer. At an intermediate exposure time of 30 s (**Figure 4.1b**) the monolayer shows approximately 25% conversion to both the m/z 145 product as well as an m/z 136 carbonyl product. The theoretical hydroxyl product should appear at m/z 137, yet is not found in the spectrum, indicating the carbonyl is the dominant first generation product. Even at an exposure time that converts over 70% of the original parent to products (**Figure 4.1c**), the first generation never accumulates to an extent to form a majority on the droplet, a marked difference between this system and the linear alkyl surfactant dodecyltrimethyl ammonium (DTA^+) previously studied. Instead, the second generation peroxy product remains a major species, along with even higher generation products. Notably, the major products for the second through fifth generations at the 60 s exposure include m/z 145 (DM^{2+} + Px), 152 (DM^{2+} + Cb + Px), 161 (DM^{2+} + 2Px), and 168 (DM^{2+} + Cb + 2Px). Interestingly, these products all correspond to products with pairs of hydroxyl shifts (+32 Da). This suggests that these two oxygen atoms are incorporated into the surfactant together. Of the known OH oxidation pathways[13, 17, 25, 39, 60-61, 100-104, 192] as shown in **Scheme 4.1**, the addition of oxygen after the initial hydrogen abstraction produces a peroxyl radical, followed by a second hydrogen abstraction by this radical, can result in the peroxyl product with an appropriate

mass and signal shift in the spectrum (reactions [1], [2], [3]). In contrast, the carbonyl product requires ultimately a second hydrogen abstraction event by a neighboring radic al, which can be achieved by degradation of the relatively unstable peroxyl radical formed in reaction [4] to an alkoxyl radical. Reaction [4] has been documented in gas phase systems via a number of proposed mechanisms. This species is long-lived enough that molecular oxygen, or a radical species can add to the radical site, abstract the alpha hydrogen, and leave causing the formation of the double bond. The higher generation products can be attributed to following the same pathways in sequence.

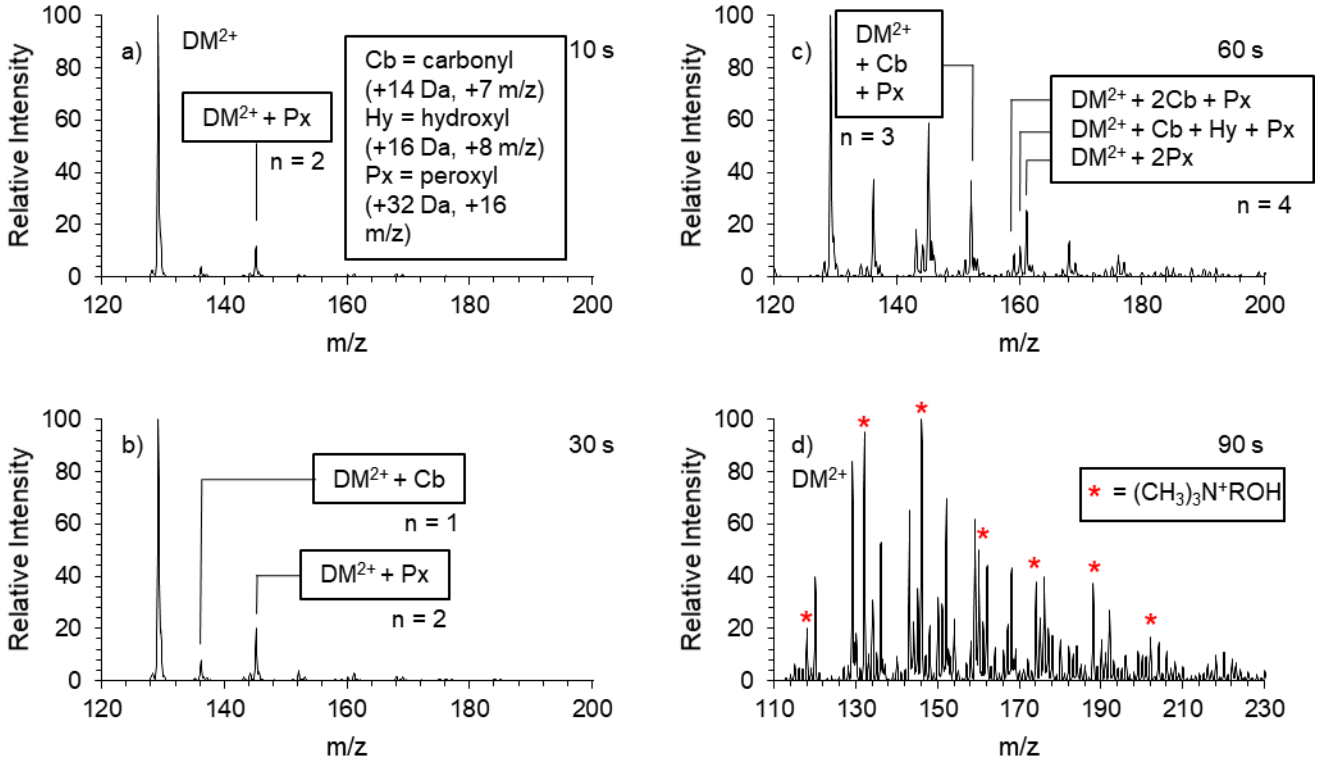

Figure 4.1. FIDI mass spectra over a nearly complete conversion of decamethonium (DM^{2+}) to oxidized products over an exposure of hydroxyl radical via the DBDS. a) 10 s DBDS exposure. N = 3. b) 30 s DBDS exposure. N = 4. c) 60 s DBDS exposure. N = 4. d) 90 s DBDS exposure. The symbol "*" represents the series of hydroxyl-containing fragmentation products. N = 4.

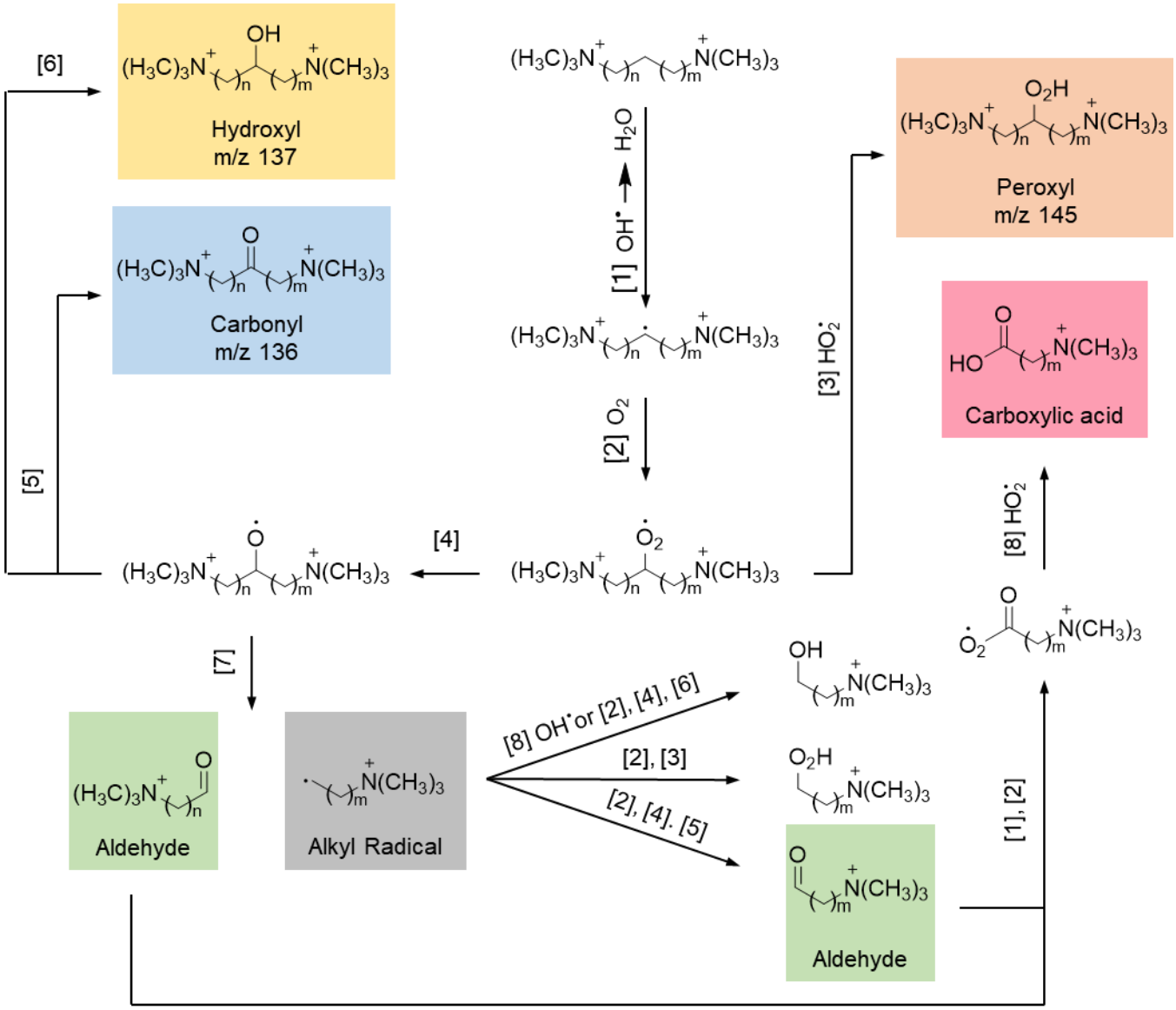

Scheme 4.1. Possible Pathways of OH-mediated oxidation of decamethonium (DM^{2+}) at the air-water interface based on known OH reactions under ambient atmospheric conditions. For DM^{2+} m + n = 9.

Collision-induced dissociation analysis was performed on the major first and second generation products to confirm the assignment of these major oxidation products. **Figure 4.2a** shows the CID of m/z 136. The major fragmentation peak at m/z 106 is indicative of head group loss. This is attributed to a carbonyl group displacing the head group by nucleophilic attack, releasing it as the neutral trimethylamine. Unlike the CID of other carbonyl-containing products of trimethyl alkyl ammonium ions, the trimethylamine species is also observed as the protonated species at m/z 60 as well as a water-bound adduct at m/z 78. The source of the labile protons and water molecules required to create these ions are likely due to stepwise processes involving the combined interaction of the carbonyl group and both head groups. The increased importance of pathways leading to these other products might be due in part to the electrostatic repulsions of the identically charged head groups. This may also be the source of the minor peaks in the spectrum. Nonetheless, the similarity of this species to the fragmentation of oxidized dodecyltrimethylammonium (**Figure 2.3** in Chapter 2) suggests the majority of signal from m/z 136 is the DM^{2+} + Cb compound.

Figure 4.2b shows the CID spectrum of the major oxidation product at m/z 145. The major dissociation produces a series of peaks corresponding to aldehydes varying from 3 to 8 carbon atoms in length, formed after scission of C–C bonds. This type of product is likely suggestive of the identification of the m/z 145 as a peroxide. Like other peroxides, upon excitation the peroxide O – O bond breaks, forming an alkoxyl radical. With no means of quenching this radical stabilizes in a manner identical to that shown in **Scheme 4.1** reaction [7] to form the aldehyde. Interestingly, the five carbon aldehyde is absent from the series. Because aldehyde functional groups occur at the site of the original oxidation, this means

peroxide groups at carbon five proceed through different fragmentation pathways. For example, the presence of m/z 136 matches DM^{2+} + Cb, which can come from the degradation of the peroxide group to a carbonyl group accompanied by water loss. This may also explain the shared peaks of the CID spectrum of m/z 136 and 145, including the cyclic m/z 106 species which is formed by carbonyl attack of a head group, and m/z 60 the head group loss. **Figure 4a** and **Figure 4b** together show that the two major products behave similarly to the carbonyl and peroxide functional groups discussed for DTA^{+} oxidation products in Chapter 2.

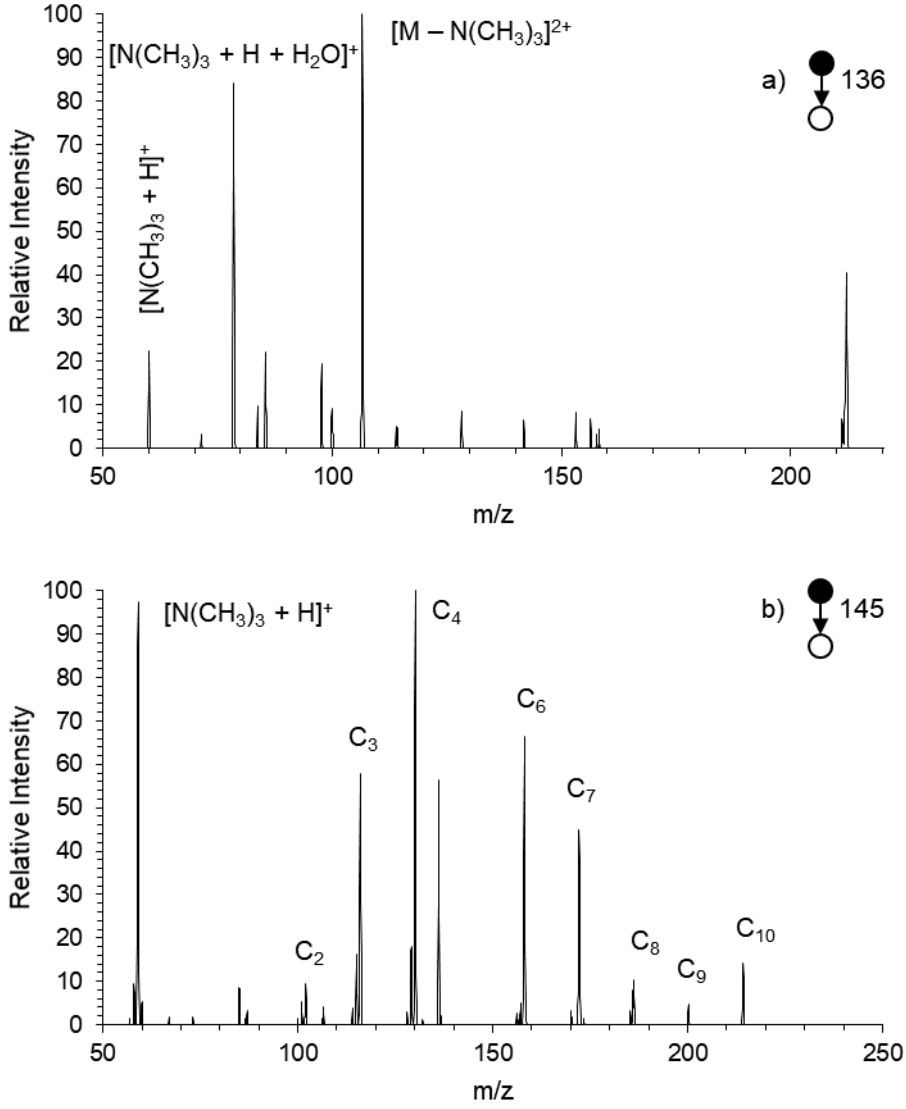

Figure 4.2. The FIDI-CID spectra for the two major initial products of OH-initiated oxidation of DM^{2+}. a) CID spectrum of m/z 136, the carbonyl product DM^{2+} + Cb. b) CID spectrum of m/z 145, the peroxide product DM^{2+} + Px.

Figure 4.1d depicts extensive oxidation of the DM^{2+} monolayer with considerable fragmentation. Fragmentation is deduced by locating comparing the spacing of ^{13}C peaks. A low mass product caused by breakage of the DM^{2+} along the alkyl moiety reduces the charge

of the species by 1, the effect of which is a decrease in the spacing of the product's charge from 0.5 m/z spacing to 1 m/z spacing. The major product is a singly charged product residing at m/z 146. One plausible structure is that of a species with a trimethylammonium head group with a five-carbon alkyl tail terminating in a hydroxyl functional group ($((CH_3)_3N^+(CH_2)_5OH)$. Furthermore, this species belongs to a series of singly charged peaks are present spaced by 14 m/z, namely m/z 118, 132, 146, 160, 174, 188, and 202 (labeled with "*" in **Figure 4.1d**), suggesting they form a series of similar products of varying methylene number in the main alkyl chain. This implies that these products are caused by scission of C–C bonds at different positions in the parent DM^{2+}, producing alcohol fragments of 3 to 8 carbon atoms in the alkyl chain. Mechanistically, this can be produced when, upon formation of an alkoxyl radical, scission of the nearest C–C bond produces an aldehyde species and an alkyl radical fragment. The alkyl species can be quenched through any of the pathway reactions. Direct addition of a hydroxyl radical (reaction [8]) can then produce the hydroxyl product, or stepwise conversion of a peroxyl radical after oxygen addition (reaction [2]) can ultimately form a hydroxyl product by forming the alkoxyl radical (reaction [4]), and a radical quenching event caused by hydrogen abstraction.

It should be noted that the m/z of this series can also be attributed to products that contain a carbonyl in addition to the hydroxyl (i.e. carboxylic acid or hydroxycarbonyl products), in which case the above-mentioned series corresponds to products with chain lengths of 2 to 7 carbon atoms. This is due to the fact that at the resolution of the mass spectrometer the addition of a carbonyl group to a saturated alkyl chain has an identical m/z shift to that of a species that contains one extra methylene unit in the chain. This species can be achieved

simply by reaction of the aldehyde fragmentation product. The aldehydic hydrogen is particularly susceptible to abstraction to form an acyl radical.[13] Carboxylic acids are known to be formed through the oxidation of aldehydes, by oxygen addition and the reaction with ambient HO_2.[39, 192] Alternatively, the hydroxycarbonyl can be produced by two oxidation events on the parent DM^{2+}, with one event imparting either a carbonyl or hydroxyl group to the main chain, while the other induces the fragmentation producing the complimentary functional group. While this complicates the identification of fragment products, based on the mass shifts accompanying the addition of oxygen atoms it can be said with certainty that it is impossible that peroxyl functional groups are incorporated into this series.

If it is assumed that the members of this series are composed mostly of the alcohol-type products, then the relative intensity of the peaks suggests that the DM^{2+} has a tendency to fragment from the center of the alkyl moiety, m/z 146 and 132 corresponding to five and four carbon species, respectively. This observation is telling of the behavior of DM^{2+} at the air-water interface. Due to the presence of two charged head groups on each end of the surfactant, each end is essentially pinned to the surface of the droplet where the two groups can interact with water molecules and bromide counterions. This imparts a looped conformation to the alkyl portion of the species, making the central methylene groups the most exposed to the gas phase and therefore susceptible to the hydroxyl radical. The further a methylene group is from the center (i.e. the closer it is to the head group), the more likely it is pulled toward the aqueous phase, making it less exposed to the gas phase and suggesting a reduced reactivity the gas phase species necessary to oxidize those carbon sites. Even if the

products are assumed to be carboxylic acids, the intensities still suggest that central atoms are more prone to be the site of fragmentation.

It should be noted that although an aldehyde is always produced as one of the fragmentation products, the predicted series of 1 to 10 carbon aldehydes at m/z 88, 102, 116, 130, 144, 158, 172, 186, 200, and 214, the intensity of peaks at these locations is relatively low, suggesting that the aldehyde is being consumed at rates comparable to its formation. This may give credence to the assignment of the alcohol-containing species as a more highly oxidized product derived from the aldehyde, specifically the carboxylic acid.

4.4.2 Direct Comparison of the Pathway Preference of a Mixture of the Looped Surfactant Decamethonium and the Free Surfactant Dodecyltrimethylammonium

In contrast to the previously studied dodecyltrimethylammonium ion (DTA^+), DM^{2+} exhibited unique product distributions upon heterogeneous oxidation at the air-water interface. The DTA^+ monolayer system produces carbonyl and hydroxyl in greatest abundance, with minor amounts of the peroxide products, while the DM^{2+} monolayer system favors the peroxide forming pathway, with carbonyl and hydroxyl functionalizations having a minor influence on the product distribution. In order to confirm that this behavior is not an artifact of some unknown procedural error, OH oxidation was carried out in a droplet containing both DTA^+ and DM^{2+} in equal amounts. **Figure 4.3** depicts the direct comparison of the initial surface oxidation of a droplet containing equimolar (150 μM total surfactant concentration) mixture of DM^{2+} and (DTA^+) by hydroxyl radicals using FIDI-MS analysis. The major product for DM^{2+} is the peroxide product at m/z 136, while DTA^+ favors the carbonyl and dicarbonyl products at m/z 242 and 256, respectively. Furthermore, DTA^+ is

more extensively oxidized, showing small amounts of five generations of products, while DM^{2+} only shows two generations of products. In a droplet containing both surfactants, each type of species.

The source of the difference between these two types of surfactants may lie in the conformation these two species adopt at the air-water interface. The DTA^{+} monolayer at the air-water interface has been studied via molecular simulation in numerous cases and has shown that for the analogous tetradecyltrimethylammonium ion, the chains themselves are quite disordered, forming a "rough" surface with considerable bending of the tetradecyl groups due to the presence 2-3 gauche methylene-methylene conformations per chain.[193] Simulations have similarly characterized the cetyltrimethylammonium monolayer as disordered.[194] If this behavior is extrapolated to the present system, the dodecyl chains of DTA^{+} are quite flexible and so the angular distribution of chains relative to the surface is sizeable. On the other hand, DM^{2+} has two head groups, each identical to that of DTA^{+}, terminating either end of the surfactant's alkyl chain. With both hydrophilic head groups behaving as the DTA^{+} case, the DM^{2+} surfactant has each head group pinned to the aqueous phase, forcing the alkyl moiety to adopt a loop curvature projecting into the gas phase. This orientation restricts the mobility of the alkyl group of DM^{2+} relative to DTA^{+}. Because the pathways found in **Scheme 4.1** require the radical site to undergo several searches for a partner, it is likely that pathways that minimize the required number of radical reactions would be favored. In this case the peroxide-forming pathway carries this advantage, despite the fact that the peroxide group is the least stable relative to the carbonyl or hydroxyl functionalization.

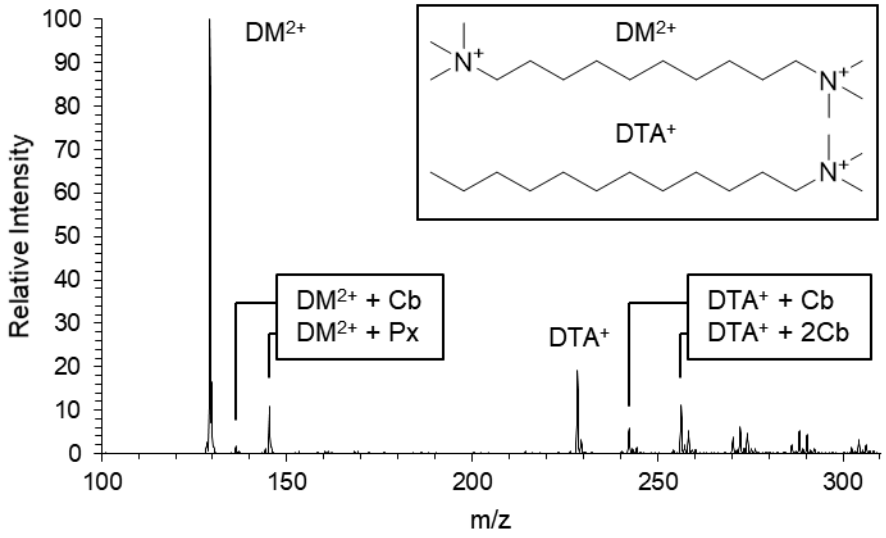

Figure 4.3. Representative FIDI mass spectrum of an aqueous 1.6 mm droplet containing 75 μM DTA^+ and 75 μM DM^{2+} after a 60 s DBDS exposure condition.

A FIDI spectrum showing the equimolar mixture of DTA^+ and DM^{2+} and an electrospray ionization spectrum of an equimolar solution of the two surfactants are found in **Appendix D**. The ratio of intensity of DTA^+ to DM^{2+} varies based on the type of ionization, and may be due to several sources, including the electrostatics of the species in the mass spectrometer, and are also dissimilar to the relative amounts of DTA^+/DM^{2+} found in **Figure 4.3**. It is for this reason that a direct comparison of the absolute amounts of all species cannot be used to comment conclusively on the reason for the unequal intensities of the DTA^+ series and the DM^{2+}

4.4.3 Testing the Influence of the Head Group Interactions on Directing the Oxidation of α,ω-Surfactants at the Air-Water Interface

The DM^{2+} system represents only a small number of surfactants that carry permanent charges in their head groups. The presence of these charges is known to play an important

part in the ordering of the main alkyl chains and water molecules at an air-water surface,[195] and so this may in part, influence how the chains behave with each other and the hydroxyl radicals at the air-water interface. Specifically, the two positively charged head groups of DM^{2+} exhibit solely repulsive interactions that would promote the elongation of the chain. It is therefore important to consider a case in which the head groups are capable of attractive intermolecular interactions, and determine whether surfactants of this type share similarities to DM^{2+} in their oxidation patterns. Two other α,ω-surfactants were chosen to determine if the head group is responsible for the unique oxidation phenomenon of this type of surfactant: the basic surfactant 1,12-diaminododecane (DAD) and acidic surfactant tetradecanedioic acid (H_2TD). These two molecules were chosen for study due to their resemblance to compounds found in natural atmospheric systems, as well as the potential attractive interaction of their head groups at the air-water interface via hydrogen bonding (RNH_2---H_3N^+R and RCO_2^----HO_2CR for DAD and H_2TD, respectively). In addition, they each form monolayers of positive or negative charge. Identical systems of DAD and H_2TD were exposed to OH using the FIDI-MS and DBDS setups in the same procedure as the DM^{2+} system.

The resulting spectra for an initial oxidation are shown in **Figure 4.4**. For the DAD system (**Figure 4.4a**), species are present in the singly charged protonated state ($[HDAD]^+$) and the doubly protonated ($[H_2DAD]^{2+}$). The major initial oxidation products are m/z 117 for the doubly charged series and m/z 233 for the singly charged series, both of which correspond to the incorporation of a peroxide functionality. For H_2TD only the singly ionized $[HTD]^-$ is detected in the FIDI spectrum at m/z 257 (**Figure 4.4b**). However, the preference

for peroxides is found for this species as well. In addition, this species is more extensively oxidized, and the third and fourth generations can be resolved. Similarly to DM^{2+}, the pattern of mass shifts suggest oxygen atoms are being incorporated in pairs of singly bonded oxygen atoms along with carbonyls. This behavior lends itself to the assertion that the incorporation of oxygen in α,ω-surfactants occurs as a peroxyl group rather than two individual hydroxyl groups.

The observation that α,ω-surfactants trimethylammonium, amino, and carboxylic acid head groups all conform to the same pattern suggests that the oxidative pathway by which α,ω-surfactants proceed is invariant to the identity of the head group. More likely, the source of the preference in peroxide product formation lies in the fact that the methylene units linking the head groups together are conformationally constrained in a looped orientation projecting into the gas phase, while the head group remains solvated. If this is the case, then the only concern is whether the terminating head groups are efficiently solubilized in the aqueous phase, which is the case for the surfactants studied.

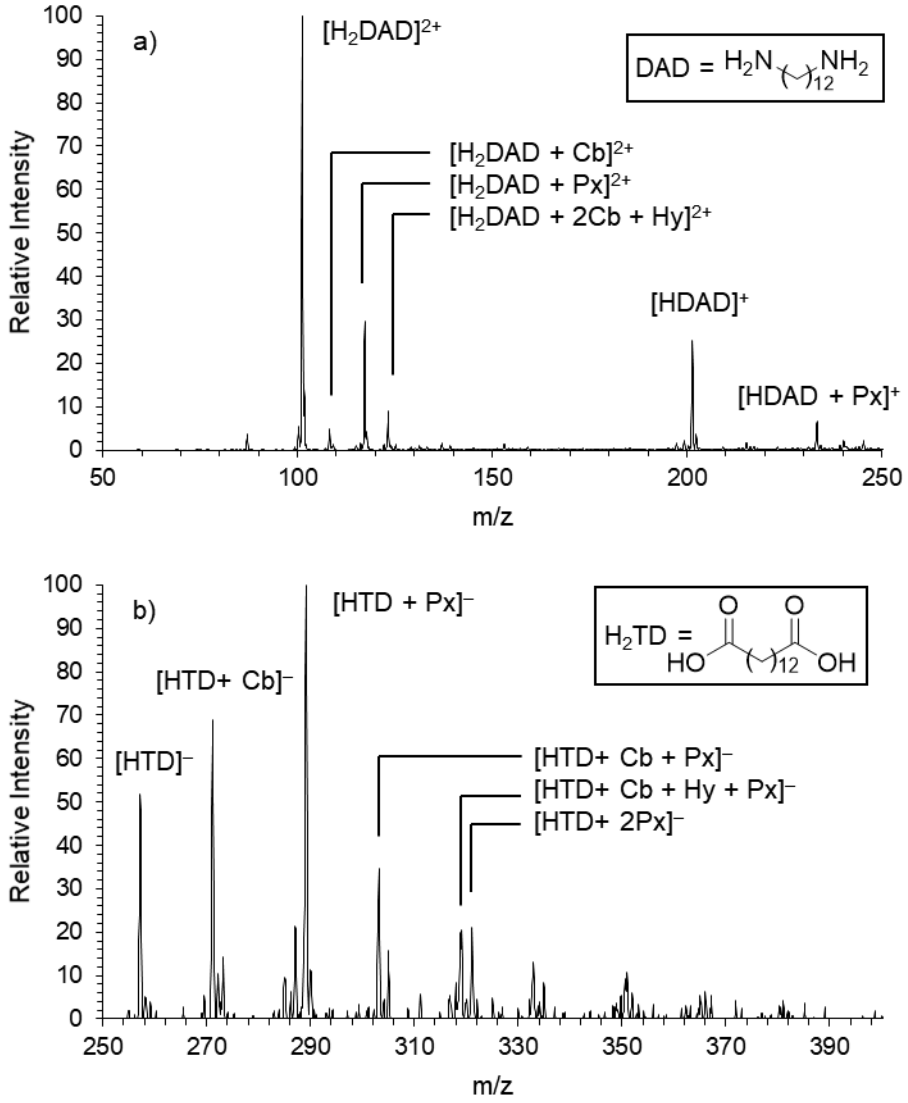

Figure 4.4. FIDI mass spectra of basic and acidic α,ω-surfactants after exposure to the DBDS. a) Positive mode spectrum of 1,12-diaminododecane (DAD) after a 30 s exposure to OH. Parent and product species are observed as the protonated and doubly protonated cations. N = 3. b) Spectrum of tetradecanedioic acid (H_2TD) after a 45 s exposure to OH. Parent and product species are observed as the deprotonated anions. N = 3.

4.5 Conclusions

This work provides insight on the ambient heterogeneous OH-oxidation of α,ω-surfactant class of molecules over a nearly complete processing at the air-water interface by utilizing FIDI-MS with DBDS OH production. The DM^{2+} provides unique detail of the reaction as its dual charged trimethylammonium head groups allow easy detection of fragmentation products of the OH-initiated reaction. The system also produces characteristic collision-induced dissociation fragments that can elucidate which of the possible product isomers is the major component of a given product signal in the spectrum, and it was successful in its ability to discern that DM^{2+} incorporates oxygen predominantly as a peroxyl group. This is in direct contrast to the linear alkyl surfactant system, whose oxidation progression favors the formation of carbonyl groups. Even in a mixed monolayer, the two species undergo their respective pathways, indicating that the FIDI-MS can observe the interfacial phenomena stemming from each surfactant's individual behavior on the droplet surface. The study of α,ω-surfactants with different head groups indicates that this unique behavior is independent of the head group identity. Finally, fragmentation products are cleanly detected and likely correspond to carboxylic acid groups, detected as a series of such species that can be clearly differentiated from high mass products by the spacing of their isotope peaks.

Chapter 5

Heterogeneous Hydroxyl Radical-Mediated Oxidation of the Amphiphilic Peptide Substance P as a Footprinting Technique

5.1 Abstract

Protein footprinting is an established analytic technique for the determination of higher order structural features of soluble proteins and peptides. However, this technique is limited to direct identification of solvent accessible residues as the oxidative reagents are generated in the aqueous phase. Information pertaining to the hydrophobic residues is not directly observed during analysis. This is particularly problematic as amphiphilic peptides are garnering interest for a variety of purposes. We have developed a novel footprinting technique that directly probes interfacial conformational features of a surface active undecapeptide substance P (RPKPQQFFGLM) localized at the air-water interface of 1.6 mm diameter droplets by generating hydroxyl radicals as the oxidant under ambient conditions via a dielectric barrier discharge source (DBDS). The resultant oxidative modification is elucidated by mass spectrometry by utilizing the surface-selective field-induced droplet ionization mass spectrometry (FIDI-MS) technique. It is found that while substance P has several residues similarly susceptible to oxidation, the C-terminal methionine is the most susceptible oxidation site, suggesting that this residue is significantly more gas phase-accessible when substance P is structured in a monolayer at the air-water interface. This technique shows promise in peptide/protein systems that adopt unique secondary structures at the air-water interface.

5.2 Introduction

Cellular systems must balance the need to allow entry of nutrients into their interior, exclude extracellular media, and communicate with their surroundings. Phospholipid membranes have evolved to be the barrier of choice for biological systems, though this barrier indiscriminately excludes small molecules from the aqueous phase. It is the role of specialized proteins to bridge the gap, both metaphorically and literally, to allow important chemical species to cross cell membranes. Since their discovery, proteins and peptides which imbed into or adsorb onto the interfacial region between hydrophobic-aqueous environments are of much interest.

Proteins and peptides are continually being considered for applications as therapeutic agents, molecular transport vectors, and industrial uses. An understanding of the behavior of such amphiphilic proteins can help in the design and investigation of synthetic proteins for use in bionanotechnology, where specially designed amphiphilic proteins can create pseudo-organelles for the generation of artificial cells.[196] Surface active peptides show promise in applications of conventional surfactants, outcompeting alkylammonium and alkyl sulfate surfactants to form monolayers at the air-water interface.[197] However, for surfactants containing amino acids, small changes in steric bulk or chirality in a residue can affect the behavior (i.e. compression isotherms) of the species.[198]

Furthermore, cell-penetrating peptides carry the necessary hydrophobic and hydrophilic domains to travel through membranes through passive processes (i.e. mechanisms that require no energy input) in addition to those that induce structural changes in the membrane to allow their transport (i.e. endocytotic mechanisms).[199-202] The source of the influence these

species have on membranes lies in the interplay of molecular distinct hydrophobic and hydrophilic domains within the species. Such peptide amphiphilicity has been shown to induce important secondary structural changes, such as the formation of helical[203-207] or hairpin[208-210] motifs under ambient biological conditions. The air-water interface is known to facilitate or imbue similar structural changes and promote conformational reorganization to surface active peptides.[211-214] Such observed macromolecular architecture has made both naturally occurring and synthetic peptides of interest. The efficient prediction and design of novel surface active peptide sequences with specific physical properties has been an active field of research in recent years.[215] This is especially important as single changes in residue change the higher order properties of proteins, such as propensity to form gels.[216]

Because secondary structure plays a large role in the properties of surface active peptides, it is of interest to monitor the native conformation under ambient conditions at air-water interfaces. Protein footprinting has long been utilized to probe conformation of proteins by subjecting a solubilized protein sample to hydroxyl radicals and detecting the oxidation products via mass spectrometry. Residue modification is a function of both side chain relative reactivity and access of the residue to the aqueous phase where hydroxyl radicals are generated, and so hydroxyl radical protein footprinting is capable of identifying residues that present themselves to the aqueous phase.

The oxidation of the biologically relevant amino acids has been studied extensively under aerobic conditions.[78, 217-222] **Scheme 5.1a** shows the result of oxidation of several sidechains during OH exposure of a protein or peptide in solution. Arginine residues form a characteristic oxidation product by the reaction of the hydroxyl radical with the δ-carbon site

on the side chain labeled in **Scheme 5.1a**.[220] This methylene, and in fact all methylene groups, are susceptible to hydrogen abstraction by the hydroxyl radical to form a carbon-centered radical. Molecular oxygen adds at this site to form a peroxyl radical RO_2. Ambient aqueous HO_2 radical is proposed to convert this radical to a hydroxyl species, which then collapses to form an aldehyde as the side chain loses the guanidine functional group. The resultant oxidized species results in a loss of 43 Da (**Scheme 5.1a**, reaction [1]). The hydroxyl radical Aromatic rings such as those in phenylalanine (**Scheme 5.1a**, reaction [2]) are susceptible to addition of the OH radical to the ring creating a radical.[78, 217] The radical is quenched by the addition of oxygen and subsequent loss of hydrogen peroxide to form a phenol-type product that carries a mass shift of + 16 Da, typically in an ortho or meta configuration.[221] Aliphatic residues such as leucine (**Scheme 5.1a**, reactions [3] and [4]) are attacked by hydroxyl radicals at C–H. Much like hydrocarbons,[17] these residues readily form carbonyl groups (+ 14 Da) and hydroxyl groups (+ 16 Da).[222] In methionine-containing residues, the hydroxyl radical adds to the sulfur atom to form a sulfur-centered radical.[219] Molecular oxygen adds to the sulfur, followed by the loss of HO_2 to form the sulfoxide species (**Scheme 5.1a**, reaction [5]) with a 16 Da increased mass.

Because some distinct modifications are reflected by the same mass shift, MS/MS analysis has been used as an integral part of protein footprinting analysis.[223-227] Post-oxidation, the product's mass-to-charge ratio is isolated within the mass spectrometer and subjected to collisions with a gas molecules, transferring their kinetic energy to the internal energy of the peptide. This energy causes the peptide to fragment in a process known as collision-induced dissociation (CID), often at the peptide backbone. Commonly, the resulting

peptide is the result of bond scission at the peptide bond as shown in **Scheme 5.1b**.[222] Using the nomenclature of proteomic studies,[228] the b-type ions, those retaining the N-terminus of the peptide, and y-type, those retaining the C-terminus of the peptide, are used to identify the location of oxidation. The presence of native b-/y-ions in the MS/MS mass spectrum are indicative that oxidation did not occur in the residues contained in the ion. However, ions that are shifted reflect the presence of an oxidized residue contained within the fragment's sequence.

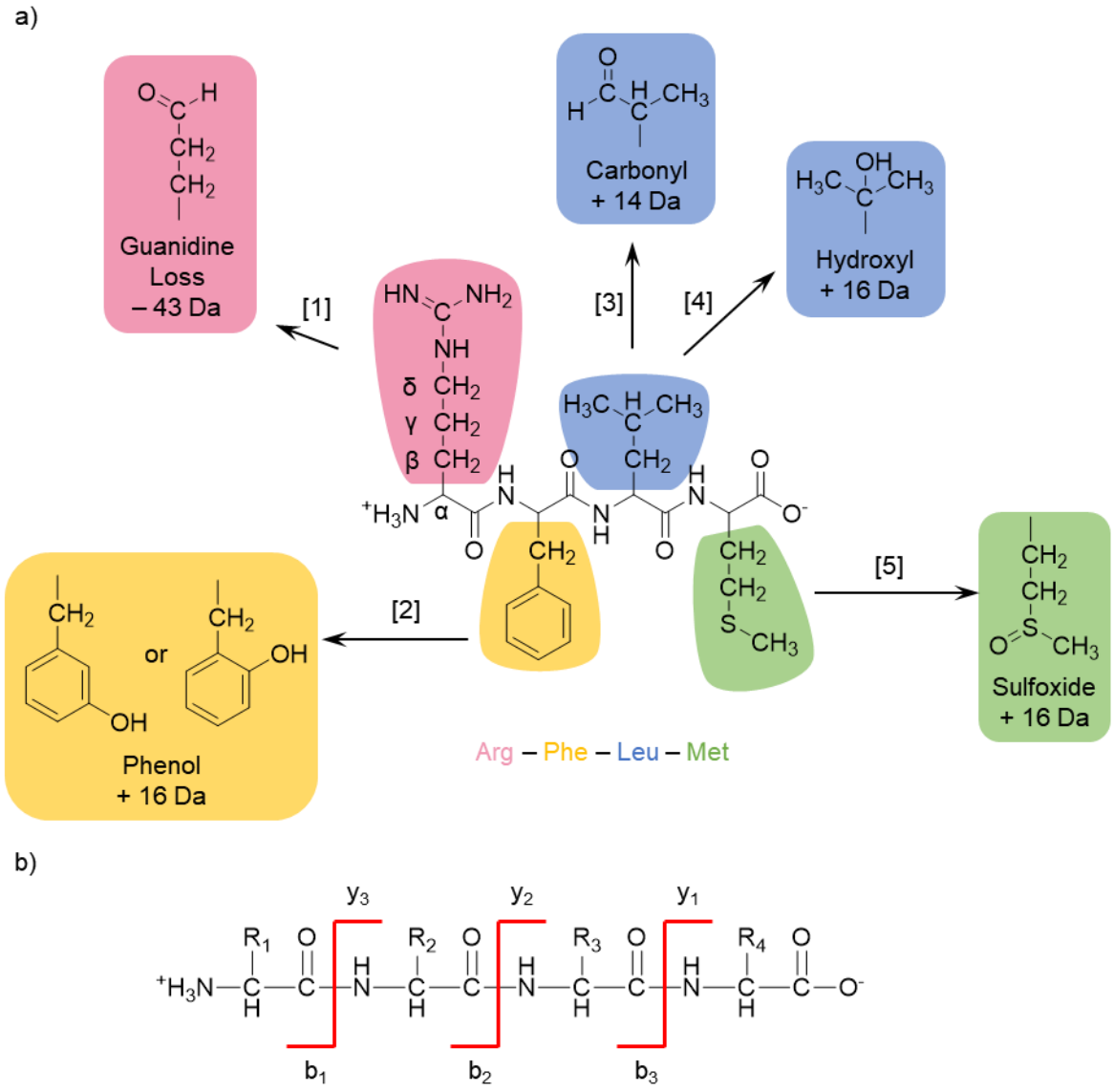

Scheme 5.1. Chemistry pertinent to footprinting experiments of a peptide. a) Pathways and mass shifts representative of the oxidation of residues arginine (Arg), phenylalanine (Phe), Leucine (Leu), and Methionine (Met) by a hydroxyl radical-initiated event in a hypothetical tetrapeptide. b) Collision-induced fragmentation sites of the peptide backbone to produce b_n- and y_n-type fragment products. The subscript n denotes the number of residues found in the ion.

Several methods of hydroxyl radical production are available for protein footprinting. Hydroxyl radical generation in aqueous protein samples can be produced through Fenton

chemistry ($Fe^{2+} + H_2O_2 \rightarrow Fe^{3+}$ OH + OH^-)[229-231] Discharges in electrospray ionization sources,[232] or the radiolysis of hydrogen peroxide[233-235] or water.[236-238] While each of these methods has proven successful in mapping the solvent-accessible residues by producing aqueous phase OH, it is of value to apply heterogeneous OH generation to map the gas-phase accessible residues of surface active peptides. We present the successful application of a dielectric barrier discharge source (DBDS) to generate OH under ambient conditions in air to expose macroscopic droplets containing the surface active peptide substance P (SP). SP is chosen for its surface activity,[239] as it contains a hydrophilic N-terminus and hydrophobic C-terminus. Sampling of the air-water interface after peptide modification is performed with field-induced droplet ionization mass spectrometry (FIDI-MS) with MS/MS analysis to identify the location of oxidation.

5.3 Materials and Methods

5.3.1 Materials

Substance P (RPKPQQFFGLM) was purchased from American Peptide Company and used without further purification. Solutions of 150 μM substance P were prepared in HPLC grade water (OmniSolv).

5.3.2 Footprinting via Heterogeneous Hydroxyl Radical Oxidation at the Air-Water Interface and Mass Spectrometry Analysis

A diagram of the heterogeneous OH footprinting setup is shown in **Figure 5.1** with major components emphasized. It is composed of the field-induced droplet ionization (FIDI) apparatus described in previous work[24, 66-70] interfaced to the atmospheric pressure inlet of a LTQ-XL mass spectrometer (Thermo-Fischer, Waltham, MA) and coupled with the

dielectric barrier discharge source (DBDS). Voltage pulses applied to the FIDI source for droplet interface sampling are controlled by a custom LabView program and power supply. The mass spectrometer is controlled using the Xcaliber software with settings optimized to the doubly protonated SP ion ($[SPH_2^{2+}]$ at m/z 674). The DBDS has been described previously (See **Appendix B** for schematic and optimization discussion). It is positioned 5 mm away from the droplet, perpendicular to the axis by which microdroplets are transferred to the mass spectrometer during sampling and is biased at the back rod electrode using a high voltage AC power supply (Trek PM04015; Trek, Inc, NY). A constant flow of water-saturated helium (technical grade) is supplied to the DBDS during operation using a bubbler containing HPLC grade water and a Type πMFC Digital Mass Flow Controller (model PFC-50, MKS Instruments). The settings of the DBDS are as follows: 1 kHz sinusoidal waveform frequency; 12 kV_{pp} applied voltage to the rod electrode; 1.4 mA current; 1000 cm^3/min flow rate of the humidified helium.

A 2.5 μL droplet (1.6 mm diameter) of the 150 μM SP aqueous solution is formed in the at the end of the capillary of the FIDI apparatus and allowed to equilibrate for 60 s, after which the DBDS voltage and gas flow are applied, exposing the droplet to a constant stream of OH for a 30 s period. FIDI sampling is then performed by biasing the FIDI apparatus electrodes with a 3 – 5 kV pulse. The electric field induces a dipole in the droplet, causing the formation of Taylor cones on each end along the direction of the field. Microdroplets containing ions from the surface of the droplet are ejected from these Taylor cones and the one aligned with the inlet of the mass spectrometer is aspirated into the instrument for analysis. FIDI-MS/MS experiments are performed by setting the mass spectrometer to isolate

the desired product m/z. Normalized collision excitation parameter is set to 25% with an isolation width of 0.8 units. Experiments are performed in triplicate.

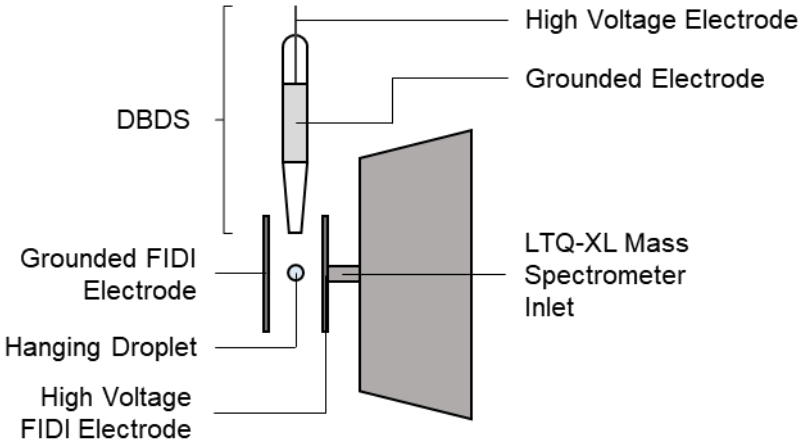

Figure 5.1. Diagram of the heterogeneous OH footprinting setup, consisting of the field-induced droplet ionization (FIDI) source, LTQ-XL mass spectrometer, and the dielectric barrier discharge source (DBDS) for the generation of gas phase OH.

5.4 Results and Discussion

5.4.1 Gas Phase OH-Initiated Footprinting of Substance P at the Air-Water Interface

The FIDI spectrum of substance P (SP) after a 30 s exposure to the DBDS is shown in **Figure 5.2**. No sodium salts were introduced during sample preparation, yet sodium is found to be a common contaminant in mass spectrometry[240] and is observed in the mass spectrum of SP in the form of positively charged adducts with the peptide. Intensities of the parent and products are found as mixtures of protonated and sodiated adducts, forming doubly and triply charged ions at m/z 674 ($[SPH_2]^{2+}$), 685 ($[SPH + Na]^{2+}$), 450 ($[SPH_3]^{3+}$), and 457 ($[SPH_2 + Na]^{3+}$). Singly charged SP species were not present. Over the OH exposure, products

incorporating a single oxygen atom are found at m/z 282 and 455, for the doubly protonated and the triply protonated species, respectively. Singly oxygenated substance P is also detected in the form of the charged sodium adducts at m/z 693 ($[SPH + Na + O]^{2+}$) and 463 ($[SPH_2 + Na + O]^{3+}$). In addition, appreciable quantities of more highly oxidized compounds are found as doubly and triply oxygenated species at m/z 690 and 698, respectively, both doubly protonated. The 16 Da mass shift is indicative that oxygen incorporation has occurred, yet is inconclusive as to which residue is the primary target of the OH radical. The hydrophobic C-terminus of SP contains phenylalanine, leucine, and methionine, all of which can produce an SP + 16 Da product based on **Scheme 5.1a**.

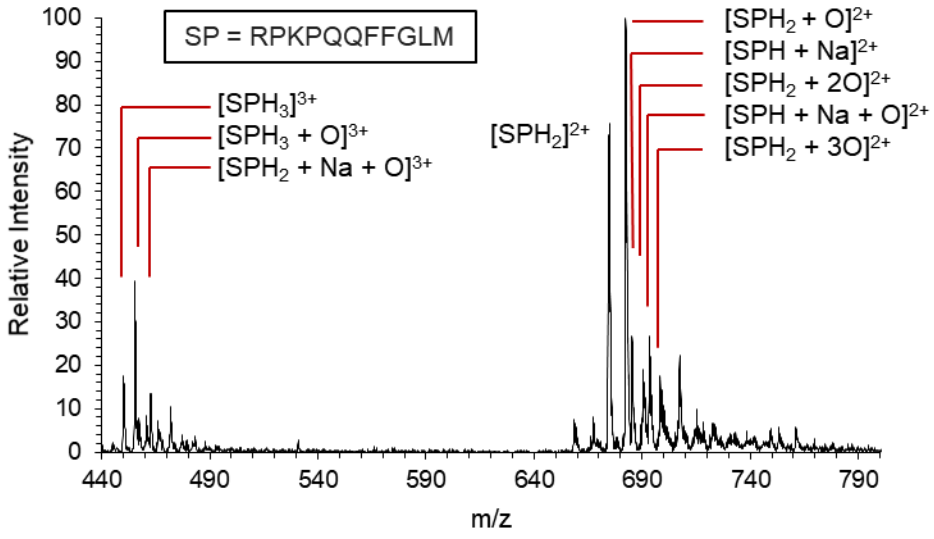

Figure 5.2. Positive mode FIDI mass spectrum of the surface of a 150 μM droplet of substance P (SP) after a 30 s exposure to the DBDS. N = 3.

The singly oxidized m/z 282 species was isolated and subjected to FIDI-MS/MS analysis. The resulting collision-induced dissociation (CID) spectrum of this species under the same oxidative conditions is found in **Figure 5.3**. The most abundant fragment is found at m/z

650.42, a loss which, when taking into account that the ions are doubly charged, corresponds to a mass of 64 Da. This loss is well-documented in the fragmentation of oxidized methionine residues in proteomic studies as the neutral methane sulfenic acid (CH_3SOH).[241-244] The pathway for this loss is shown in **Scheme 5.2**. The sulfoxide oxygen deprotonates a neighboring methylene unit, enabling the formation of the carbon-carbon double bond while displacing neutral methanesulfenic acid (CH_3SOH). The large abundance of this species confirms that the methionine residue is the primary site of oxidation in SP. Furthermore, the presence of b-type ions, N-terminal positively charged fragment ions produced by scission of the peptide bond, is found with varying residue numbers. Importantly, the b_{10} fragment is observed as both the singly charged and doubly charged species at m/z 1199.58 and 600.33, respectively. The existence of these ions in significant quantities in the mass spectrum reveals that the site of oxidation does not occur appreciably on the ten N-terminal residues of substance P, but rather provides a second source of evidence that the site of oxidation is the methionine residue. Many b_n ions reside at a mass-to-charge ratio identical to native SP, indicating that the constituent n residues are not oxidation sites. The mass shifted $[b_7 + O]^+$ and $[b_8 + O]^+$ at m/z 899.50 and m/z 1046.50, respectively, suggest a product with oxidation site within the first 7 and 8 residues. With no other evidence that residues 1 – 6 carry the oxidation site, these peaks imply oxidation at residue 7 or 8, both of which are phenylalanine residues. However, the total relative intensity makes up only 10% of the major peak at m/z 650.42, which is definitive proof of methionine oxidation. This suggests that there is a significant bias toward methionine oxidation rather than phenylalanine oxidation.

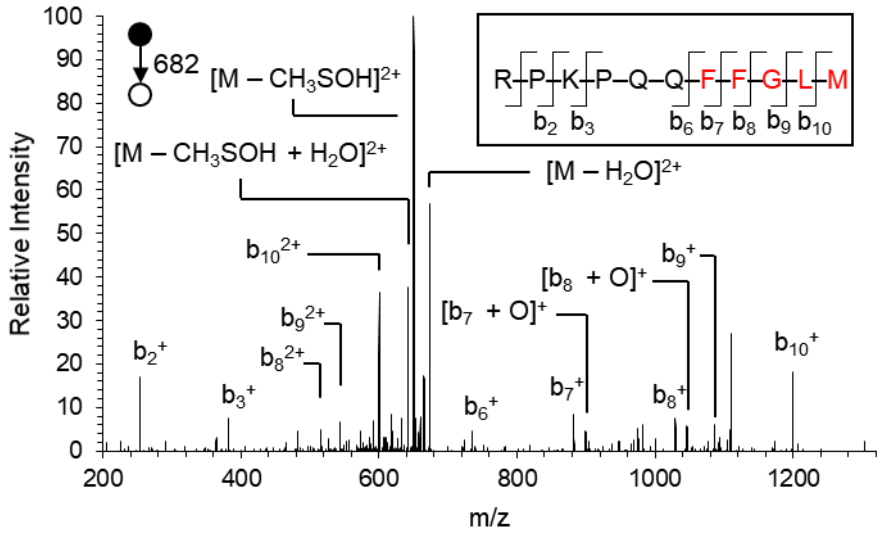

Figure 5.3. Collision-induced dissociation (CID) analysis of the singly oxidized substance P at m/z 682. Fragment ions are labeled using b- and y-type ion designation commonly used in proteomics. Inset: diagram of the locations of the peptide bond breakage along the SP backbone that produces the b_n ions found in the spectrum. Hydrophobic residues are highlighted in red. N = 3.

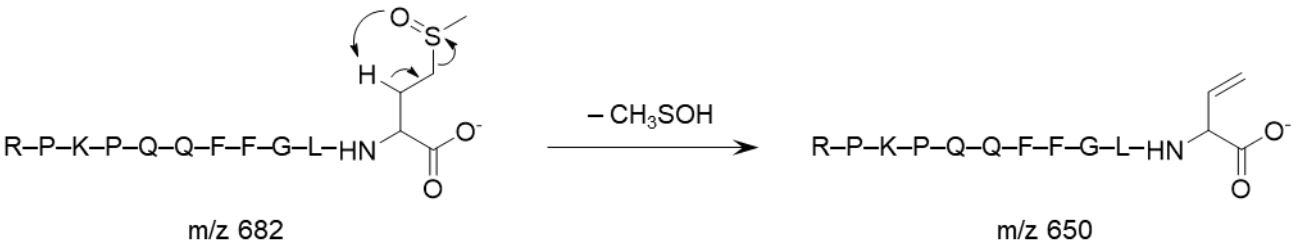

Scheme 5.2. Proposed mechanism of the formation of m/z 650 in the collision-induced dissociation of singly oxidized substance P ($[SPH_2 + O]^{2+}$) during FIDI-MS/MS analysis by the loss of methanesulfenic acid (CH_3SOH) from oxidized methionine.

The results of **Figure 5.3** implicate the air-water interface as an environment that influences peptide reactivity with the hydroxyl radical to a considerable degree. Aqueous phase reaction rates predict that the methionine, phenylalanine, and arginine are the most susceptible to OH-mediated oxidation, with reaction rates within an order of magnitude of

each other (8.5×10^9, 6.9×10^9, 3.5×10^9 M^{-1} s^{-1}, respectively).[218, 245] However, the CID spectrum indicates that the oxidation of the phenylalanine residue constitutes a minor pathway relative to the oxidation of the methionine residue. The striking difference in relative amounts of phenylalanine versus methionine oxidation product despite their similar kinetics suggest the experiment detects differences in accessibility of the two residue types to the gas phase OH. Furthermore, the absence of the characteristic SP – 43 Da species caused by arginine oxidation is also indicative of residue accessibility to the gas phase, as arginine is found on as the N-terminus. The results suggest that the OH does not appreciably penetrate the surface of the SP monolayer in order to oxidize this and other residues in this hydrophilic region.

5.5 Conclusions

The heterogeneous OH footprinting apparatus coupling the DBDS to FIDI-MS product detection can produce the same level of proteomic analysis for surface-active peptides as is seen with other protein footprinting methods. The ability to control the exposure of OH to promote mostly a single oxidation event SP + O exemplifies that heterogeneous OH footprinting can probe the most likely oxidation target found at the air-water interface. By utilization of MS/MS capabilities to determine oxidation site location suggests the structural or conformational features of peptides at the air-water interface. The effective oxidation of methionine over all other peptides in SP has shown that these residues are effectively gas phase accessible. The result indicates that gas phase OH generated from the DBDS effectively initiates the oxidation of a monolayer of a surface active peptide originating from the aqueous phase of a droplet.

Appendix A

Supplemental Information for Chapter 2

A.1. Calculation of a Monolayer Concentration of DTA^+ for FIDI Experiments

The concentration of DTA^+ necessary to form a monolayer in a 2.5 μL spherical droplet with radius of 0.84 mm is found as follows: the surface area A of the droplet is

$$A = 4\pi r^2 = 4\pi(8.4 \times 10^{-4} m)^2 = 8.9 \times 10^{-6} m^2 = 8.9 \times 10^{14} Å^2$$

Assuming DTA^+ has a surface area of approximately 44 $Å^2$/molecules as reported in the literature,[246] the required number of molecules needed to form a monolayer on the droplet is

$$\frac{8.9 \times 10^{14} Å^2}{44 Å/molecule} = 2.0 \times 10^{13}\ molecules$$

The concentration C required to provide a monolayer on the surface of a 2.5 μL droplet is therefore

$$C = \frac{2.0 \times 10^{13}\ molecules}{2.5\ \times 10^{-6}\ L} \times \frac{1}{6.02 \times 10^{23} molecules/mol} = 1.3 \times 10^{-5}\ M = 13\ \mu M$$

A.2. Calculation of the Diffusion Length of DTA^+ over a 1 Minute Equilibration Period in the FIDI Droplet

The diffusion length l, the distance a molecule travels in a given time period, is given by

$$l = 2\sqrt{Dt}$$

where D is the diffusion constant and t is the time. The diffusion constant of 8.2×10^{-6} cm^2/s is given in the literature.[247] The diffusion length over a 60 s equilibration period is

$$l = 2\sqrt{(8.2 \times 10^{-6} cm^2/s)(60s)} = 0.044cm = 0.44mm$$

which is approximately half the radius of the droplet.

A.3 Calculations of Relative Intensity Changes due to Hydrogen/Deuterium Exchange

The ^{13}C isotope ratio for the surfactant species at the air-water interface is taken from the H_2O condition at 50 s DBDS exposure DTA^+ FIDI spectrum and was found the ratio of DTA^+/1 ^{13}C DTA^+/2 ^{13}C DTA^+ is 1/0.167/0.030

The normalized FIDI-MS intensity data for up to the first two generations (DTA^+ + O, DTA^+ + 2O) is shown:

m/z	H_2O	D_2O
228	0.535976	0.645455
229	0.089336	0.108677
230	0.016471	0.01943
242	1	1
243	0.159551	0.182988
244	0.174417	0.147285
245	0.03527	0.084258
246	0.014003	0.025741
256	0.561619	0.600184
257	0.1068	0.114645
258	0.700527	0.465249
259	0.127514	0.295368
260	0.260855	0.19538
261	0.044622	0.107389
262	0.010057	0.030741

The change in intensity of a given m/z corrected for ^{13}C, $I_{m/z}^{corr}$, is given by

$$I_{m/z}^{corr} = I_{m/z}^{obs} - I_{m/z-1}^{C13} - I_{m/z-2}^{2C13}$$

Defining the intensity of the base peak, I_{BP}^{corr}, in a series as the corrected intensity for the parent product (m/z 242, 244, 256, 258, and 260), relative percentage change for the D_2O intensity for a peak, $\Delta_{m/z}$, is given by:

$$\Delta_{m/z} = \frac{I_{m/z}^{corr}}{I_{BP}^{corr}} \times 100\%$$

m/z	corrected	Ratio to base peak in series	Percentage
242	1	1	100
243	0.015988	0.015987899	1.59879
244	0.086726	1	100
245	0.054172	0.624638592	62.46386
246	0.007251	0.083607685	8.360769
256	0.600184	1	100
257	0.014414	0.024016222	2.401622
258	0.428098	1	100
259	0.214232	0.500427137	50.04271
260	0.132096	1	100
261	0.065899	0.49887365	49.88736
262	0.006945	0.052576719	5.257672

Assuming Δ_{245} corresponds to the extent a single hydroxyl group undergoes H/D exchange, and this corresponds to a probability of exchange, Pr(H/D) = 0.625, then we can calculate the extent a dihydroxy product exchanges by considering a sequence of independent events each with a probability Pr(H/D)

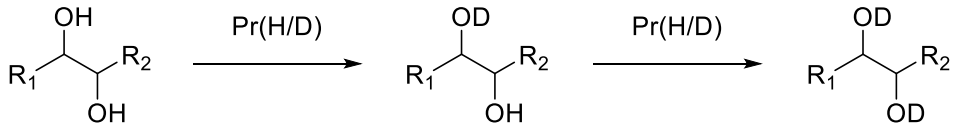

The probabilities of no exchange (Pr(0 H/D)), 1 exchange (Pr(1 H/D)), and 2 exchanges (Pr(2 H/D)) are

$$\Pr(0\ H/D) = [1 - \Pr(H/D)]^2 = 0.141$$

$$\Pr(1\ H/D) = 2\{\Pr(H/D) * [1 - \Pr(H/D)]\} = 0.469$$

$$\Pr(2\ H/D) = [\Pr(H/D)]^2 = 0.390$$

So the relative amounts of the supposed dihydroxy product m/z 260 after H/D exchange should conform to a ratio of intensities of (m/z 260)/(m/z 261)/(m/z 262) = 0.141/0.469/0.390, or 0.300/1.00/0.832. Because the extent of H/D exchange does not conform to these ratios, it is unlikely a dihydroxy species composes the majority of the population of the m/z 260 species.

A.4 Comparison of the CID Spectrum of m/z 228 after a 30 s DBDS Exposure

The FIDI CID spectrum of the m/z 228 species was taken at 25% collision excitation parameter and an isolation width of 2, both without exposure to the DBDS and 60 s DBDS exposure condition. The resulting spectra are shown in Figure S4. The DTA^+ spectrum with no DBDS exposure (**Figure A.1**) shows no significant fragmentation. After 60 s DBDS exposure the CID spectrum of m/z 228 shows a small amount of head group loss, indicating the presence of a distinct species with the same m/z as DTA^+. The fragmentation pattern suggests the C_{11} aldehyde product is present.

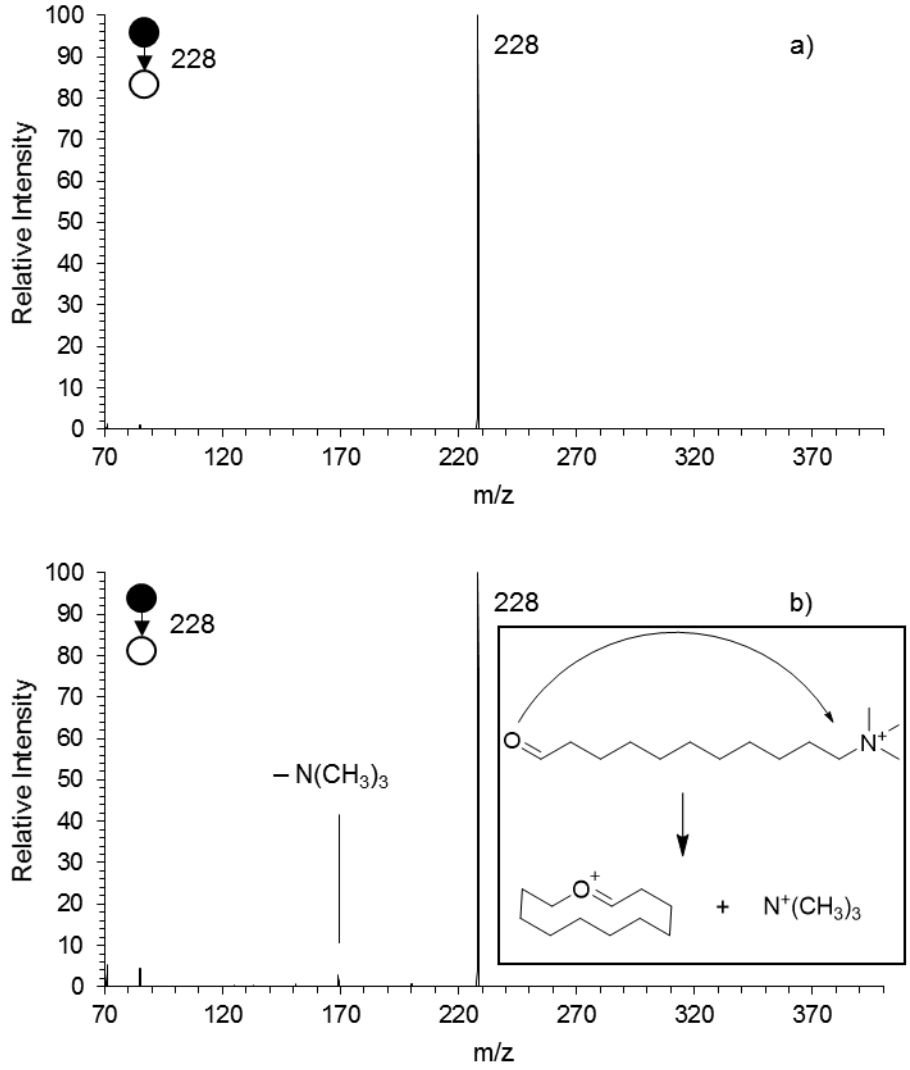

Figure A.1. Comparison of the FIDI-CID spectrum of m/z 228. a) CID spectrum of m/z 228 in the absence of oxidation. b) CID of m/z 228 after a 60 s exposure to the DBDS.

A.5 Estimation of OH Concentration Based on Kinetics Data

The molecular flux (J_z) of a gas phase species through a planar surface normal to the z axis is given by

$$J_z = \frac{1}{4} n * \langle v \rangle$$

where n* is the concentration of the gas phase species and <v> is the average velocity of the gas species given by

$$\langle v \rangle = \left(\frac{8k_B T}{\pi m} \right)^{1/2}$$

where k_B is the Boltzmann constant, T is temperature in Kelvin, and m is the mass of the gas phase species (mass of OH = 17.0 amu). At 298 K the average velocity is

$$\langle v \rangle = \frac{8\left(1.381\times10^{-23}\,\text{kg m}^2\,\text{s}^{-2}\,\text{K}^{-1}\right)(298\text{K})}{\pi(17.0\text{amu})(1.6605\times10^{-27}\,\text{kg amu}^{-1})}^{1/2} = 609.3\text{m/s} = 6.09\times10^{4}\,\text{cm/s}$$

The trend line in **Figure 2.7** is given by f(t) = (0.0381 s^{-1})t (R^2 = 0.987), and represents the average number of oxygen atoms incorporated per DTA^+ Using this equation, the time it takes to incorporate a single oxygen into every DTA hydrocarbon chain is

$$f(t) = 1 = \left(0.0381 s^{-1}\right) t$$
$$t = \frac{1}{0.0381 s^{-1}} = 26.2 s$$

As discussed previously, assuming a surface area of 44 Å^2 ($4.4\times10^{-15} cm^2$), the number of DTA molecules in a square centimeter is $2.27\times10^{14} cm^{-2}$. So the necessary flux is

$$\frac{2.27\times10^{14} cm^{-2}}{26.2 s} = 8.66\times10^{12} cm^{-2}\cdot s^{-1}$$

Assuming a moderate accommodation coefficient of 0.3,[59] the actual flux of OH needed is

$$J_z = \frac{8.66\times10^{12} cm^{-2}\cdot s^{-1}}{0.3} = 2.89\times10^{13} cm^{-2}\cdot s^{-1}$$

Solving for number density, this means the concentration of OH radicals is

$$n^* = \frac{4\left(2.89\times10^{13} cm^{-2}\cdot s^{-1}\right)}{6.09\times10^{4} cm/s} = 2\times10^{9} molecules\cdot cm^{-3}$$

This is 4 orders of magnitude larger than atmospheric OH concentration (~10^5 molecules/cm^3)

A.6 Mathematical Fits for Kinetics Data

A fit of the DTA + O to a least-squares best fit function results in the equation:

$f(t) = (8.52799 \times 10^{-8})t^4 - (1.17646 \times 10^{-5})t^3 + (2.82696 \times 10^{-4})t^2 + (9.54184 \times 10^{-3})t - (4.03723 \times 10^{-4})$ ($R^2 = 0.999139$).

The maximum, reflecting the time at which the rate of production and consumption of DTA + O products is equal is 36.1 s. Similarly, a fit of the DTA + 2O data results in the equation

$f(t) = (-5.46318 \times 10^{-8})t^4 + (4.66435 \times 10^{-6})t^3 - (1.15056 \times 10^{-4})t^2 + (6.86966 \times 10^{-3})t - (1.24902 \times 10^{-3})$ ($R^2 = 0.998174$).

The maximum, reflecting the time at which the rate of production and consumption of DTA + 2O products is equal is 55.3 s.

Appendix B

Characterization of the Dielectric Barrier Discharge Source

A schematic of the dielectric barrier discharge source (DBDS) is shown in **Figure B.1**. The main body is made from standard 6.35 mm (1/4 in) O.D. borosilicate glass tube tapered to a 3.5 mm O.D., 2 mm I.D. outlet. The gas inlet is formed by fusing a 3.175 mm (1/8 in) borosilicate tube approximately 10 mm from the end of the main body. The tungsten rod extends through the main body up to the tapered portion and extends out of the closed end approximately 10 mm. Gas connections from the flow controller are made using copper tubing (Restek Corporation, U.S., Bellefonte, PA) and PTFE Swagelok fittings (Swagelok, Los Angeles, CA).

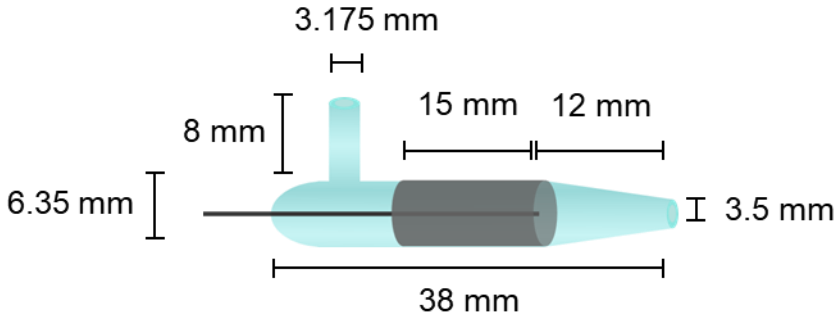

Figure B.1. Schematic of dielectric barrier discharge source for hydroxyl radical

The emission spectrum of the DBDS was taken by placing an Ocean Optics S2000 Fiber Optic Spectrometer's optical cable 5 mm away from the outlet of the DBDS as shown in **Figure B.2a**. The emission spectrum for the DBDS is shown in **Figure B.2b** for the following operating settings: 12 kV_{pp}, 1 kHz sine waveform, 1.414 mA current, and 1000

cm^3/min He/H_2O flowrate. The excited state OH emission was identified in the plasma around 310 nm corresponding to the $A^2\Sigma \rightarrow X^2\Pi$ transition is identified, along with emissions from excited state N_2 and He, which is typical of low temperature plasmas.[93-94] While the presence of excited state OH is confirmed, the radiative lifetime of the species is on the order of 700 ns,[248-250] indicating that the OH will have relaxed before exiting the DBDS.

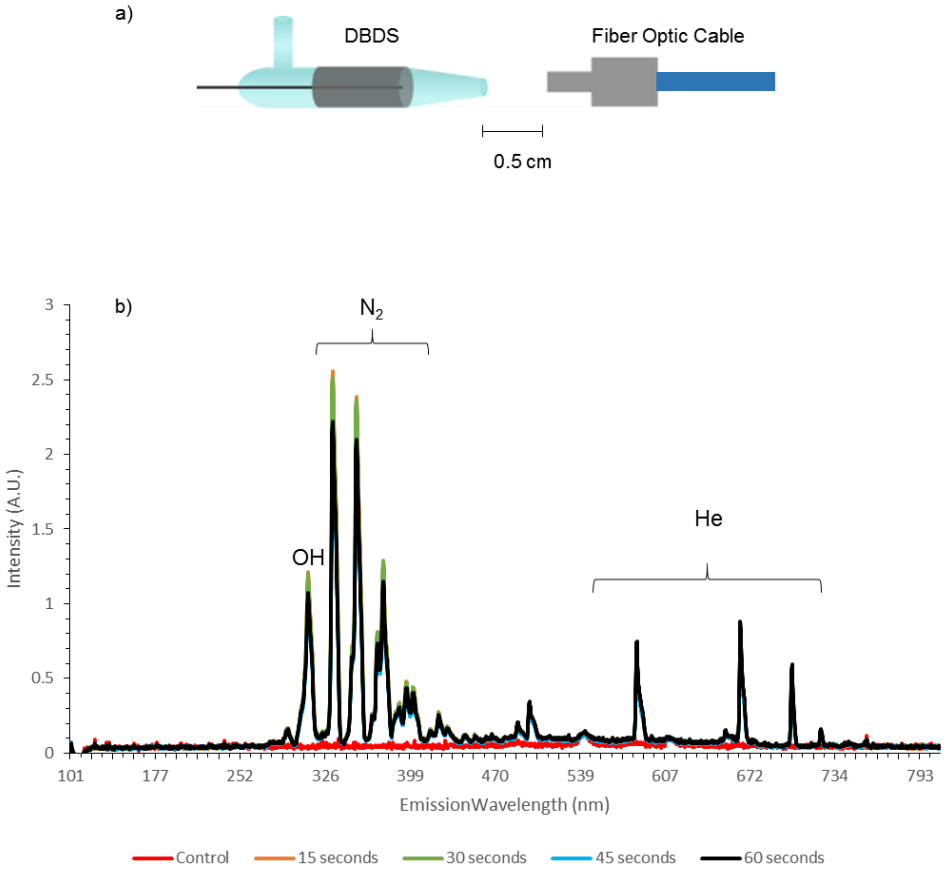

Figure B.2. Spectroscopic Analysis of DBDS. a) Placement of the UV-visible spectrometer probe in relation to the DBDS. b) Emission spectrum of the DBDS plasma over a 60 s period.

Caffeine was chosen to test for the presence of hydroxyl radicals in the exiting gas stream of the DBDS because of its known antioxidant properties.[110-111, 251] The setup for caffeine

oxidation is shown in **Figure B.3a**. A granule of solid caffeine (Sigma-Aldrich Corp., St. Louis, MO) was placed on a glass melting point capillary 0.5 cm from the atmospheric pressure inlet of a LTQ-XL mass spectrometer (Thermo-Fischer, Waltham, MA). The DBDS was positioned 1 cm from the inlet, such that the gas flow passed over the caffeine granule. The DBDS oxidation was performed at 14 kV_{pp} bias, 1 kHz frequency, and 500 cm^3/min flowrate of water-saturated helium. The full mass spectrum is shown in **Figure B.3b**. Approximately 1% of the desorbed caffeine is oxidized to the product 8-oxocaffeine (m/z 211) on the timescale of ionization. Signal of more extensively oxidized caffeine was observed at m/z 227 ($[M + 2O + H]^+$). Adducts of ammonia and water were also observed at m/z 212 ($[M + NH_3 + H]^+$) and m/z 245 ($[M + 2O + H + H_2O]^+$).

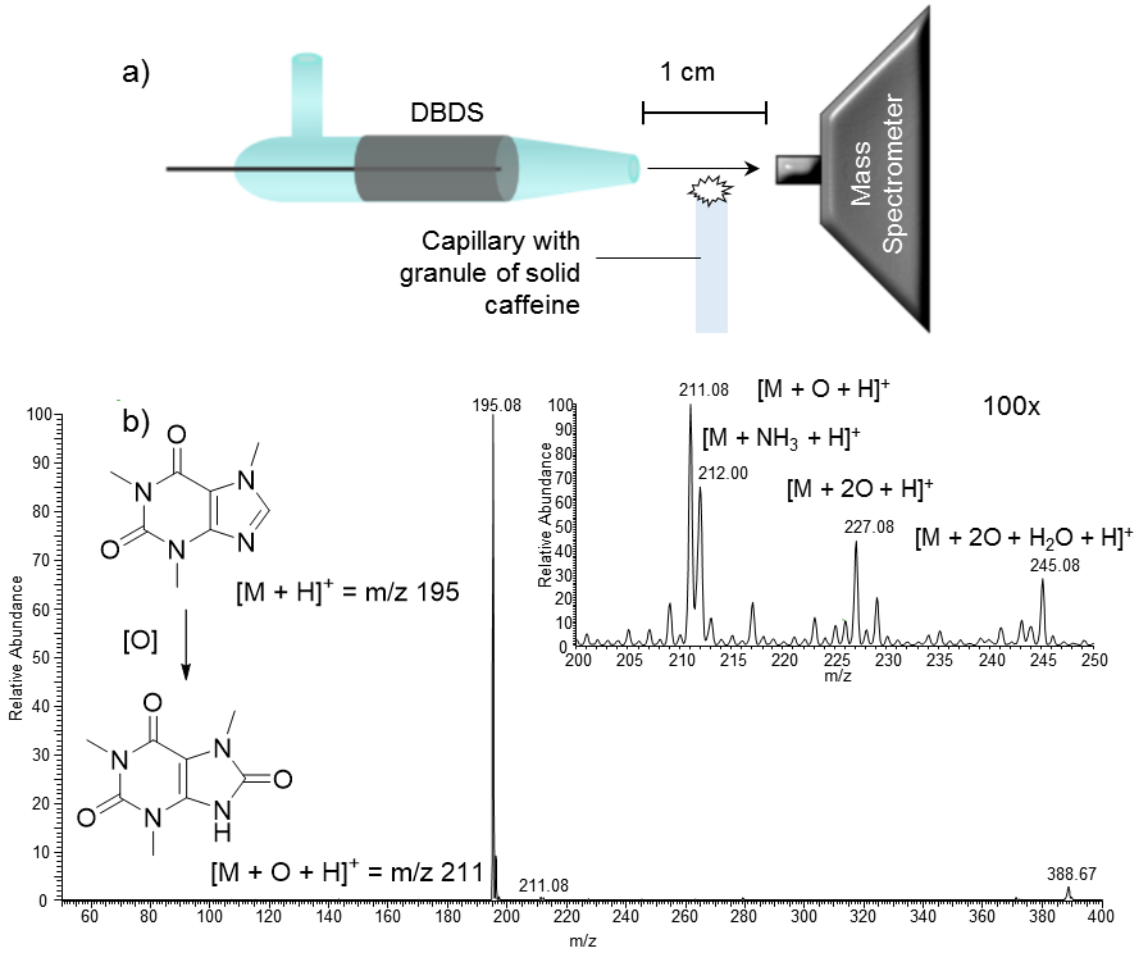

Figure B.3. Oxidation of caffeine using the DBDS. a) The setup for the caffeine oxidation test. A granule of solid caffeine at the end of a glass capillary is placed between the DBDS flow and the inlet of the LTQ-XL mass spectrometer. b) The full mass spectrum of caffeine during DBDS operation at an electrode bias of 14 kV_{pp}. Proton-bound caffeine $[M + H]^+$ at m/z 195 is the most abundant ion. Inset: 100x magnification of the m/z 200 – 250 range.

The DBDS settings were optimized for oxidation using caffeine as the oxidation target. Voltage and flowrate were varied in order to maximize 8-oxocaffeine signal. **Figure B.4** shows the caffeine spectrum for 5 different DBDS settings. Oxidation product signal increased as electrode voltage increased, maximizing for a bias of 14 kV_{pp}. Signal also

increased as gas flowrate increased, maximizing for 1000 cm^3/min. While 14 kV_{pp} and 1000 cm^3/min flowrate showed the most product signal, the final DBDS settings for FIDI-MS oxidation were chosen to be 12 kV_{pp} and 1000 cm^3/min flowrate to avoid arcing from the DBDS to the metal components of the FIDI-MS setup.

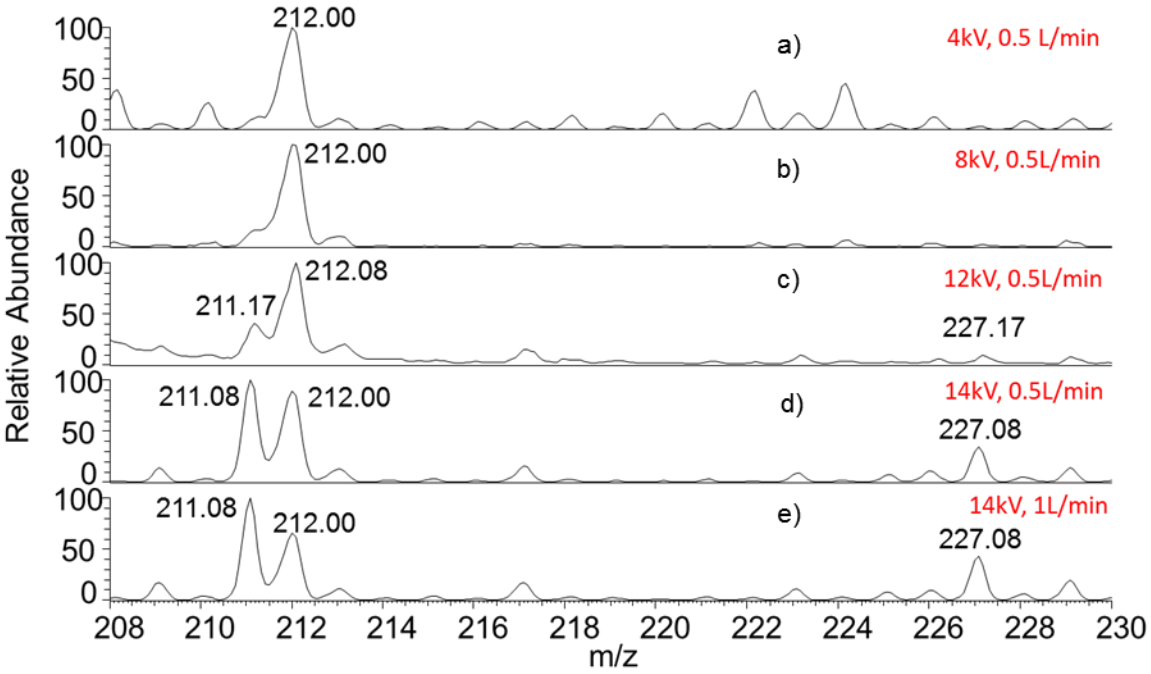

Figure B.4. Mass spectra of the caffeine oxidation product region for various DBDS settings. a) DBDS biased at 4 kV_{pp} with a flowrate of 500 cm^3/min. b) DBDS biased at 8 kV_{pp} with a flowrate of 500 cm^3/min. c) DBDS biased at 12 kV_{pp} with a flowrate of 500 cm^3/min. d) DBDS biased at 14 kV_{pp} with a flowrate of 500 cm^3/min. e) DBDS biased at 14 kV_{pp} with a flowrate of 1000 cm^3/min.

Appendix C

Supplemental Information for Chapter 3

C.1 Characterization of Gemini Synthesis Intermediate and Products

Crude product of the synthesis of intermediate 1 (**Scheme 3.3a**) was subjected to ESI-MS analysis by dissolving a small crystal in HPLC acetonitrile. **Figure C.1** shows the spectrum of the intermediate. The major spectrum feature includes a doublet at m/z 404 and 406. This agrees with the theoretical ion location of intermediate 1 at m/z 404.298 and 406.287. The presence of nearly equal intensity peaks is due to the presence of bromine, which has a characteristic isotope spacing of two mass units.

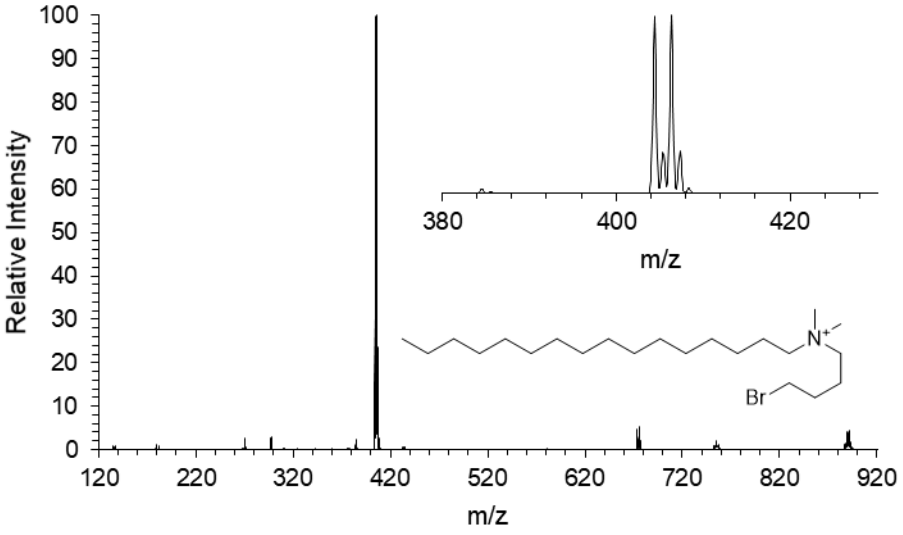

Figure C.1. ESI-MS spectrum of intermediate 1 in acetonitrile. Inset: m/z 380 – 440 region.

The spectrum for the dissymmetric product 16-4-12 is shown in **Figure C.2**, showing good agreement with the theoretical m/z 269.308.

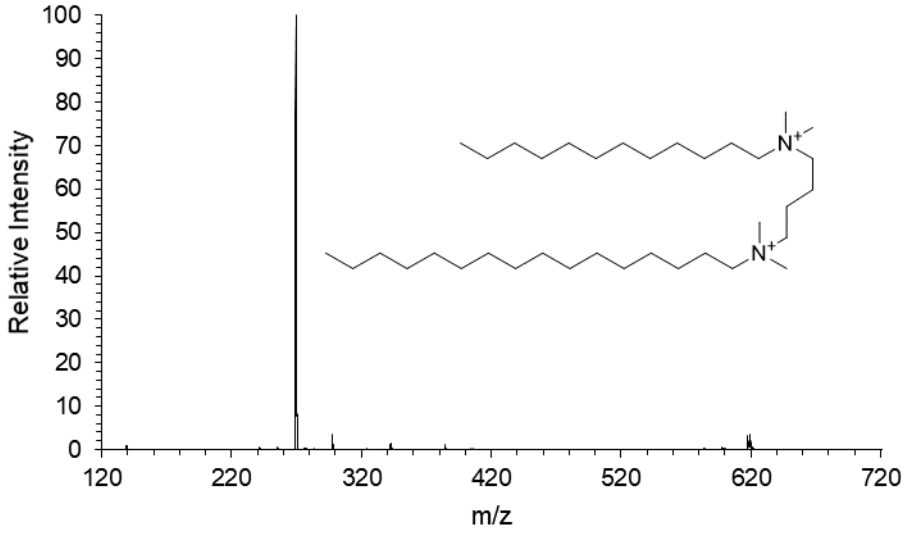

Figure C.2. ESI-MS spectrum of product 16-4-12.

The ESI-MS spectrum of the product from the synthesis of the symmetric gemini 16-4-16 (**Scheme 3.3b**) is found in **Figure C.3**. The major peak at m/z 297 matches the expected m/z of 297.339 of the doubly charged gemini product. The minor peak at m/z 270 is the protonated form of the unreacted N,N'-dimethylhexadecylamine.

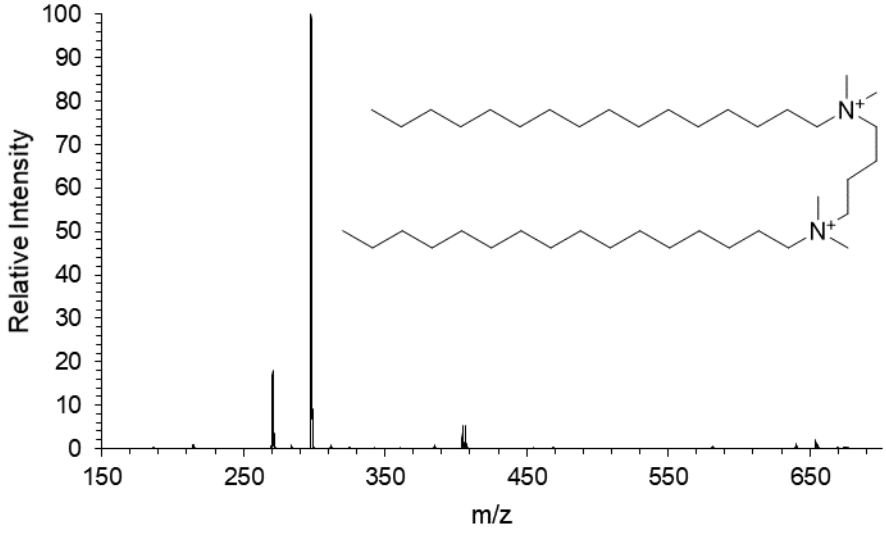

Figure C.3 ESI-MS spectrum of product 16-4-16.

C.2 CID Spectrum of First Generation Oxidation Product [DG + Hy]$^{2+}$

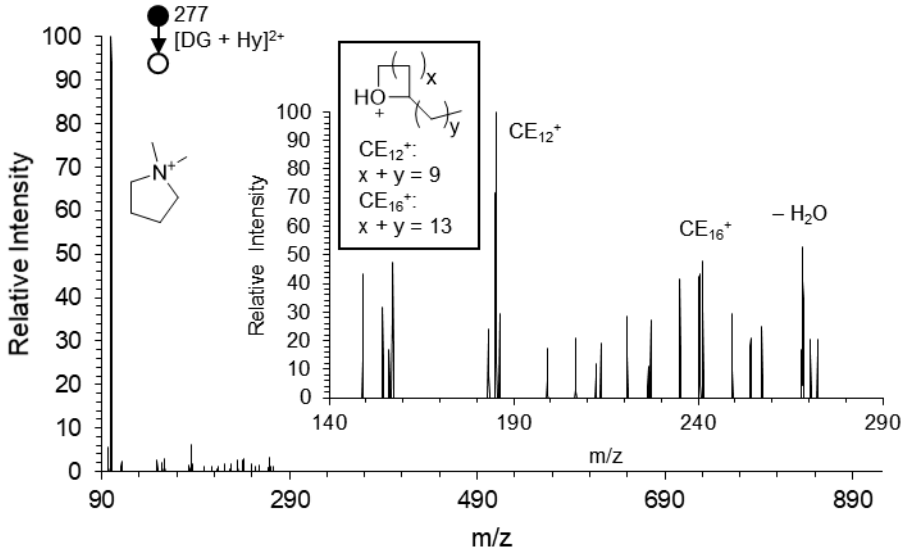

Figure C.4. The CID spectrum of [DG + Hy]$^{2+}$.

C.3 CID Spectra of the First Generation Oxidation Products of Symmetric Gemini 16-4-16

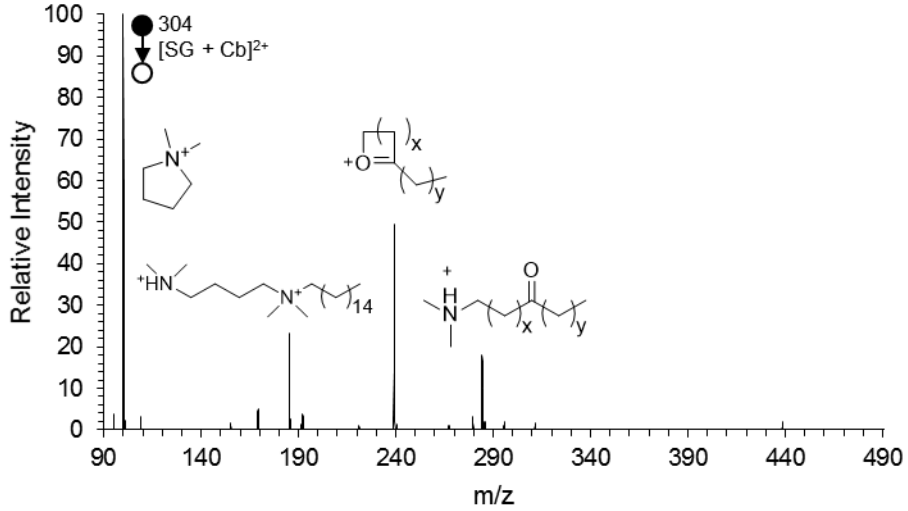

Figure C.5. The CID spectrum of m/z 304, the [SG + Cb]$^{2+}$ product.

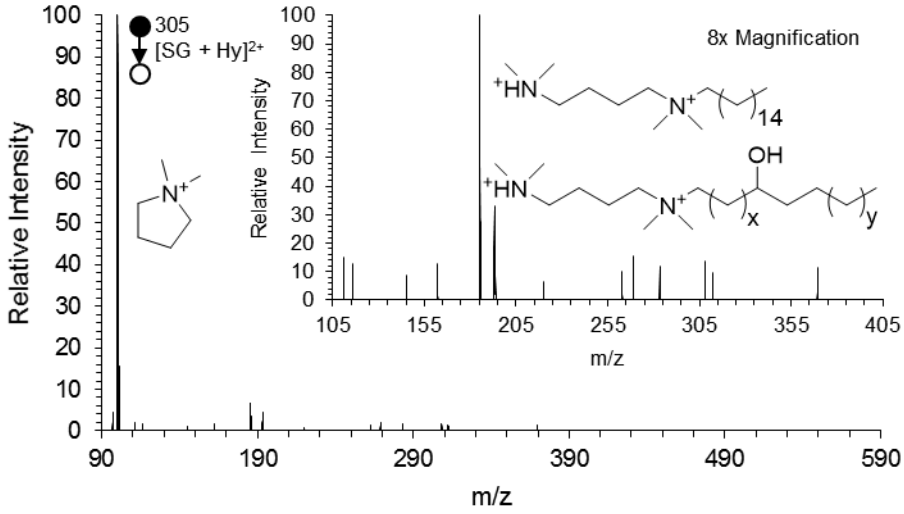

Figure C.6 The CID spectrum of m/z 305, the $[SG + Hy]^{2+}$ product.

Appendix D

Supplemental Information for Chapter 4

D.1 Spectra of the Decamethonium Ion and Dodecyltrimethylammonium Ion in an Equimolar Solution

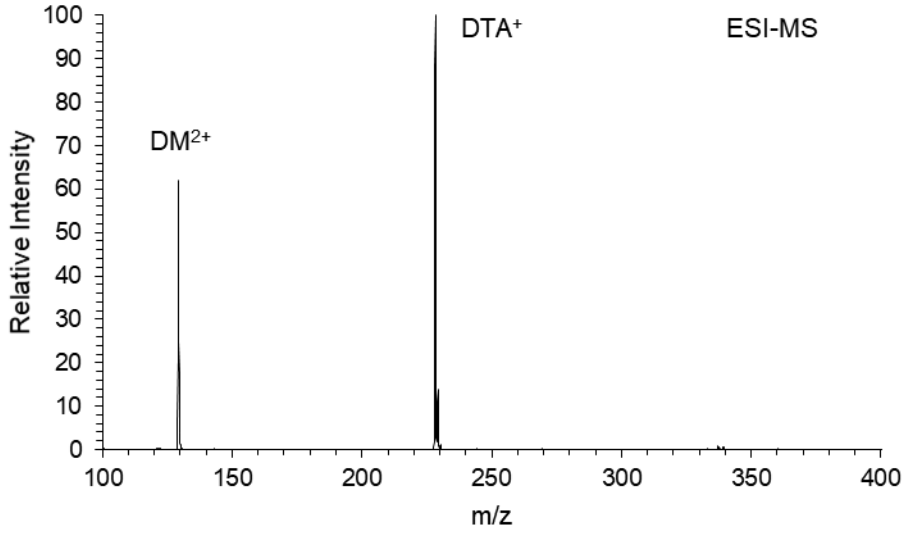

Figure D1. ESI-MS positive mode spectrum of an equimolar aqueous solution of decamethonium ion (DM^{2+}) and dodecyltrimethylammonium ion (DTA^{+}), each at 75 μM concentration.

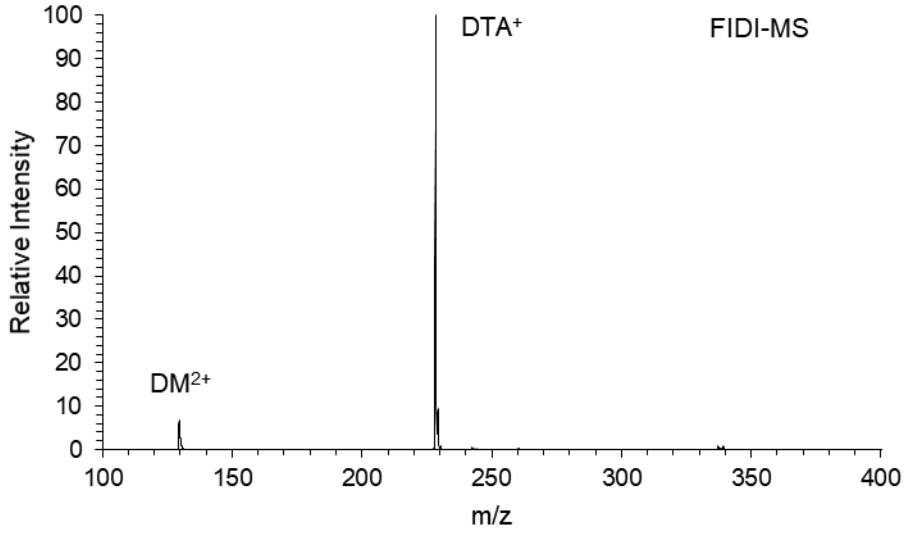

Figure D2. FIDI-MS positive mode spectrum of an aqueous solution of 75μM decamethonium ion (DM^{2+}) and 75μM dodecyltrimethylammonium ion (DTA^{+}).

BIBLIOGRAPHY

1.Na, K.; Kim, Y. P.; Moon, I.; Moon, K.-C., Chemical composition of major VOC emission sources in the Seoul atmosphere. *Chemosphere* **2004,** *55* (4), 585-594.
2.Piccot, S. D.; Watson, J. J.; Jones, J. W., A global inventory of volatile organic compound emissions from anthropogenic sources. *Journal of Geophysical Research: Atmospheres* **1992,** *97* (D9), 9897-9912.
3.Rogge, W. F.; Hildemann, L. M.; Mazurek, M. A.; Cass, G. R.; Simoneit, B. R., Sources of fine organic aerosol. 3. Road dust, tire debris, and organometallic brake lining dust: roads as sources and sinks. *Environmental Science & Technology* **1993,** *27* (9), 1892-1904.
4.Sahu, L.; Yadav, R.; Pal, D., Source identification of VOCs at an urban site of western India: Effect of marathon events and anthropogenic emissions. *Journal of Geophysical Research: Atmospheres* **2016**.
5.Satsumabayashi, H.; Kurita, H.; Yokouchi, Y.; Ueda, H., Mono- and di-carboxylic acids under long-range transport of air pollution in central Japan. *Tellus B: Chemical and Physical Meteorology* **1989,** *41* (3), 219-229.
6.Yang, L.; Nguyen, D. M.; Jia, S.; Reid, J. S.; Yu, L. E., Impacts of biomass burning smoke on the distributions and concentrations of C2–C5 dicarboxylic acids and dicarboxylates in a tropical urban environment. *Atmospheric Environment* **2013,** *78*, 211-218.
7.Kawamura, K.; Yasui, O., Diurnal changes in the distribution of dicarboxylic acids, ketocarboxylic acids and dicarbonyls in the urban Tokyo atmosphere. *Atmospheric Environment* **2005,** *39* (10), 1945-1960.
8.Kawamura, K.; Kasukabe, H.; Barrie, L. A., Source and reaction pathways of dicarboxylic acids, ketoacids and dicarbonyls in arctic aerosols: One year of observations. *Atmospheric Environment* **1996,** *30* (10), 1709-1722.
9.Kanakidou, M.; Seinfeld, J. H.; Pandis, S. N.; Barnes, I.; Dentener, F. J.; Facchini, M. C.; Van Dingenen, R.; Ervens, B.; Nenes, A.; Nielsen, C. J.; Swietlicki, E.; Putaud, J. P.; Balkanski, Y.; Fuzzi, S.; Horth, J.; Moortgat, G. K.; Winterhalter, R.; Myhre, C. E. L.; Tsigaridis, K.; Vignati, E.; Stephanou, E. G.; Wilson, J., Organic aerosol and global climate modelling: a review. *Atmos. Chem. Phys.* **2005,** *5* (4), 1053-1123.
10.Guenther, A.; Zimmerman, P.; Wildermuth, M., Natural volatile organic compound emission rate estimates for U.S. woodland landscapes. *Atmospheric Environment* **1994,** *28* (6), 1197-1210.
11.Goldstein, A. H.; Galbally, I. E., Known and Unexplored Organic Constituents in the Earth's Atmosphere. *Environmental Science & Technology* **2007,** *41* (5), 1514-1521.
12.Corchnoy, S. B.; Arey, J.; Atkinson, R., Hydrocarbon emissions from twelve urban shade trees of the Los Angeles, California, Air Basin. *Atmospheric Environment. Part B. Urban Atmosphere* **1992,** *26* (3), 339-348.
13.Finlayson-Pitts, B. J.; Pitts Jr, J. N., *Chemistry of the upper and lower atmosphere: theory, experiments, and applications*. Academic press: 1999.
14.Seinfeld, J. H.; Pandis, S. N., *Atmospheric chemistry and physics: from air pollution to climate change*. John Wiley & Sons: 2012.

15.Lim, Y. B.; Ziemann, P. J., Products and Mechanism of Secondary Organic Aerosol Formation from Reactions of n-Alkanes with OH Radicals in the Presence of NOx. *Environmental Science & Technology* **2005,** *39* (23), 9229-9236.
16.Donahue, N. M.; Henry, K. M.; Mentel, T. F.; Kiendler-Scharr, A.; Spindler, C.; Bohn, B.; Brauers, T.; Dorn, H. P.; Fuchs, H.; Tillmann, R.; Wahner, A.; Saathoff, H.; Naumann, K.-H.; Möhler, O.; Leisner, T.; Müller, L.; Reinnig, M.-C.; Hoffmann, T.; Salo, K.; Hallquist, M.; Frosch, M.; Bilde, M.; Tritscher, T.; Barmet, P.; Praplan, A. P.; DeCarlo, P. F.; Dommen, J.; Prévôt, A. S. H.; Baltensperger, U., Aging of biogenic secondary organic aerosol via gas-phase OH radical reactions. *Proceedings of the National Academy of Sciences* **2012,** *109* (34), 13503-13508.
17.Atkinson, R., Kinetics and mechanisms of the gas-phase reactions of the hydroxyl radical with organic compounds under atmospheric conditions. *Chemical Reviews* **1986,** *86* (1), 69-201.
18.Logan, J. A.; Prather, M. J.; Wofsy, S. C.; McElroy, M. B., Tropospheric chemistry: A global perspective. *Journal of Geophysical Research: Oceans* **1981,** *86* (C8), 7210-7254.
19.Kwok, E. S. C.; Arey, J.; Atkinson, R., Alkoxy Radical Isomerization in the OH Radical-Initiated Reactions of C4−C8 n-Alkanes. *The Journal of Physical Chemistry* **1996,** *100* (1), 214-219.
20.Kwok, E. S. C.; Atkinson, R., Estimation of hydroxyl radical reaction rate constants for gas-phase organic compounds using a structure-reactivity relationship: An update. *Atmospheric Environment* **1995,** *29* (14), 1685-1695.
21.Larsen, B. R.; Di Bella, D.; Glasius, M.; Winterhalter, R.; Jensen, N. R.; Hjorth, J., Gas-Phase OH Oxidation of Monoterpenes: Gaseous and Particulate Products. *Journal of Atmospheric Chemistry* **2001,** *38* (3), 231-276.
22.Ruehl, C. R.; Nah, T.; Isaacman, G.; Worton, D. R.; Chan, A. W. H.; Kolesar, K. R.; Cappa, C. D.; Goldstein, A. H.; Wilson, K. R., The Influence of Molecular Structure and Aerosol Phase on the Heterogeneous Oxidation of Normal and Branched Alkanes by OH. *The Journal of Physical Chemistry A* **2013,** *117* (19), 3990-4000.
23.Sinha, V.; Williams, J.; Lelieveld, J.; Ruuskanen, T. M.; Kajos, M. K.; Patokoski, J.; Hellen, H.; Hakola, H.; Mogensen, D.; Boy, M.; Rinne, J.; Kulmala, M., OH Reactivity Measurements within a Boreal Forest: Evidence for Unknown Reactive Emissions. *Environmental Science & Technology* **2010,** *44* (17), 6614-6620.
24.Thomas, D. A.; Coggon, M. M.; Lignell, H.; Schilling, K. A.; Zhang, X.; Schwantes, R. H.; Flagan, R. C.; Seinfeld, J. H.; Beauchamp, J. L., Real-Time Studies of Iron Oxalate-Mediated Oxidation of Glycolaldehyde as a Model for Photochemical Aging of Aqueous Tropospheric Aerosols. *Environmental Science & Technology* **2016,** *50* (22), 12241-12249.
25.Tully, F. P.; Droege, A. T.; Koszykowski, M. L.; Melius, C. F., Hydrogen-atom abstraction from alkanes by hydroxyl. 2. Ethane. *The Journal of Physical Chemistry* **1986,** *90* (4), 691-698.
26.Zhou, S.; Barnes, I.; Zhu, T.; Bejan, I.; Albu, M.; Benter, T., Atmospheric Chemistry of Acetylacetone. *Environmental Science & Technology* **2008,** *42* (21), 7905-7910.
27.Jungkamp, T. P. W.; Smith, J. N.; Seinfeld, J. H., Atmospheric Oxidation Mechanism of n-Butane: The Fate of Alkoxy Radicals. *The Journal of Physical Chemistry A* **1997,** *101* (24), 4392-4401.

28.Droege, A. T.; Tully, F. P., Hydrogen-atom abstraction from alkanes by hydroxyl. 3. Propane. *The Journal of Physical Chemistry* **1986,** *90* (9), 1949-1954.
29.Atkinson, R., Kinetics of the gas-phase reactions of OH radicals with alkanes and cycloalkanes. *Atmos. Chem. Phys.* **2003,** *3* (6), 2233-2307.
30.Atkinson, R., A structure-activity relationship for the estimation of rate constants for the gas-phase reactions of OH radicals with organic compounds. *International Journal of Chemical Kinetics* **1987,** *19* (9), 799-828.
31.Heard, D. E.; Pilling, M. J., Measurement of OH and HO2 in the Troposphere. *Chemical Reviews* **2003,** *103* (12), 5163-5198.
32.Levy, H., Photochemistry of the lower troposphere. *Planetary and Space Science* **1972,** *20* (6), 919-935.
33.Kroll, J. H.; Seinfeld, J. H., Chemistry of secondary organic aerosol: Formation and evolution of low-volatility organics in the atmosphere. *Atmospheric Environment* **2008,** *42* (16), 3593-3624.
34.Lambe, A. T.; Onasch, T. B.; Croasdale, D. R.; Wright, J. P.; Martin, A. T.; Franklin, J. P.; Massoli, P.; Kroll, J. H.; Canagaratna, M. R.; Brune, W. H.; Worsnop, D. R.; Davidovits, P., Transitions from Functionalization to Fragmentation Reactions of Laboratory Secondary Organic Aerosol (SOA) Generated from the OH Oxidation of Alkane Precursors. *Environmental Science & Technology* **2012,** *46* (10), 5430-5437.
35.Lambe, A. T.; Zhang, J.; Sage, A. M.; Donahue, N. M., Controlled OH Radical Production via Ozone-Alkene Reactions for Use in Aerosol Aging Studies. *Environmental Science & Technology* **2007,** *41* (7), 2357-2363.
36.Molina, M. J.; Ivanov, A. V.; Trakhtenberg, S.; Molina, L. T., Atmospheric evolution of organic aerosol. *Geophysical Research Letters* **2004,** *31* (22), n/a-n/a.
37.Ng, N. L.; Canagaratna, M. R.; Zhang, Q.; Jimenez, J. L.; Tian, J.; Ulbrich, I. M.; Kroll, J. H.; Docherty, K. S.; Chhabra, P. S.; Bahreini, R.; Murphy, S. M.; Seinfeld, J. H.; Hildebrandt, L.; Donahue, N. M.; DeCarlo, P. F.; Lanz, V. A.; Prévôt, A. S. H.; Dinar, E.; Rudich, Y.; Worsnop, D. R., Organic aerosol components observed in Northern Hemispheric datasets from Aerosol Mass Spectrometry. *Atmos. Chem. Phys.* **2010,** *10* (10), 4625-4641.
38.Zhang, Q.; Jimenez, J. L.; Canagaratna, M. R.; Allan, J. D.; Coe, H.; Ulbrich, I.; Alfarra, M. R.; Takami, A.; Middlebrook, A. M.; Sun, Y. L.; Dzepina, K.; Dunlea, E.; Docherty, K.; DeCarlo, P. F.; Salcedo, D.; Onasch, T.; Jayne, J. T.; Miyoshi, T.; Shimono, A.; Hatakeyama, S.; Takegawa, N.; Kondo, Y.; Schneider, J.; Drewnick, F.; Borrmann, S.; Weimer, S.; Demerjian, K.; Williams, P.; Bower, K.; Bahreini, R.; Cottrell, L.; Griffin, R. J.; Rautiainen, J.; Sun, J. Y.; Zhang, Y. M.; Worsnop, D. R., Ubiquity and dominance of oxygenated species in organic aerosols in anthropogenically-influenced Northern Hemisphere midlatitudes. *Geophysical Research Letters* **2007,** *34* (13), n/a-n/a.
39.Griffin, R. J.; Dabdub, D.; Seinfeld, J. H., Secondary organic aerosol 1. Atmospheric chemical mechanism for production of molecular constituents. *Journal of Geophysical Research: Atmospheres* **2002,** *107* (D17), AAC 3-1-AAC 3-26.
40.George, I. J.; Abbatt, J. P. D., Chemical evolution of secondary organic aerosol from OH-initiated heterogeneous oxidation. *Atmos. Chem. Phys.* **2010,** *10* (12), 5551-5563.
41.Browne, E. C.; Franklin, J. P.; Canagaratna, M. R.; Massoli, P.; Kirchstetter, T. W.; Worsnop, D. R.; Wilson, K. R.; Kroll, J. H., Changes to the Chemical Composition of Soot

from Heterogeneous Oxidation Reactions. *The Journal of Physical Chemistry A* **2015,** *119* (7), 1154-1163.
42.Bertram, A. K.; Ivanov, A. V.; Hunter, M.; Molina, L. T.; Molina, M. J., The Reaction Probability of OH on Organic Surfaces of Tropospheric Interest. *The Journal of Physical Chemistry A* **2001,** *105* (41), 9415-9421.
43.Angelino, S.; Suess, D. T.; Prather, K. A., Formation of Aerosol Particles from Reactions of Secondary and Tertiary Alkylamines: Characterization by Aerosol Time-of-Flight Mass Spectrometry. *Environmental Science & Technology* **2001,** *35* (15), 3130-3138.
44.McClements, D. J.; Decker, E. A., Lipid Oxidation in Oil-in-Water Emulsions: Impact of Molecular Environment on Chemical Reactions in Heterogeneous Food Systems. *Journal of Food Science* **2000,** *65* (8), 1270-1282.
45.McNeill, V. F.; Yatavelli, R. L. N.; Thornton, J. A.; Stipe, C. B.; Landgrebe, O., Heterogeneous OH oxidation of palmitic acid in single component and internally mixed aerosol particles: vaporization and the role of particle phase. *Atmos. Chem. Phys.* **2008,** *8* (17), 5465-5476.
46.Moise, T.; Rudich, Y., Reactive Uptake of Ozone by Aerosol-Associated Unsaturated Fatty Acids: Kinetics, Mechanism, and Products. *The Journal of Physical Chemistry A* **2002,** *106* (27), 6469-6476.
47.Vlasenko, A.; George, I. J.; Abbatt, J. P. D., Formation of Volatile Organic Compounds in the Heterogeneous Oxidation of Condensed-Phase Organic Films by Gas-Phase OH. *The Journal of Physical Chemistry A* **2008,** *112* (7), 1552-1560.
48.Park, J.-H.; Ivanov, A. V.; Molina, M. J., Effect of Relative Humidity on OH Uptake by Surfaces of Atmospheric Importance. *The Journal of Physical Chemistry A* **2008,** *112* (30), 6968-6977.
49.Roeselová, M.; Vieceli, J.; Dang, L. X.; Garrett, B. C.; Tobias, D. J., Hydroxyl Radical at the Air−Water Interface. *Journal of the American Chemical Society* **2004,** *126* (50), 16308-16309.
50.Slade, J. H.; Knopf, D. A., Heterogeneous OH oxidation of biomass burning organic aerosol surrogate compounds: assessment of volatilisation products and the role of OH concentration on the reactive uptake kinetics. *Physical Chemistry Chemical Physics* **2013,** *15* (16), 5898-5915.
51.Che, D. L.; Smith, J. D.; Leone, S. R.; Ahmed, M.; Wilson, K. R., Quantifying the reactive uptake of OH by organic aerosols in a continuous flow stirred tank reactor. *Physical Chemistry Chemical Physics* **2009,** *11* (36), 7885-7895.
52.Pflieger, M.; Monod, A.; Wortham, H., Heterogeneous Oxidation of Terbuthylazine by "Dark" OH Radicals under Simulated Atmospheric Conditions in a Flow Tube. *Environmental Science & Technology* **2013,** *47* (12), 6239-6246.
53.Salo, K.; Hallquist, M.; Jonsson, Å. M.; Saathoff, H.; Naumann, K. H.; Spindler, C.; Tillmann, R.; Fuchs, H.; Bohn, B.; Rubach, F.; Mentel, T. F.; Müller, L.; Reinnig, M.; Hoffmann, T.; Donahue, N. M., Volatility of secondary organic aerosol during OH radical induced ageing. *Atmos. Chem. Phys.* **2011,** *11* (21), 11055-11067.
54.Segal-Rosenheimer, M.; Linker, R.; Dubowski, Y., Heterogeneous oxidation of the insecticide cypermethrin as thin film and airborne particles by hydroxyl radicals and ozone. *Physical Chemistry Chemical Physics* **2011,** *13* (2), 506-517.

55.Smith, J. D.; Kroll, J. H.; Cappa, C. D.; Che, D. L.; Liu, C. L.; Ahmed, M.; Leone, S. R.; Worsnop, D. R.; Wilson, K. R., The heterogeneous reaction of hydroxyl radicals with sub-micron squalane particles: a model system for understanding the oxidative aging of ambient aerosols. *Atmos. Chem. Phys.* **2009,** *9* (9), 3209-3222.
56.Kolesar, K. R.; Buffaloe, G.; Wilson, K. R.; Cappa, C. D., OH-Initiated Heterogeneous Oxidation of Internally-Mixed Squalane and Secondary Organic Aerosol. *Environmental Science & Technology* **2014,** *48* (6), 3196-3202.
57.George, I. J.; Slowik, J.; Abbatt, J. P. D., Chemical aging of ambient organic aerosol from heterogeneous reaction with hydroxyl radicals. *Geophysical Research Letters* **2008,** *35* (13), n/a-n/a.
58.George, I. J.; Chang, R. Y. W.; Danov, V.; Vlasenko, A.; Abbatt, J. P. D., Modification of cloud condensation nucleus activity of organic aerosols by hydroxyl radical heterogeneous oxidation. *Atmospheric Environment* **2009,** *43* (32), 5038-5045.
59.George, I. J.; Abbatt, J. P. D., Heterogeneous oxidation of atmospheric aerosol particles by gas-phase radicals. *Nat Chem* **2010,** *2* (9), 713-722.
60.Enami, S.; Hoffmann, M. R.; Colussi, A. J., Stepwise Oxidation of Aqueous Dicarboxylic Acids by Gas-Phase OH Radicals. *The Journal of Physical Chemistry Letters* **2015,** *6* (3), 527-534.
61.Enami, S.; Hoffmann, M. R.; Colussi, A. J., In Situ Mass Spectrometric Detection of Interfacial Intermediates in the Oxidation of RCOOH(aq) by Gas-Phase OH-Radicals. *The Journal of Physical Chemistry A* **2014,** *118* (23), 4130-4137.
62.Eliason, T. L.; Gilman, J. B.; Vaida, V., Oxidation of organic films relevant to atmospheric aerosols. *Atmospheric Environment* **2004,** *38* (9), 1367-1378.
63.Dilbeck, C. W.; Finlayson-Pitts, B. J., Hydroxyl radical oxidation of phospholipid-coated NaCl particles. *Physical Chemistry Chemical Physics* **2013,** *15* (24), 9833-9844.
64.D'Andrea, T. M.; Zhang, X.; Jochnowitz, E. B.; Lindeman, T. G.; Simpson, C. J. S. M.; David, D. E.; Curtiss, T. J.; Morris, J. R.; Ellison, G. B., Oxidation of Organic Films by Beams of Hydroxyl Radicals. *The Journal of Physical Chemistry B* **2008,** *112* (2), 535-544.
65.George, I. J.; Vlasenko, A.; Slowik, J. G.; Broekhuizen, K.; Abbatt, J. P. D., Heterogeneous oxidation of saturated organic aerosols by hydroxyl radicals: uptake kinetics, condensed-phase products, and particle size change. *Atmos. Chem. Phys.* **2007,** *7* (16), 4187-4201.
66.Grimm, R. L.; Beauchamp, J. L., Field-Induced Droplet Ionization Mass Spectrometry. *The Journal of Physical Chemistry B* **2003,** *107* (51), 14161-14163.
67.Grimm, R. L.; Beauchamp, J. L., Dynamics of Field-Induced Droplet Ionization: Time-Resolved Studies of Distortion, Jetting, and Progeny Formation from Charged and Neutral Methanol Droplets Exposed to Strong Electric Fields. *The Journal of Physical Chemistry B* **2005,** *109* (16), 8244-8250.
68.Grimm, R. L.; Hodyss, R.; Beauchamp, J. L., Probing Interfacial Chemistry of Single Droplets with Field-Induced Droplet Ionization Mass Spectrometry: Physical Adsorption of Polycyclic Aromatic Hydrocarbons and Ozonolysis of Oleic Acid and Related Compounds. *Analytical Chemistry* **2006,** *78* (11), 3800-3806.
69.Kim, H. I.; Kim, H.; Shin, Y. S.; Beegle, L. W.; Goddard, W. A.; Heath, J. R.; Kanik, I.; Beauchamp, J. L., Time Resolved Studies of Interfacial Reactions of Ozone with Pulmonary

Phospholipid Surfactants Using Field Induced Droplet Ionization Mass Spectrometry. *The Journal of Physical Chemistry B* **2010,** *114* (29), 9496-9503.
70.Kim, H. I.; Kim, H.; Shin, Y. S.; Beegle, L. W.; Jang, S. S.; Neidholdt, E. L.; Goddard, W. A.; Heath, J. R.; Kanik, I.; Beauchamp, J. L., Interfacial Reactions of Ozone with Surfactant Protein B in a Model Lung Surfactant System. *Journal of the American Chemical Society* **2010,** *132* (7), 2254-2263.
71.Maleknia, S. D.; Chance, M. R.; Downard, K. M., Electrospray-assisted modification of proteins: a radical probe of protein structure. *Rapid Communications in Mass Spectrometry* **1999,** *13* (23), 2352-2358.
72.Rafat Husain, S.; Cillard, J.; Cillard, P., Hydroxyl radical scavenging activity of flavonoids. *Phytochemistry* **1987,** *26* (9), 2489-2491.
73.Stefan, M. I.; Hoy, A. R.; Bolton, J. R., Kinetics and Mechanism of the Degradation and Mineralization of Acetone in Dilute Aqueous Solution Sensitized by the UV Photolysis of Hydrogen Peroxide. *Environmental Science & Technology* **1996,** *30* (7), 2382-2390.
74.Beltrán, F. J.; Ovejero, G.; Acedo, B., Oxidation of atrazine in water by ultraviolet radiation combined with hydrogen peroxide. *Water Research* **1993,** *27* (6), 1013-1021.
75.Liao, C.-H.; Gurol, M. D., Chemical oxidation by photolytic decomposition of hydrogen peroxide. *Environmental science & technology* **1995,** *29* (12), 3007-3014.
76.Harbour, J. R.; Chow, V.; Bolton, J. R., An Electron Spin Resonance Study of the Spin Adducts of OH and HO2 Radicals with Nitrones in the Ultraviolet Photolysis of Aqueous Hydrogen Peroxide Solutions. *Canadian Journal of Chemistry* **1974,** *52* (20), 3549-3553.
77.Hochanadel, C. J., Photolysis of Dilute Hydrogen Peroxide Solution in the Presence of Dissolved Hydrogen and Oxygen: Evidence Relating to the Nature of the Hydroxyl Radical and the Hydrogen Atom Produced in the Radiolysis of Water. *Radiation Research* **1962,** *17* (3), 286-301.
78.Garrison, W. M., Reaction mechanisms in the radiolysis of peptides, polypeptides, and proteins. *Chemical Reviews* **1987,** *87* (2), 381-398.
79.Draganic, Z.; Draganic, I., Formation of primary yields of hydroxyl radical and hydrated electron in the. gamma.-radiolysis of water. *The Journal of Physical Chemistry* **1973,** *77* (6), 765-772.
80.Westerhoff, P.; Mezyk, S. P.; Cooper, W. J.; Minakata, D., Electron Pulse Radiolysis Determination of Hydroxyl Radical Rate Constants with Suwannee River Fulvic Acid and Other Dissolved Organic Matter Isolates. *Environmental Science & Technology* **2007,** *41* (13), 4640-4646.
81.Burns, W. G.; Sims, H. E., Effect of radiation type in water radiolysis. *Journal of the Chemical Society, Faraday Transactions 1: Physical Chemistry in Condensed Phases* **1981,** *77* (11), 2803-2813.
82.Uchida, H.; Tanabe, K.; Nojiri, Y.; Haraguchi, H.; Fuwa, K., Spatial distributions of metastable argon, temperature and electron number density in an inductively coupled argon plasma. *Spectrochimica Acta Part B: Atomic Spectroscopy* **1981,** *36* (7), 711-718.
83.Heywood, M. S.; Taylor, N.; Farnsworth, P. B., Measurement of Helium Metastable Atom Densities in a Plasma-Based Ambient Ionization Source. *Analytical Chemistry* **2011,** *83* (17), 6493-6499.

84.Carroll, D. I.; Dzidic, I.; Stillwell, R. N.; Haegele, K. D.; Horning, E. C., Atmospheric pressure ionization mass spectrometry. Corona discharge ion source for use in a liquid chromatograph-mass spectrometer-computer analytical system. *Analytical Chemistry* **1975,** *47* (14), 2369-2373.
85.Tabrizchi, M.; Khayamian, T.; Taj, N., Design and optimization of a corona discharge ionization source for ion mobility spectrometry. *Review of Scientific Instruments* **2000,** *71* (6), 2321-2328.
86.Hippler, R.; Kersten, H.; Schmidt, M., *Low temperature plasmas: fundamentals, technologies and techniques*. Wiley-VCH: 2008; Vol. 1.
87.Harper, J. D.; Charipar, N. A.; Mulligan, C. C.; Zhang, X.; Cooks, R. G.; Ouyang, Z., Low-Temperature Plasma Probe for Ambient Desorption Ionization. *Analytical Chemistry* **2008,** *80* (23), 9097-9104.
88.Kogelschatz, U.; Eliasson, B.; Egli, W., From ozone generators to flat television screens: history and future potential of dielectric-barrier discharges. *Pure and Applied Chemistry* **1999,** *71* (10), 1819-1828.
89. Fridman, A.; Kennedy, L. A., *Plasma physics and engineering*. CRC press: 2004.
90.Na, N.; Zhao, M.; Zhang, S.; Yang, C.; Zhang, X., Development of a Dielectric Barrier Discharge Ion Source for Ambient Mass Spectrometry. *Journal of the American Society for Mass Spectrometry* **2007,** *18* (10), 1859-1862.
91.Na, N.; Zhang, C.; Zhao, M.; Zhang, S.; Yang, C.; Fang, X.; Zhang, X., Direct detection of explosives on solid surfaces by mass spectrometry with an ambient ion source based on dielectric barrier discharge. *Journal of Mass Spectrometry* **2007,** *42* (8), 1079-1085.
92.Liu, Y.; Ma, X.; Lin, Z.; He, M.; Han, G.; Yang, C.; Xing, Z.; Zhang, S.; Zhang, X., Imaging Mass Spectrometry with a Low-Temperature Plasma Probe for the Analysis of Works of Art. *Angewandte Chemie International Edition* **2010,** *49* (26), 4435-4437.
93.Laroussi, M.; Lu, X., Room-temperature atmospheric pressure plasma plume for biomedical applications. *Applied Physics Letters* **2005,** *87* (11), 113902.
94.Zhang, H.; Xu, Z. M.; Shen, J.; Li, X.; Ding, L. L.; Ma, J.; Lan, Y.; Xia, W. D.; Cheng, C.; Sun, Q.; Zhang, Z. L.; Chu, P. K., Effects and Mechanism of Atmospheric-Pressure Dielectric Barrier Discharge Cold Plasma on Lactate Dehydrogenase (LDH) Enzyme. *Scientific Reports* **2015,** *5*.
95.Tang, S.; Lu, N.; Shang, K.; Li, J.; Wu, Y. In *Detection of hydroxyl radicals during regeneration of granular activated carbon in dielectric barrier discharge plasma system*, Journal of Physics: Conference Series, IOP Publishing: 2013; p 012104.
96.Greenslade, M. E.; Lester, M. I.; Radenović, D. Č.; van Roij, A. J.; Parker, D. H., (2+ 1) Resonance-enhanced ionization spectroscopy of a state-selected beam of OH radicals. *The Journal of chemical physics* **2005,** *123* (7), 074309.
97.Valsaraj, K. T., Hydrophobic compounds in the environment: Adsorption equilibrium at the air-water interface. *Water Research* **1994,** *28* (4), 819-830.
98.Chakraborty, A.; Ervens, B.; Gupta, T.; Tripathi, S. N., Characterization of organic residues of size-resolved fog droplets and their atmospheric implications. *Journal of Geophysical Research: Atmospheres* **2016,** *121* (8), 4317-4332.

99.Mitroka, S.; Zimmeck, S.; Troya, D.; Tanko, J. M., How Solvent Modulates Hydroxyl Radical Reactivity in Hydrogen Atom Abstractions. *Journal of the American Chemical Society* **2010,** *132* (9), 2907-2913.
100.von Sonntag, C.; Schuchmann, H.-P., The Elucidation of Peroxyl Radical Reactions in Aqueous Solution with the Help of Radiation-Chemical Methods. *Angewandte Chemie International Edition in English* **1991,** *30* (10), 1229-1253.
101.Bennett, J. E.; Summers, R., Product Studies of the Mutual Termination Reactions of sec-Alkylperoxy Radicals: Evidence for Non-Cyclic Termination. *Canadian Journal of Chemistry* **1974,** *52* (8), 1377-1379.
102.Russell, G. A., Deuterium-isotope Effects in the Autoxidation of Aralkyl Hydrocarbons. Mechanism of the Interaction of PEroxy Radicals1. *Journal of the American Chemical Society* **1957,** *79* (14), 3871-3877.
103.Gilbert, B. C.; Holmes, R. G. G.; Laue, H. A. H.; Norman, R. O. C., Electron spin resonance studies. Part L. Reactions of alkoxyl radicals generated from alkyl hydroperoxides and titanium(III) ion in aqueous solution. *Journal of the Chemical Society, Perkin Transactions 2* **1976,** (9), 1047-1052.
104.Seinfeld, J. H.; Pandis, S. N., *Atmospheric chemistry and physics: from air pollution to climate change*. John Wiley & Sons: 2016.
105.Nelson, D. D.; Shorter, J. H.; McManus, J. B.; Zahniser, M. S., Sub-part-per-billion detection of nitric oxide in air using a thermoelectrically cooled mid-infrared quantum cascade laser spectrometer. *Applied Physics B* **2002,** *75* (2), 343-350.
106.Berdnikov, V. M.; Bazhin, N. M.; Fedorov, V. K.; Polyakov, O. V., Isomerization of the Ethoxyl Radical to the alpha-Hydroxyethyl Radical in Aqueous Solution. *Kinet. Catal.* **1972,** *13*, 986-987.
107.Saebo, S.; Radom, L.; Schaefer, H. F., The weakly exothermic rearrangement of methoxy radical (CH3O·) to the hydroxymethyl radical (CH2OH·). *The Journal of Chemical Physics* **1983,** *78* (2), 845-853.
108.Batt, L.; Burrows, J. P.; Robinson, G. N., On the isomerisation of the methoxy radical relevance to atmospheric chemistry and combustion. *Chemical Physics Letters* **1981,** *78* (3), 467-470.
109.Domínguez, A.; Fernández, A.; González, N.; Iglesias, E.; Montenegro, L., Determination of critical micelle concentration of some surfactants by three techniques. *Journal of Chemical Education* **1997,** *74* (10), 1227.
110.Stadler, R. H.; Fay, L. B., Antioxidative Reactions of Caffeine: Formation of 8-Oxocaffeine (1,3,7-Trimethyluric Acid) in Coffee Subjected to Oxidative Stress. *Journal of Agricultural and Food Chemistry* **1995,** *43* (5), 1332-1338.
111.Shi, X.; Dalal, N. S.; Jain, A. C., Antioxidant behaviour of caffeine: Efficient scavenging of hydroxyl radicals. *Food and Chemical Toxicology* **1991,** *29* (1), 1-6.
112.León-Carmona, J. R.; Galano, A., Is Caffeine a Good Scavenger of Oxygenated Free Radicals? *The Journal of Physical Chemistry B* **2011,** *115* (15), 4538-4546.
113.Grossert, J. S.; Fancy, P. D.; White, R. L., Fragmentation pathways of negative ions produced by electrospray ionization of acyclic dicarboxylic acids and derivatives. *Canadian Journal of Chemistry* **2005,** *83* (11), 1878-1890.

114.Sahetchian, K. A.; Rigny, R.; Blin, N.; Heiss, A., HOMOGENEOUS DECOMPOSITION OF DIALKYLPEROXIDES IN OXYGEN. *Journal of the Chemical Society-Faraday Transactions Ii* **1987,** *83*, 2035-2043.
115.Molyneux, P., The arrhenius parameters for the thermal decomposition of organic peroxides, and the dissociation energy of the peroxide bond. *Tetrahedron* **1966,** *22* (9), 2929-2943.
116.Hudzik, J. M.; Bozzelli, J. W., Thermochemistry and Bond Dissociation Energies of Ketones. *The Journal of Physical Chemistry A* **2012,** *116* (23), 5707-5722.
117.Kroll, J. H.; Smith, J. D.; Che, D. L.; Kessler, S. H.; Worsnop, D. R.; Wilson, K. R., Measurement of fragmentation and functionalization pathways in the heterogeneous oxidation of oxidized organic aerosol. *Physical Chemistry Chemical Physics* **2009,** *11* (36), 8005-8014.
118.Atkinson, R., Atmospheric reactions of alkoxy and β-hydroxyalkoxy radicals. *International Journal of Chemical Kinetics* **1997,** *29* (2), 99-111.
119.Reeves, J. P.; Dowben, R. M., Formation and properties of thin-walled phospholipid vesicles. *Journal of Cellular Physiology* **1969,** *73* (1), 49-60.
120.Enoch, H. G.; Strittmatter, P., Formation and properties of 1000-A-diameter, single-bilayer phospholipid vesicles. *Proceedings of the National Academy of Sciences* **1979,** *76* (1), 145-149.
121.Mueller, P.; Chien, T. F.; Rudy, B., Formation and properties of cell-size lipid bilayer vesicles. *Biophysical Journal* **1983,** *44* (3), 375-381.
122.von Tscharner, V.; McConnell, H. M., Physical Properties of Lipid Monolayers on Alkylated Planar Glass Surfaces. *Biophysical Journal* **1981,** *36* (2), 421-427.
123.Gebicki, J. M.; Hicks, M., Preparation and properties of vesicles enclosed by fatty acid membranes. *Chemistry and Physics of Lipids* **1976,** *16* (2), 142-160.
124.Cronan, J. E.; Gelmann, E. P., Physical properties of membrane lipids: biological relevance and regulation. *Bacteriological Reviews* **1975,** *39* (3), 232-256.
125.Poste, G.; Papahadjopoulos, D., Lipid vesicles as carriers for introducing materials into cultured cells: influence of vesicle lipid composition on mechanism(s) of vesicle incorporation into cells. *Proceedings of the National Academy of Sciences* **1976,** *73* (5), 1603-1607.
126.Stamatatos, L.; Leventis, R.; Zuckermann, M. J.; Silvius, J. R., Interactions of cationic lipid vesicles with negatively charged phospholipid vesicles and biological membranes. *Biochemistry* **1988,** *27* (11), 3917-3925.
127.Niki, E.; Yamamoto, Y.; Komuro, E.; Sato, K., Membrane damage due to lipid oxidation. *The American Journal of Clinical Nutrition* **1991,** *53* (1), 201S-205S.
128.Halliwell, B.; Chirico, S., Lipid peroxidation: its mechanism, measurement, and significance. *The American Journal of Clinical Nutrition* **1993,** *57* (5), 715S-724S.
129.Esterbauer, H., Cytotoxicity and genotoxicity of lipid-oxidation products. *The American Journal of Clinical Nutrition* **1993,** *57* (5), 779S-785S.
130.Jain, S. K.; McVie, R.; Duett, J.; Herbst, J. J., Erythrocyte Membrane Lipid Peroxidation and Glycosylated Hemoglobin in Diabetes. *Diabetes* **1989,** *38* (12), 1539-1543.

131.Catalá, A., Lipid peroxidation of membrane phospholipids generates hydroxy-alkenals and oxidized phospholipids active in physiological and/or pathological conditions. *Chemistry and Physics of Lipids* **2009,** *157* (1), 1-11.
132.Simonian, N.; Coyle, J., Oxidative stress in neurodegenerative diseases. *Annual review of pharmacology and toxicology* **1996,** *36* (1), 83-106.
133.Parhami, F.; Morrow, A. D.; Balucan, J.; Leitinger, N.; Watson, A. D.; Tintut, Y.; Berliner, J. A.; Demer, L. L., Lipid Oxidation Products Have Opposite Effects on Calcifying Vascular Cell and Bone Cell Differentiation. *A Possible Explanation for the Paradox of Arterial Calcification in Osteoporotic Patients* **1997,** *17* (4), 680-687.
134.Stewart, R. R. C.; Bewley, J. D., Lipid Peroxidation Associated with Accelerated Aging of Soybean Axes. *Plant Physiology* **1980,** *65* (2), 245-248.
135.Halliwell, B.; Murcia, M. A.; Chirico, S.; Aruoma, O. I., Free radicals and antioxidants in food and in vivo: What they do and how they work. *Critical Reviews in Food Science and Nutrition* **1995,** *35* (1-2), 7-20.
136.Coupland, J. N.; McClements, D. J., Lipid oxidation in food emulsions. *Trends in Food Science & Technology* **1996,** *7* (3), 83-91.
137.Schaich, K. M., Metals and lipid oxidation. Contemporary issues. *Lipids* **1992,** *27* (3), 209-218.
138.Fong, K.-L.; McCay, P. B.; Poyer, J. L.; Keele, B. B.; Misra, H., Evidence that Peroxidation of Lysosomal Membranes Is Initiated by Hydroxyl Free Radicals Produced during Flavin Enzyme Activity. *Journal of Biological Chemistry* **1973,** *248* (22), 7792-7797.
139. Frankel, E. N., Lipid oxidation. *Progress in Lipid Research* **1980,** *19* (1), 1-22.
140.Howard, J. A.; Ingold, K. U., Absolute rate constants for hydrocarbon autoxidation. VI. Alkyl aromatic and olefinic hydrocarbons. *Canadian Journal of Chemistry* **1967,** *45* (8), 793-802.
141.Hawco, F. J.; O'Brien, C. R.; O'Brien, P. J., Singlet oxygen formation during hemoprotein catalyzed lipid peroxide decomposition. *Biochemical and Biophysical Research Communications* **1977,** *76* (2), 354-361.
142.Bus, J. S.; Aust, S. D.; Gibson, J. E., Superoxide- and singlet oxygen-catalyzed lipid peroxidation as a possible mechanism for paraquat (methyl viologen) toxicity. *Biochemical and Biophysical Research Communications* **1974,** *58* (3), 749-755.
143.Thomas, C. E.; Morehouse, L. A.; Aust, S. D., Ferritin and superoxide-dependent lipid peroxidation. *Journal of Biological Chemistry* **1985,** *260* (6), 3275-3280.
144.Porter, N. A.; Caldwell, S. E.; Mills, K. A., Mechanisms of free radical oxidation of unsaturated lipids. *Lipids* **1995,** *30* (4), 277-290.
145.Till, G. O.; Hatherill, J. R.; Tourtellotte, W. W.; Lutz, M. J.; Ward, P. A., Lipid peroxidation and acute lung injury after thermal trauma to skin. Evidence of a role for hydroxyl radical. *The American Journal of Pathology* **1985,** *119* (3), 376-384.
146.Laguerre, M.; Lecomte, J.; Villeneuve, P., Evaluation of the ability of antioxidants to counteract lipid oxidation: Existing methods, new trends and challenges. *Progress in Lipid Research* **2007,** *46* (5), 244-282.
147.Creuwels, L. A. J. M.; van Golde, L. M. G.; Haagsman, H. P., The Pulmonary Surfactant System: Biochemical and Clinical Aspects. *Lung* **1997,** *175* (1), 1-39.

148.Kahn, M. C.; Anderson, G. J.; Anyan, W. R.; Hall, S. B., Phosphatidylcholine molecular species of calf lung surfactant. *American Journal of Physiology - Lung Cellular and Molecular Physiology* **1995,** *269* (5), L567-L573.
149.Goerke, J., Pulmonary surfactant: functions and molecular composition. *Biochimica et Biophysica Acta (BBA) - Molecular Basis of Disease* **1998,** *1408* (2–3), 79-89.
150.Shin, Y. S.; Choi, T. S.; Kim, H.; Beauchamp, J. L.; Heath, J. R.; Kim, H. I., A microfluidic-based bubble generation platform enables analysis of physical property change in phospholipid surfactant layers by interfacial ozone reaction(). *Lab on a chip* **2012,** *12* (24), 5243-5248.
151.Qiao, L.; Ge, A.; Osawa, M.; Ye, S., Structure and stability studies of mixed monolayers of saturated and unsaturated phospholipids under low-level ozone. *Physical Chemistry Chemical Physics* **2013,** *15* (41), 17775-17785.
152.Qiao, L.; Ge, A.; Liang, Y.; Ye, S., Oxidative Degradation of the Monolayer of 1-Palmitoyl-2-Oleoyl-sn-Glycero-3-Phosphocholine (POPC) in Low-Level Ozone. *The Journal of Physical Chemistry B* **2015,** *119* (44), 14188-14199.
153.Menger, F. M.; Littau, C. A., Gemini-surfactants: synthesis and properties. *Journal of the American Chemical Society* **1991,** *113* (4), 1451-1452.
154.Menger, F. M.; Littau, C. A., Gemini surfactants: a new class of self-assembling molecules. *Journal of the American Chemical Society* **1993,** *115* (22), 10083-10090.
155.Rosen, M. J., Geminis: a new generation of surfactants: these materials have better properties than conventional ionic surfactants as well as positive synergistic effects with non-ionics. *Chemtech* **1993,** *23* (3), 30-33.
156.Zhu, Y.-P.; Masuyama, A.; Kobata, Y.; Nakatsuji, Y.; Okahara, M.; Rose, M. J., Double-Chain Surfactants with Two Carboxylate Groups and Their Relation to Similar Double-Chain Compounds. *Journal of Colloid and Interface Science* **1993,** *158* (1), 40-45.
157.Kang, P.; Xu, H., Synthesis and Properties of Dissymmetric Gemini Surfactants. *Journal of Surfactants and Detergents* **2013,** *16* (6), 921-925.
158.Zana, R., Dimeric (Gemini) Surfactants: Effect of the Spacer Group on the Association Behavior in Aqueous Solution. *Journal of Colloid and Interface Science* **2002,** *248* (2), 203-220.
159.Zana, R.; Benrraou, M.; Rueff, R., Alkanediyl-.alpha.,.omega.-bis(dimethylalkylammonium bromide) surfactants. 1. Effect of the spacer chain length on the critical micelle concentration and micelle ionization degree. *Langmuir* **1991,** *7* (6), 1072-1075.
160.Zana, R.; Lévy, H., Alkanediyl-α,ω-bis(dimethylalkylammonium bromide) surfactants (dimeric surfactants) Part 6. CMC of the ethanediyl-1,2-bis(dimethylalkylammonium bromide) series. *Colloids and Surfaces A: Physicochemical and Engineering Aspects* **1997,** *127* (1), 229-232.
161.Brun, A.; Brezesinski, G.; Möhwald, H.; Blanzat, M.; Perez, E.; Rico-Lattes, I., Interaction between phospholipids and new Gemini catanionic surfactants having anti-HIV activity. *Colloids and Surfaces A: Physicochemical and Engineering Aspects* **2003,** *228* (1–3), 3-16.

162.Naqvi, A. Z.; Noori, S.; Kabir ud, D., Effect of surfactant structure on the mixed micelle formation of cationic gemini–zwitterionic phospholipid systems. *Colloids and Surfaces A: Physicochemical and Engineering Aspects* **2015,** *477*, 9-18.
163.Scarzello, M.; Klijn, J. E.; Wagenaar, A.; Stuart, M. C. A.; Hulst, R.; Engberts, J. B. F. N., pH-Dependent Aggregation Properties of Mixtures of Sugar-Based Gemini Surfactants with Phospholipids and Single-Tailed Surfactants. *Langmuir* **2006,** *22* (6), 2558-2568.
164.Obłąk, E.; Piecuch, A.; Krasowska, A.; Łuczyński, J., Antifungal activity of gemini quaternary ammonium salts. *Microbiological Research* **2013,** *168* (10), 630-638.
165.Imam, T.; Devinsky, F.; Lacko, I.; Mlynarcik, D.; Krasnec, L., Preparation and antimicrobial activity of some new bisquaternary ammonium salts. *Die Pharmazie* **1983,** *38* (5), 308-310.
166.Pavlíková, M.; Lacko, I.; Devínský, F.; Mlynarčík, D., Quantitative relationships between structure, aggregation properties and antimicrobial activity of quaternary ammonium bolaamphiphiles. *Collection of Czechoslovak chemical communications* **1995,** *60* (7), 1213-1228.
167.Toyama, A.; Nakagawa, H.; Matsuda, K.; Sato, T.-A.; Nakamura, Y.; Ueda, K., Quantitative Structural Characterization of Local N-Glycan Microheterogeneity in Therapeutic Antibodies by Energy-Resolved Oxonium Ion Monitoring. *Analytical Chemistry* **2012,** *84* (22), 9655-9662.
168.Sun, Y.; Feng, Y.; Dong, H.; Chen, Z.; Han, L., Synthesis and aqueous solution properties of homologous gemini surfactants with different head groups. *Central European Journal of Chemistry* **2007,** *5* (2), 620-634.
169.Banks, J. L.; Beard, H. S.; Cao, Y.; Cho, A. E.; Damm, W.; Farid, R.; Felts, A. K.; Halgren, T. A.; Mainz, D. T.; Maple, J. R.; Murphy, R.; Philipp, D. M.; Repasky, M. P.; Zhang, L. Y.; Berne, B. J.; Friesner, R. A.; Gallicchio, E.; Levy, R. M., Integrated Modeling Program, Applied Chemical Theory (IMPACT). *Journal of Computational Chemistry* **2005,** *26* (16), 1752-1780.
170.Glasius, M.; Lahaniati, M.; Calogirou, A.; Di Bella, D.; Jensen, N. R.; Hjorth, J.; Kotzias, D.; Larsen, B. R., Carboxylic Acids in Secondary Aerosols from Oxidation of Cyclic Monoterpenes by Ozone. *Environmental Science & Technology* **2000,** *34* (6), 1001-1010.
171.Zhang, Y. Y.; Müller, L.; Winterhalter, R.; Moortgat, G. K.; Hoffmann, T.; Pöschl, U., Seasonal cycle and temperature dependence of pinene oxidation products, dicarboxylic acids and nitrophenols in fine and coarse air particulate matter. *Atmos. Chem. Phys.* **2010,** *10* (16), 7859-7873.
172.Vesna, O.; Sax, M.; Kalberer, M.; Gaschen, A.; Ammann, M., Product study of oleic acid ozonolysis as function of humidity. *Atmospheric Environment* **2009,** *43* (24), 3662-3669.
173.Ackman, R. G.; Retson, M. E.; Gallay, L. R.; Vandenheuvel, F. A., OZONOLYSIS OF UNSATURATED FATTY ACIDS: I. OZONOLYSIS OF OLEIC ACID. *Canadian Journal of Chemistry* **1961,** *39* (10), 1956-1963.
174.Ziemann, P. J., Aerosol products, mechanisms, and kinetics of heterogeneous reactions of ozone with oleic acid in pure and mixed particles. *Faraday Discussions* **2005,** *130*, 469-490.

175.Reynolds, J. C.; Last, D. J.; McGillen, M.; Nijs, A.; Horn, A. B.; Percival, C.; Carpenter, L. J.; Lewis, A. C., Structural Analysis of Oligomeric Molecules Formed from the Reaction Products of Oleic Acid Ozonolysis. *Environmental Science & Technology* **2006,** *40* (21), 6674-6681.
176.Zahardis, J.; LaFranchi, B. W.; Petrucci, G. A., Direct observation of polymerization in the oleic acid–ozone heterogeneous reaction system by photoelectron resonance capture ionization aerosol mass spectrometry. *Atmospheric Environment* **2006,** *40* (9), 1661-1670.
177.Jen, C. N.; Bachman, R.; Zhao, J.; McMurry, P. H.; Hanson, D. R., Diamine-sulfuric acid reactions are a potent source of new particle formation. *Geophysical Research Letters* **2016,** *43* (2), 867-873.
178.Elm, J.; Passananti, M.; Kurtén, T.; Vehkamäki, H., Diamines Can Initiate New Particle Formation in the Atmosphere. *The Journal of Physical Chemistry A* **2017,** *121* (32), 6155-6164.
179.Ge, X.; Wexler, A. S.; Clegg, S. L., Atmospheric amines – Part I. A review. *Atmospheric Environment* **2011,** *45* (3), 524-546.
180.Sipilä, M.; Sarnela, N.; Jokinen, T.; Junninen, H.; Hakala, J.; Rissanen, M. P.; Praplan, A.; Simon, M.; Kürten, A.; Bianchi, F.; Dommen, J.; Curtius, J.; Petäjä, T.; Worsnop, D. R., Bisulfate – cluster based atmospheric pressure chemical ionization mass spectrometer for high-sensitivity (< 100 ppqV) detection of atmospheric dimethyl amine: proof-of-concept and first ambient data from boreal forest. *Atmos. Meas. Tech.* **2015,** *8* (10), 4001-4011.
181.Kieloaho, A.-J.; Pihlatie, M.; Launiainen, S.; Kulmala, M.; Riekkola, M.-L.; Parshintsev, J.; Mammarella, I.; Vesala, T.; Heinonsalo, J., Soil concentrations and soil-atmosphere exchange of alkylamines in a boreal Scots pine forest. *Biogeosciences* **2017,** *14* (5), 1075.
182.Hellén, H.; Kieloaho, A. J.; Hakola, H., Gas-phase alkyl amines in urban air; comparison with a boreal forest site and importance for local atmospheric chemistry. *Atmospheric Environment* **2014,** *94*, 192-197.
183.Facchini, M. C.; Decesari, S.; Rinaldi, M.; Carbone, C.; Finessi, E.; Mircea, M.; Fuzzi, S.; Moretti, F.; Tagliavini, E.; Ceburnis, D.; O'Dowd, C. D., Important Source of Marine Secondary Organic Aerosol from Biogenic Amines. *Environmental Science & Technology* **2008,** *42* (24), 9116-9121.
184.Nölscher, A.; Williams, J.; Sinha, V.; Custer, T.; Song, W.; Johnson, A.; Axinte, R.; Bozem, H.; Fischer, H.; Pouvesle, N., Summertime total OH reactivity measurements from boreal forest during HUMPPA-COPEC 2010. *Atmospheric chemistry and Physics* **2012,** *12* (17), 8257-8270.
185.Wilm, M., Principles of Electrospray Ionization. *Molecular & Cellular Proteomics* **2011,** *10* (7).
186.Takáts, Z.; Wiseman, J. M.; Gologan, B.; Cooks, R. G., Mass Spectrometry Sampling Under Ambient Conditions with Desorption Electrospray Ionization. *Science* **2004,** *306* (5695), 471-473.
187.Ho, C. S.; Lam, C. W. K.; Chan, M. H. M.; Cheung, R. C. K.; Law, L. K.; Lit, L. C. W.; Ng, K. F.; Suen, M. W. M.; Tai, H. L., Electrospray Ionisation Mass Spectrometry: Principles and Clinical Applications. *The Clinical Biochemist Reviews* **2003,** *24* (1), 3-12.

188.Hoang, K.; Pophristic, M.; Horan, A. J.; Johnston, M. V.; McEwen, C. N., High Sensitivity Analysis of Nanoliter Volumes of Volatile and Nonvolatile Compounds using Matrix Assisted Ionization (MAI) Mass Spectrometry. *J Am Soc Mass Spectrom* **2016,** *27* (10), 1590-6.
189.King, R.; Bonfiglio, R.; Fernandez-Metzler, C.; Miller-Stein, C.; Olah, T., Mechanistic investigation of ionization suppression in electrospray ionization. *Journal of the American Society for Mass Spectrometry* **2000,** *11* (11), 942-950.
190.Bonfiglio, R.; King, R. C.; Olah, T. V.; Merkle, K., The effects of sample preparation methods on the variability of the electrospray ionization response for model drug compounds. *Rapid Communications in Mass Spectrometry* **1999,** *13* (12), 1175-1185.
191.Beaudry, F.; Vachon, P., Electrospray ionization suppression, a physical or a chemical phenomenon? *Biomedical Chromatography* **2006,** *20* (2), 200-205.
192.Madronich, S.; Calvert, J. G., Permutation reactions of organic peroxy radicals in the troposphere. *Journal of Geophysical Research: Atmospheres* **1990,** *95* (D5), 5697-5715.
193.Tarek, M.; Tobias, D. J.; Klein, M. L., Molecular dynamics simulation of tetradecyltrimethylammonium bromide monolayers at the air/water interface. *The Journal of Physical Chemistry* **1995,** *99* (5), 1393-1402.
194.Yuan, S.; Ma, L.; Zhang, X.; Zheng, L., Molecular dynamics studies on monolayer of cetyltrimethylammonium bromide surfactant formed at the air/water interface. *Colloids and Surfaces A: Physicochemical and Engineering Aspects* **2006,** *289* (1), 1-9.
195.Strazdaite, S.; Versluis, J.; Bakker, H. J., Interplay of Electrostatic Interactions and Hydrophobic Hydration at the Surface of Tetra-n-alkylammonium Bromide Solutions. *The Journal of Physical Chemistry C* **2016,** *120* (31), 17290-17295.
196.Huber, M. C.; Schreiber, A.; von Olshausen, P.; Varga, B. R.; Kretz, O.; Joch, B.; Barnert, S.; Schubert, R.; Eimer, S.; Kele, P.; Schiller, S. M., Designer amphiphilic proteins as building blocks for the intracellular formation of organelle-like compartments. *Nat Mater* **2015,** *14* (1), 125-132.
197.Zhang, X. L.; Penfold, J.; Thomas, R. K.; Tucker, I. M.; Petkov, J. T.; Bent, J.; Cox, A., Adsorption Behavior of Hydrophobin and Hydrophobin/Surfactant Mixtures at the Solid–Solution Interface. *Langmuir* **2011,** *27* (17), 10464-10474.
198.Heath, J. G.; Arnett, E. M., Chiral molecular recognition in monolayers of diastereomeric N-acylamino acid methyl esters at the air/water interface. *Journal of the American Chemical Society* **1992,** *114* (12), 4500-4514.
199.Madani, F.; Lindberg, S.; Langel; #220; lo; Futaki, S.; Gr; #228; slund, A., Mechanisms of Cellular Uptake of Cell-Penetrating Peptides. *Journal of Biophysics* **2011,** *2011*.
200.Vives, E.; Brodin, P.; Lebleu, B., A truncated HIV-1 Tat protein basic domain rapidly translocates through the plasma membrane and accumulates in the cell nucleus. *Journal of Biological Chemistry* **1997,** *272* (25), 16010-16017.
201.Derossi, D.; Calvet, S.; Trembleau, A.; Brunissen, A.; Chassaing, G.; Prochiantz, A., Cell internalization of the third helix of the Antennapedia homeodomain is receptor-independent. *Journal of Biological Chemistry* **1996,** *271* (30), 18188-18193.
202.Nakase, I.; Hirose, H.; Tanaka, G.; Tadokoro, A.; Kobayashi, S.; Takeuchi, T.; Futaki, S., Cell-surface Accumulation of Flock House Virus-derived Peptide Leads to Efficient Internalization via Macropinocytosis. *Molecular Therapy* **2009,** *17* (11), 1868-1876.

203.Roise, D.; Horvath, S. J.; Tomich, J. M.; Richards, J. H.; Schatz, G., A chemically synthesized pre-sequence of an imported mitochondrial protein can form an amphiphilic helix and perturb natural and artificial phospholipid bilayers. *The EMBO Journal* **1986,** *5* (6), 1327-1334.
204.Johansson, J.; Gudmundsson, G. H.; Rottenberg, M. n. E.; Berndt, K. D.; Agerberth, B., Conformation-dependent antibacterial activity of the naturally occurring human peptide LL-37. *Journal of Biological Chemistry* **1998,** *273* (6), 3718-3724.
205.Fletcher, J. M.; Harniman, R. L.; Barnes, F. R. H.; Boyle, A. L.; Collins, A.; Mantell, J.; Sharp, T. H.; Antognozzi, M.; Booth, P. J.; Linden, N.; Miles, M. J.; Sessions, R. B.; Verkade, P.; Woolfson, D. N., Self-Assembling Cages from Coiled-Coil Peptide Modules. *Science* **2013,** *340* (6132), 595-599.
206.Stahl, P. J.; Yu, S. M., Encoding cell-instructive cues to PEG-based hydrogels via triple helical peptide assembly. *Soft Matter* **2012,** *8* (40), 10409-10418.
207.Chandra, S.; Chen, X.; Rizo, J.; Jahn, R.; Südhof, T. C., A Broken α-Helix in Folded α-Synuclein. *Journal of Biological Chemistry* **2003,** *278* (17), 15313-15318.
208.Kaul, R.; Angeles, A. R.; Jäger, M.; Powers, E. T.; Kelly, J. W., Incorporating β-Turns and a Turn Mimetic out of Context in Loop 1 of the WW Domain Affords Cooperatively Folded β-Sheets. *Journal of the American Chemical Society* **2001,** *123* (22), 5206-5212.
209.Amit, M.; Cheng, G.; Hamley, I. W.; Ashkenasy, N., Conductance of amyloid [small beta] based peptide filaments: structure-function relations. *Soft Matter* **2012,** *8* (33), 8690-8696.
210.Lin, Y.-A.; Ou, Y.-C.; Cheetham, A. G.; Cui, H., Rational Design of MMP Degradable Peptide-Based Supramolecular Filaments. *Biomacromolecules* **2014,** *15* (4), 1419-1427.
211.Vaiser, V.; Rapaport, H., Compressibility and Elasticity of Amphiphilic and Acidic β-Sheet Peptides at the Air−Water Interface. *The Journal of Physical Chemistry B* **2011,** *115* (1), 50-56.
212.Engin, O.; Villa, A.; Sayar, M.; Hess, B., Driving Forces for Adsorption of Amphiphilic Peptides to the Air−Water Interface. *The Journal of Physical Chemistry B* **2010,** *114* (34), 11093-11101.
213.Segman, S.; Lee, M.-r.; Vaiser, V.; Gellman, S. H.; Rapaport, H., Highly Stable Pleated-Sheet Secondary Structure in Assemblies of Amphiphilic α/β-Peptides at the Air–Water Interface. *Angewandte Chemie International Edition* **2010,** *49* (4), 716-719.
214.Roach, P.; Farrar, D.; Perry, C. C., Interpretation of Protein Adsorption: Surface-Induced Conformational Changes. *Journal of the American Chemical Society* **2005,** *127* (22), 8168-8173.
215.Gu, C.; Lustig, S.; Jackson, C.; Trout, B. L., Design of Surface Active Soluble Peptide Molecules at the Air/Water Interface. *The Journal of Physical Chemistry B* **2008,** *112* (10), 2970-2980.
216.Micklitsch, C. M.; Medina, S. H.; Yucel, T.; Nagy-Smith, K. J.; Pochan, D. J.; Schneider, J. P., Influence of Hydrophobic Face Amino Acids on the Hydrogelation of β-Hairpin Peptide Amphiphiles. *Macromolecules* **2015,** *48* (5), 1281-1288.
217.Maleknia, S. D.; Brenowitz, M.; Chance, M. R., Millisecond Radiolytic Modification of Peptides by Synchrotron X-rays Identified by Mass Spectrometry. *Analytical Chemistry* **1999,** *71* (18), 3965-3973.

218.Xu, G.; Chance, M. R., Radiolytic Modification and Reactivity of Amino Acid Residues Serving as Structural Probes for Protein Footprinting. *Analytical Chemistry* **2005,** *77* (14), 4549-4555.
219.Xu, G.; Chance, M. R., Radiolytic Modification of Sulfur-Containing Amino Acid Residues in Model Peptides: Fundamental Studies for Protein Footprinting. *Analytical Chemistry* **2005,** *77* (8), 2437-2449.
220.Xu, G.; Takamoto, K.; Chance, M. R., Radiolytic Modification of Basic Amino Acid Residues in Peptides: Probes for Examining Protein−Protein Interactions. *Analytical Chemistry* **2003,** *75* (24), 6995-7007.
221.Stadtman, E. R.; Levine, R. L., Free radical-mediated oxidation of free amino acids and amino acid residues in proteins. *Amino Acids* **2003,** *25* (3), 207-218.
222.Takamoto, K.; Chance, M. R., RADIOLYTIC PROTEIN FOOTPRINTING WITH MASS SPECTROMETRY TO PROBE THE STRUCTURE OF MACROMOLECULAR COMPLEXES. *Annual Review of Biophysics and Biomolecular Structure* **2006,** *35* (1), 251-276.
223.Hunt, D. F.; Yates, J. R.; Shabanowitz, J.; Winston, S.; Hauer, C. R., Protein sequencing by tandem mass spectrometry. *Proceedings of the National Academy of Sciences* **1986,** *83* (17), 6233-6237.
224.Johnson, R. S.; Martin, S. A.; Biemann, K.; Stults, J. T.; Watson, J. T., Novel fragmentation process of peptides by collision-induced decomposition in a tandem mass spectrometer: differentiation of leucine and isoleucine. *Analytical chemistry* **1987,** *59* (21), 2621-2625.
225.Tabb, D. L.; Huang, Y.; Wysocki, V. H.; Yates, J. R., Influence of Basic Residue Content on Fragment Ion Peak Intensities in Low-Energy Collision-Induced Dissociation Spectra of Peptides. *Analytical Chemistry* **2004,** *76* (5), 1243-1248.
226.Tang, X. J.; Thibault, P.; Boyd, R. K., Fragmentation reactions of multiply-protonated peptides and implications for sequencing by tandem mass spectrometry with low-energy collision-induced dissociation. *Analytical Chemistry* **1993,** *65* (20), 2824-2834.
227.Mitchell Wells, J.; McLuckey, S. A., Collision-Induced Dissociation (CID) of Peptides and Proteins. *Methods in Enzymology* **2005,** *402*, 148-185.
228.Biemann, K., Contributions of mass spectrometry to peptide and protein structure. *Biological Mass Spectrometry* **1988,** *16* (1-12), 99-111.
229.Sharp, J. S.; Becker, J. M.; Hettich, R. L., Protein surface mapping by chemical oxidation: Structural analysis by mass spectrometry. *Analytical Biochemistry* **2003,** *313* (2), 216-225.
230.Tullius, T. D.; Dombroski, B. A., Hydroxyl radical "footprinting": high-resolution information about DNA-protein contacts and application to lambda repressor and Cro protein. *Proceedings of the National Academy of Sciences* **1986,** *83* (15), 5469-5473.
231.Zepp, R. G.; Faust, B. C.; Hoigne, J., Hydroxyl radical formation in aqueous reactions (pH 3-8) of iron (II) with hydrogen peroxide: the photo-Fenton reaction. *Environmental Science & Technology* **1992,** *26* (2), 313-319.
232.Boys, B. L.; Kuprowski, M. C.; Noël, J. J.; Konermann, L., Protein Oxidative Modifications During Electrospray Ionization: Solution Phase Electrochemistry or Corona Discharge-Induced Radical Attack? *Analytical Chemistry* **2009,** *81* (10), 4027-4034.

233.Sharp, J. S.; Becker, J. M.; Hettich, R. L., Analysis of Protein Solvent Accessible Surfaces by Photochemical Oxidation and Mass Spectrometry. *Analytical Chemistry* **2004,** *76* (3), 672-683.
234.Sharp, J. S.; Guo, J.-t.; Uchiki, T.; Xu, Y.; Dealwis, C.; Hettich, R. L., Photochemical surface mapping of C14S-Sml1p for constrained computational modeling of protein structure. *Analytical Biochemistry* **2005,** *340* (2), 201-212.
235.Hambly, D. M.; Gross, M. L., Laser Flash Photolysis of Hydrogen Peroxide to Oxidize Protein Solvent-Accessible Residues on the Microsecond Timescale. *Journal of the American Society for Mass Spectrometry* **2005,** *16* (12), 2057-2063.
236.Watson, C.; Janik, I.; Zhuang, T.; Charvátová, O.; Woods, R. J.; Sharp, J. S., Pulsed Electron Beam Water Radiolysis for Submicrosecond Hydroxyl Radical Protein Footprinting. *Analytical Chemistry* **2009,** *81* (7), 2496-2505.
237.Hayes, J. J.; Kam, L.; Tullius, T. D., [56] Footprinting protein-DNA complexes with γ-rays. *Methods in Enzymology* **1990,** *186*, 545-549.
238.Sclavi, B.; Woodson, S.; Sullivan, M.; Chance, M.; Brenowitz, M., [19] Following the folding of RNA with time-resolved synchrotron X-ray footprinting. *Methods in Enzymology* **1998,** *295*, 379-402.
239.Seelig, A., Substance P and antagonists. Surface activity and molecular shapes. *Biochimica et Biophysica Acta (BBA) - Biomembranes* **1990,** *1030* (1), 111-118.
240.Keller, B. O.; Sui, J.; Young, A. B.; Whittal, R. M., Interferences and contaminants encountered in modern mass spectrometry. *Analytica Chimica Acta* **2008,** *627* (1), 71-81.
241.Turecek, F.; Drinkwater, D. E.; McLafferty, F. W., Gas-phase chemistry of CH3SOH, -CH2+SHOH, CH3SO.cntdot., and .cntdot.CH2SOH by neutralization-reionization mass spectrometry. *Journal of the American Chemical Society* **1989,** *111* (20), 7696-7701.
242.O'Hair, R. A. J.; Reid, G. E., Neighboring Group versus Cis-Elimination Mechanisms for Side Chain Loss from Protonated Methionine, Methionine Sulfoxide and Their Peptides. *European Mass Spectrometry* **1999,** *5* (5), 325-334.
243.Lioe, H.; Laskin, J.; Reid, G. E.; O'Hair, R. A. J., Energetics and Dynamics of the Fragmentation Reactions of Protonated Peptides Containing Methionine Sulfoxide or Aspartic Acid via Energy- and Time-Resolved Surface Induced Dissociation. *The Journal of Physical Chemistry A* **2007,** *111* (42), 10580-10588.
244.Paizs, B.; Suhai, S., Fragmentation pathways of protonated peptides. *Mass Spectrometry Reviews* **2005,** *24* (4), 508-548.
245.Xu, G.; Chance, M. R., Hydroxyl Radical-Mediated Modification of Proteins as Probes for Structural Proteomics. *Chemical Reviews* **2007,** *107* (8), 3514-3543.
246.Lyttle, D. J.; Lu, J. R.; Su, T. J.; Thomas, R. K.; Penfold, J., Structure of a Dodecyltrimethylammonium Bromide Layer at the Air/Water Interface Determined by Neutron Reflection: Comparison of the Monolayer Structure of Cationic Surfactants with Different Chain Lengths. *Langmuir* **1995,** *11* (3), 1001-1008.
247.Parker, R. A.; Wasik, S. P., Diffusion Coefficient of Dodecyltrimethylammonium Chloride in Aqueous Solution at 23°. *The Journal of Physical Chemistry* **1959,** *63* (11), 1921-1924.
248.Jr., C. W. B.; Langhoff, S. R., Theoretical determination of the radiative lifetime of the A 2Σ+ state of OH. *The Journal of Chemical Physics* **1987,** *87* (8), 4665-4672.

249.German, K. R., Direct measurement of the radiative lifetimes of the A 2Σ+ (V′ = 0) states of OH and OD. *The Journal of Chemical Physics* **1975,** *62* (7), 2584-2587.
250.Brzozowski, J.; Erman, P.; Lyyra, M., Precision Estimates of the Predissociation Rates of the OH A2Σ State (v⩽ 2). *Physica scripta* **1978,** *17* (5), 507.
251.Devasagayam, T. P. A.; Kamat, J. P.; Mohan, H.; Kesavan, P. C., Caffeine as an antioxidant: inhibition of lipid peroxidation induced by reactive oxygen species. *Biochimica et Biophysica Acta (BBA) - Biomembranes* **1996,** *1282* (1), 63-70.